Fundamental Analysis of Wood Adhesion Primers

Joshua C. Hosen

Thesis submitted to the faculty of the

Virginia Polytechnic Institute and State University

in partial fulfillment of the requirements for the degree of

Master of Science

in

Forest Products

Charles E. Frazier

Kevin J. Edgar

Scott H. Renneckar

September 8th, 2010

Blacksburg, VA

Keywords: hydroxymethyl resorcinol, solvent submersion dynamic mechanical analysis, mode-I fracture, rheology, wood primers

Fundamental Analysis of Wood Adhesion Primers

Josh Hosen

ABSTRACT

Hydroxymethyl resorcinol (HMR) is an effective adhesion promoter (primer) for wood bonding; it dramatically improves adhesion and enhances bond durability against moisture exposure. In an effort to improve understanding of the HMR mechanism, this work compared HMR with two other chemical treatments investigated as wood primers: alkyl-HMR (a-HMR), an HMR variant having reduced crosslink density; and a 5% solution of polymeric methylenebis(phenylisocyanate) in N-methylpyrrolidone (solution referred to as "pMDI"). The experimental system was red oak (*Quercus rubra*) bonded with a moisture-cure polyurethane adhesive (PUR). The objective was to document wood rheological changes induced by the three primers, and determine if these changes correlated to primer efficacy. Adhesion was tested in mode-I fracture using dual cantilever beam specimens. HMR and a-HMR proved to be highly effective primers for PUR-bonded red oak; both primers dramatically improved bondline toughness and durability. Relative to HMR, the reduced crosslink density in a-HMR did not impair primer efficacy. In contrast, the pMDI primer reduced bondline toughness and durability. Solvent-submersion, torsional dynamic mechanical analysis (DMA) was conducted on primer-treated red oak (with specimens immersed in dimethylformamide). Using all three grain orientations, the lignin glass/rubber transition was carefully studied with attention directed towards primer-induced changes in storage modulus, the glass transition temperature (T_g), tan δ maximum intensity, and the breadth of tan δ transition. It was found that primer effectiveness correlated with a reduction in damping intensity, and also with a T_g increase greater than 5˚C. Determination of these correlations was complicated by grain dependency, and also by rheological changes caused by solvent treatments that were used as primer control treatments.

Acknowledgements

I would first like to thank my major advisor, Dr. Charles Frazier, for all of the support and guidance he has lent to me over the course of this work. Without question, his endless enthusiasm for research has propelled my own scientific curiosity to new heights; the patience he exhibited as he molded this forest products marketing student into a rigorous scientist is truly remarkable. I would also like to thank my committee members Dr. Scott Renneckar and Dr. Kevin Edgar for all of their comments and support on this research; Dr. Renneckar especially has been a friend since the beginning of my collegiate career, and I will always remember fondly his devastating hook shot. This work would not have been possible without the superior work of David Jones, who toiled endlessly to produce the wood specimens I required; thank you. The tremendous support of friendly faces Debbie Garnand and Angie Riegel also did not go unnoticed; this department could not function without you. Dr. Audrey Zink-Sharp was also always there to lend her support when times were tough. Rick and Linda Caudill were integral to my growth as both a student and a person. Many thanks to Kevin Knight, Taylor Bertschy, and Charlie Schlosser for being my social life these past two years. Of course I must also acknowledge my friends in the Virginia Tech Wood Adhesion Group: Sudip Chowdhury, Dakai Ren, Jessie Paris, and James Fabiyi. My deepest gratitude is extended to Sudip and Dakai, whose never-ending supply of patience, kindness, and knowledge I took advantage of as often as possible – your friendship, as well as your wives' cooking, really kept me going. And it is not possible to have an acknowledgements section without mentioning Jessica Wolfe, who has been with me through feast and famine; it is only because of your love and support that I was able to succeed in this endeavor. This work is dedicated to my friends and family, who I have so selfishly neglected over the course of this work; thank you for your support and understanding.

TABLE OF CONTENTS

LIST OF FIGURES

LIST OF TABLES

1 Introduction

Moisture durability of wood-adhesive bonds is a critical issue in the wood-based composites industry, not only because of in-use water exposure, but also because structural adhesive certification imposes demanding test procedures that include extreme, cyclic water exposures. In 1995, a wood primer was developed which mitigated the damaging effects caused by extreme simulated weathering. This chemical treatment is known as hydroxymethyl resorcinol (HMR).

HMR is a 5% solids, dilute alkaline solution of resorcinol and formaldehyde, and is currently the most well-known and effective wood primer available; it remarkably enhances the moisture durability of wood-adhesive bonds. The treatment is suggested to enhance the dimensional stability of the wood, and its effectiveness is implicated by its ability to crosslink within the wood cell wall (Christiansen 2005; Son and Gardner 2004; Sun and Frazier 2005). The goal of this project is to investigate the impact of HMR and HMR-related primers on red oak (*Quercus rubra*) using primarily dynamic mechanical analysis and mode-I fracture adhesion testing. A possible link between the rheological properties of primer-treated wood and its resulting bond performance will also be studied. What follows is an overview of HMR, followed by a review of the major analytical methods used in this project.

2 Literature Review

2.1 Hydroxymethyl Resorcinol

2.1.1 Origination

HMR was disclosed in 1995 by Vick and coworkers at the United Sates Forest Products Laboratory (Vick et al. 1995). It was originally developed for use with epoxies, which are known to produce moisture-sensitive wood bonds. HMR was found to dramatically improve the moisture durability of epoxy bonds to sitka spruce (Vick et al. 1995). The discovery was revealed through the ASTM D 2559 (2004) delamination test; this procedure is a critical hurdle towards the structural certification of wood adhesives, involving a harsh cyclic water-weathering process. With no HMR treatment, bisphenol-A epoxy adhesives failed the ASTM test, while HMR-treated samples passed this rigorous test

The HMR primer is prepared by reacting formaldehyde and resorcinol in a 1.54 mole ratio (F/R) under slightly alkaline conditions (Figure 2-1). This mole ratio provides a slight formaldehyde excess therefore ensuring the formation of a theoretically perfect network, where the functionalities of formaldehyde and resorcinol are respectively 2 and 3.

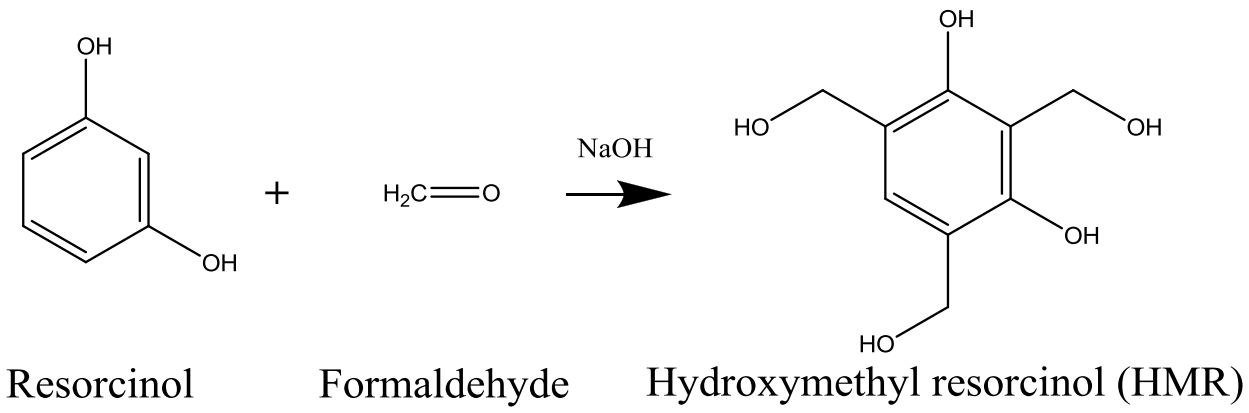

Figure 2-1. Chemical reaction for hydroxymethyl resorcinol.

The ingredients in Table 2-1 are reacted at room temperature for 3 to 8 hours before application to wood surfaces (Vick et al. 1998). This reaction time was deemed critical – if either too short or too long, the primer treatment could not enable the bonded system to meet the delamination test criterion (Vick et al. 1995). After the appropriate reaction time, the HMR solution is applied to the bonding surface and allowed to dry for approximately 24 hours, whereafter adhesive application and bonding occur.

Table 2-1. Ingredients for hydroxymethyl resorcinol synthesis.

Ingredient	% by weight	F/R mole ratio
Water, deionized	90.43	1.54
Formaldehyde, 37% (formalin)	3.79	
Resorcinol, crystalline	3.34	
Sodium Hydroxide, 3 molar	2.44	

2.1.2 Effects of Treatment

Besides epoxy adhesives, the HMR bond durability enhancement was also found for several other thermosetting wood adhesives, including emulsion polymer isocyanates (EPIs), polymeric methylenebis(phenylisocyanates) (pMDIs) (Christiansen and Conner 1995), and also one-part moisture-cure polyurethanes (Vick and Okkonen 2000).

Beyond promoting moisture durability, HMR treatment was also shown to improve adhesive bond test strengths. Follrich et al. (Follrich et al. 2007) found that HMR treatment doubled the tensile strength of polyurethane-bonded spruce end-grain joints. Most recently Kurt et al. (Kurt et al. 2008) found HMR to increase the tensile shear strength and percent wood failure of wax-treated specimens bonded with polyvinyl acetate (PVAc) and melamine formaldehyde (MF).

HMR has also been found to promote bonding of preservative-treated wood, a notoriously difficult substrate for adhesive bonding. Vick et al. (Vick et al. 1996a) found that HMR treatment significantly increased internal bond strength of flakeboards made with chromated copper arsenate (CCA)-treated wood flakes and a phenol-formaldehyde (PF) adhesive. However, the HMR treatment showed no effect on the mechanical properties of flakeboards made with preservative-free flakes (Vick et al. 1996a). Christiansen and Conner (Christiansen and Conner 1995) also found the HMR treatment to enhance the durability of epoxy, pMDI, EPI, and phenol resorcinol formaldehyde (PRF) bonds to CCA-treated lumber in the ASTM D 2559 delamination test.

The bond performance of alkaline copper quaternary-(ACQ) and copper azole-(CA-B) treated wood primed with a so-called novolak HMR (n-HMR, which will be described in more detail later) was also investigated. The n-HMR primer was found to reduce delamination of the PRF-bonded CA-B-treated southern yellow pine samples in the ASTM delamination test (Lorenz and Frihart 2006). The ACQ-treated samples did not pass the ASTM standard, even with n-HMR treatment (Lorenz and Frihart 2006). n-HMR was found to absorb slowly into some of the preservative-treated wood, and the researchers hypothesized this observation to be correlated to high delamination rates in testing (Lorenz and Frihart 2006).

HMR has clearly proven to enhance the bond durability of a variety of thermoset adhesives in wood-to-wood bonding. Fiber-reinforced polymers (FRPs) are another substrate of importance; they have been thoroughly researched in the field of laminated beam (glulam) reinforcement due to their light weight and high tensile strength properties (Dagher et al. 1996; Lopez-Anido et al. 2000). Glulam panels approximately 4' wide by 6" thick have recently been implemented in timber girder bridges (Wipf et al. 1999). Lopez-Anido et al. (Lopez-Anido et al. 2000) investigated the use of an E-glass /vinyl ester resin as a means of reinforcing eastern hemlock glulam panels. HMR was used to improve the durability of the wood/vinyl ester resin bond. The ASTM D 1101 (1997) cyclic delamination test was used to test the durability of the wood-FRP laminates (Lopez-Anido et al. 2000). The HMR treatment was found to promote strong, exterior-grade bonds between the wood and FRP. These bonds were comparable in strength and durability to PRF adhesive bonds; PRF adhesives are commonly considered as the most durable structural wood adhesives (Lopez-Anido et al. 2000).

Pirvu et al. (Pirvu et al. 2004) also examined vinyl ester bonds between FRPs and wood using HMR as a durability promoter. Southern yellow pine laminates treated with novolak HMR (n-HMR) and reinforced with carbon fiber/vinyl ester resin produced a durable composite (Pirvu et al. 2004). This result is consistent with the work of Lopez-Anido et al. (Lopez-Anido et al. 2000) mentioned above, expanding HMR's utility beyond FRP's and into unidirectional carbon fiber mats.

2.1.3 Recent Developments

While HMR is a remarkable wood primer, it has not enjoyed any significant industrial use because of a number of practical limitations. HMR has a critical reaction period of 3-8 hours; too short or too long of a reaction time renders the primer incapable of meeting the ASTM

delamination criterion (Vick et al. 1998). Once the treatment is applied, the user must wait 12-24 hours before bonding to allow for drying. Another limitation is economic feasibility; resorcinol is an expensive reagent. Efforts have been made to alleviate these problems in order to make HMR more suitable for use in industry.

In an effort to make HMR more industrially feasible, Christiansen et al. (Christiansen et al. 2000) created the so-called "novolak-HMR" (n-HMR). The primer begins as a stable novolak prepolymer, in which formaldehyde and resorcinol are mixed at low mole ratio (0.39 F:R); at this stage, storage life is essentially infinite (Christiansen et al. 2000). Prior to wood application, the mole ratio is increased to 1.54 (Christiansen et al. 2000). Once the additional formaldehyde is added, the n-HMR solution can be applied to the wood substrate immediately and up to 7 hours later (Christiansen et al. 2000). Weather durability tests using n-HMR treatment and an epoxy adhesive yielded similar results seen by Vick et al. (Vick et al. 1995). Note that the term "novolak-HMR" is somewhat of a misnomer; novolaks are acid-cured phenol-formaldehyde thermosets also prepared in two stages; final cure is achieved with a second addition of formaldehyde. Christiansen's use of the term novolak reflects the two-stage curing process, but n-HMR is prepared under alkaline conditions.

Christiansen and Okkonen (Christiansen and Okkonen 2003) later demonstrated that lowering the final F/R ratio (from 1.54 to 1.34) improved the delamination resistance. The n-HMR treatment could also be applied to wood up to 16 days prior to bonding without decreasing its effectiveness (Christiansen and Okkonen 2003). This finding could prove commercially useful, as wood manufacturing elements could be treated with HMR at one industrial site and subsequently bonded at another site.

Utilizing infrared heat lamps for fast curing of n-HMR, Eisenheld and Gardner (Eisenheld and Gardner 2005) found that an infrared drying time between 15 and 20 minutes dramatically improved the shear strength and percent wood failure in both dry and wet epoxy-bonded laminates. These results were compared to n-HMR-treated samples which were dried 24 hours in ambient conditions prior to bonding. No significant improvements in bond performance were observed when adjustments to solids content and spread rate were made (Eisenheld and Gardner 2005).

2.1.4 Theories on the HMR Mechanism

HMR has inspired much research in understanding exactly how it interacts with wood and/or the adhesive to enhance bondline durability. At the time of its discovery, HMR was postulated to react with the epoxy adhesive and the wood substrate, as for a true "coupling agent," the term first used to describe HMR. HMR hydroxymethyl groups were thought to condense with epoxy-resin hydroxyl groups to form ether linkages (Vick et al. 1995). The remaining hydroxymethyl groups were thought capable of forming ether linkages with the wood polymers. Hydrogen bonding was also believed to be possible if the hydroxyl-rich wood polymers were unavailable for cross-linking. It was postulated that a multimolecular layer of HMR adsorbed to the wood surface, allowing wood polymers to interact with the abundance of hydroxyl groups on the HMR molecules (Vick et al. 1995).

After Vick et al. patented HMR for use as a wood coupling agent in 1996 (Vick et al. 1996b), they investigated the reactivity of HMR as it affects the weather durability of epoxy bonds to douglas-fir (Vick et al. 1998). Important chemical characteristics of HMR were determined using gel permeation chromatography (GPC), differential scanning calorimetry (DSC), and ^{13}C nuclear magnetic resonance (NMR). Employing the ASTM D 2559

delamination test, HMR-treated samples were tested after a variety of HMR reaction times prior to bonding; the optimum time was determined to be between 3 and 8 hours (delamination was less than 5% only within this timeframe) (Vick et al. 1998). Through the use of GPC and NMR, an ideal molecular weight distribution was associated with this optimum reaction time; however the molecular weight distribution was only qualified, and not precisely quantified (Christiansen 2000; Vick et al. 1998). Between 3 and 8 hours reaction time, the HMR solution consists mostly of monomers, dimers, and trimers that are capable of penetrating the cell wall because their molecular weight is less than 1,000 g/mole (Christiansen 2000; Gardner et al. 2005; Vick et al. 1998). However, within this time frame a lower percentage of HMR exists as larger polymers with a molecular weight greater than 1000 g/mole (Vick et al. 1998). These higher polymers are thought incapable of penetrating the cell wall, perhaps suggesting that the mode of action involves more than HMR reactions within the wood cell wall.

Gardner et al. (Gardner et al. 2000) examined how HMR affects wood surface chemistry through contact angle analysis. HMR was shown to reduce the dispersive (non-polar) surface free energy, while increasing the polar surface free energy (Gardner et al. 2000). The HMR treatment was found to produce a higher contact angle and lower k-value (penetration and spreading constant) for both pMDI and PF adhesives, demonstrating a decrease in adhesive wettability. Conversely, water wettability increased; HMR treatment resulted in a lower contact angle and greater k-value (Gardner et al. 2000). Gardner et al. (Gardner et al. 2000) concluded that HMR bond enhancement could not be attributed to increased adhesive wettability, and stated that his results were consistent with the HMR mechanism postulated by Vick et al. (1995).

X-ray photoelectron spectroscopy (XPS) was employed by Tze and coworkers to gain insight into HMR's effect on wood surface chemistry. HMR was found to increase the

percentage of non-oxidized carbons on the wood surface (Tze et al. 2005), hence, HMR is present on the wood surface. Otherwise, no clear insights were gained about HMR's impact on surface chemistry.

Son and Gardner (Son and Gardner 2004) also investigated the effect of HMR on the dimensional stability and water uptake behavior of maple veneers. HMR treatment was found to reduce wood swelling, thereby improving the veneer's dimensional stability (Son and Gardner 2004). In a subsequent water uptake experiment, the HMR treatment outperformed a commercial water repellent treatment (Son and Gardner 2004).

While increased wood dimensional stability appeared to be a result of HMR treatment, a molecular explanation of the effect required further investigation. Christiansen (Christiansen 2005) examined this by studying the chemical and mechanical aspects of HMR in relationship to wood bonding. To study the impact of HMR crosslinking, a varying amount of resorcinol was replaced with 2-methylresorcinol (Christiansen 2005). Using high pressure liquid chromatography, Christiansen found resorcinol to react more quickly with formaldehyde compared to 2-methylresorcinol, at slightly alkaline conditions (pH = 8). After 40 minutes of reaction time, the rate of consumption, on a per site basis, had equalized; after this point, the two resorcinolic monomers were believed to be incorporating at equal molar ratios (Christiansen 2005). The replacement of resorcinol with 2-methylresorcinol was therefore theorized to reduce HMR crosslink density: resorcinol has a functionality of 3, enabling network formation, while 2-methylresorcinol can only extend existing chains since its functionality is 2 (Figure 2-2). This decrease in reactivity with formaldehyde due to the presence of an alkyl group at the *ortho* position is in agreement with previous work which found that, for phenolic compounds, an alkyl group *ortho*- or *para*- to the hydroxyl group dramatically lowered its reactivity; alternatively, an

alkyl group placed *meta*- to the hydroxyl group substantially increased the phenolic molecule's reactivity with formaldehyde (Sprung 1941).

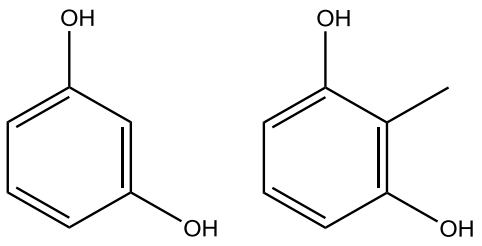

Figure 2-2. Left: Resorcinol. Right: 2-methylresorcinol.

At 30% resorcinol replacement, the delamination resistance of epoxy-wood bonds was enhanced compared to unprimed wood, but ultimately failed the ASTM D 2559 delamination criterion (Figure 2-3). Christiansen therefore demonstrated that the HMR mechanism of action depends upon some minimum level of crosslinking the HMR network.

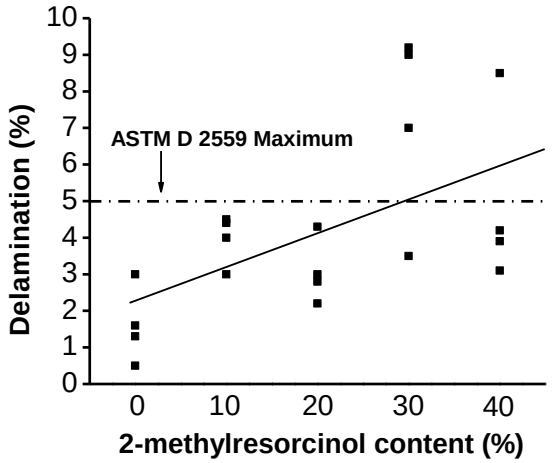

Figure 2-3. Effect of 2-methylresorcinol substitution for resorcinol in HMR primer on delamination resistance (adapted from (Christiansen 2005)).

Furthering this study, Christiansen imposed thermal treatments that would hinder any potential HMR/adhesive chemical reactions (Christiansen 2005). Prior to adhesive application, Christiansen exposed HMR-primed substrates to a variety of thermal treatments that would promote HMR crosslinking and thereby reduce its ability to react with the adhesive. The resulting epoxy-wood bonds still passed the ASTM D 2559 delamination test. This suggested that the priming mechanism was not dependent on HMR reaction with the adhesive, and that reaction with the wood cell wall was required (Christiansen 2005).

In an effort to view the effects of HMR on the mobility of *in situ* wood polymers, Son et al. (Son et al. 2005) investigated the thermal behavior of HMR-treated maple veneers. Dynamic Mechanical Thermal Analysis (DMTA) results found no evidence of HMR-induced wood reinforcement, as measured through stiffness changes (Son et al. 2005). The authors claimed that HMR reduced the temperature of what was identified as a glass transition in wood having a moisture content of 7%; the transition temperature was reported to have been reduced from 56.9°C to 42.2°C. The authors postulated that this change would provide a toughening mechanism that explains the improved durability. However, it is well known that glass transitions in 7% moisture-content wood occur at temperatures above 150°C (Back and Salmen 1982). So while the observations of Son et al. (Son et al. 2005) may have been accurate, their interpretation of HMR's impact on the wood glass transition is in question.

Son et al. (Son et al. 2005) also calculated the solubility parameters of HMR and the primary lignocellulosic polymers of wood (cellulose, hemicellulose, and lignin) in an effort to predict which wood polymers interact with HMR. Lignin and HMR were found to have very similar solubility parameters, and were thus postulated as most likely capable of interaction.

Sun and Frazier (Sun and Frazier 2005) used isothermal stress relaxation to study HMR-treated samples. HMR was found to effectively stiffen yellow-poplar samples against stress relaxation, showing the greatest impact at 25°C (Sun and Frazier 2005). The stiffening effect was likely caused by chemical crosslinking within the wood cell wall, most likely with hemicellulose and lignin. This finding contradicts the work of Son et al. (Son et al. 2005) mentioned previously, who found no stiffness enhancement due to HMR treatment. It was also suggested that HMR does not act through a simple bulking effect, where chemical treatments occupy wood-polymer free volume and adsorption sites. To examine this, Sun and Frazier (Sun and Frazier 2005) tested specimens impregnated to 5% by dry weight with phenol, a compound known for preferential adsorption to wood (Sun and Frazier 2005). Phenol treatment had little or no effect on wood stress relaxation. This further suggested chemical crosslinking in the wood cell wall was related to HMR's effectiveness as a wood adhesion primer.

While clearly much research has been conducted on the topic, the effect of HMR treatment on wood and its resulting bond performance is still not fully understood. This research attempts to elucidate its impact by further investigating the effects of hydroxymethyl resorcinol and its derivatives on red oak. Dynamic mechanical analysis was used to study the molecular impact on the cell wall polymers, while mode-I fracture was used to examine the corresponding bond performance due to these primer treatments. A commercial moisture cure polyurethane adhesive was used in the preparation of fracture specimens. What follows is a brief review of polyurethane adhesives, and also some of the analytical procedures that are used in this research.

2.2 Analytical Methods

2.2.1 Polyurethane Adhesive Analysis

2.2.1.1 Polyurethane History

Polyurethanes were first developed by Dr. Otto Bayer at Germany's I.G. Farben-industrie in 1937 (Rogers and Long 2003). By the 1950's, polyurethanes were being produced on a large scale, and were being implemented into the coatings and adhesives industry via use in seating, bedding, and carpeting manufacture (Rogers and Long 2003). Since then, polyurethane adhesives have expanded their use to a number of applications (shoe assembly, composite wood, automotive interiors, etc.) because of their versatility and ability to produce strong adhesive bonds (Rogers and Long 2003).

2.2.1.2 Types of Polyurethane Adhesives

A polyurethane is a material that results from reaction between isocyanates and hydroxyl functional compounds such as alcohols and phenols. Polyurethane adhesives are generally either two-component or one-component systems. Two-component adhesives use either a polyol/polyisocyanate combination or an isocyanate-terminated prepolymer with a low molar weight diol, triol, or diamine curative (Sebenik and Krajnc 2007).

One-component systems are based on low isocyanate content prepolymers, and are also known as moisture-cure polyurethane (MCPU) adhesives. These systems utilize available moisture to form highly crosslinked bonds. As a result of chemical crosslinking, both one- and two-component polyurethane adhesives exhibit good thermal stability compared to non-reactive, solvent- or water-borne polyurethane adhesives (Randall and Lee 2002). MCPU adhesives have several clear benefits compared to two-component systems: they are manufactured in one

package for ease of use; they do not require special mixing equipment; they have a longer pot-life, as long as the adhesive is protected from exposure to moisture; and they release less volatile organic compounds (VOCs) due to reaction with only available moisture (Randall and Lee 2002; Rath et al. 2008; Szycher 1999).

While not technically moisture-cure polyurethane adhesives, moisture-cured isocyanate-based resins have established themselves in the wood-based composites industry due to their ability to rapidly penetrate and bond to most types of wood, their excellent resistance to hydrolysis, and their very low VOC release (Randall and Lee 2002). Polymeric methylenebis(phenylisocyanate) (pMDI) is one such resin which is used in production of smaller particle composites such as medium density fiberboard and oriented strandboard; pMDI is also a common precursor to MCPU adhesives. MCPU adhesives are used in composites which utilize larger wood members, such as laminated veneer lumber and glulam. These formulated resins are used in place of pMDI resins due to their improved resistance to creep, as well as good gap filling properties (Randall and Lee 2002). Comparable advantages of PUR adhesives over more traditional formaldehyde-based adhesives include having shorter cure times without additional thermal acceleration or pressing, and being formaldehyde-free (Meier-Westhues 2007).

In this research, a commercial moisture-cure polyurethane adhesive was used.

2.2.1.3 Concentric Cylinder Viscometry

The narrow-gap concentric cylinder geometry is ideal for measuring the viscosity of non-newtonian fluids; it allows for a uniform shear rate almost everywhere in the flowing liquid due to the narrowness of the gap (Barnes 2000). It is often used for measuring the steady shear viscosity and dynamic mechanical properties of low-viscosity fluids, polymer solutions, solid-in-liquid suspensions, and emulsions (Gupta 2000). The liquid sample is simply loaded between

two concentric cylinders (see Figure 2-4), and the inner cylinder rotates with a given number of rotations per minute (Swarbick 2004). Due to the viscous nature of the liquid, a torque is produced which is proportional to the shear stress applied (Swarbick 2004). The shear rate on the sample can be calculated as:

$$\dot{\gamma} = \frac{a_2 \omega}{a_2 - a_1} \qquad \text{[Equation 2-1]}$$

where a_2 and a_1 correspond to the radii of the outer and inner cylinders, respectively, and ω represents the rotation rate. The shear stress in the sample depends on the torque (T), or couple, and the immersed length (H) of the inner cylinder (Swarbick 2004):

$$\sigma = \frac{T}{2\pi a_2^2 H} \qquad \text{[Equation 2-2]}$$

Combining equations 2-1 and 2-2, the viscosity can be calculated as:

$$\eta = \frac{T(a_2 - a_1)}{2\pi a_2^3 \omega H} \qquad \text{[Equation 2-3]}$$

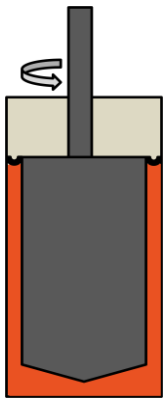

Figure 2-4. Schematic diagram of concentric cylinder geometry.

Compared to the cone and plate geometry, which is perhaps more common, the concentric cylinder geometry is advantageous because it is easier to operate, and it can tolerate

larger particles (Barnes 2000). However, the concentric cylinder geometry requires a greater specimen volume than does the cone and plate system.

2.2.1.4 Determination of Isocyanate Content

The isocyanate (NCO) content of a moisture-cure polyurethane adhesive is defined as the weight percent of the NCO groups present. NCO content is a critical property of polyurethane adhesives because it reveals the potential adhesive reactivity, and it allows one to monitor adhesive changes that may occur from reaction with ambient moisture.

Method C of the ASTM D 5155 (2007) standard was used for determining the isocyanate content of the MCPU used in this research. In this standard an isocyanate sample is reacted with an excess of dibutylamine to form the corresponding urea. The isocyanate content is then determined from the amount of dibutylamine consumed in this reaction.

2.2.1.5 Nuclear Magnetic Resonance

Solution-state nuclear magnetic resonance (NMR) spectroscopy is a very useful technique for revealing the molecular structure of organic compounds (Balci 2005). This technique is based on the magnetic nuclear spin of certain isotopes (^{13}C, ^{1}H, ^{15}N, etc.). A variety of magnetic nuclei may be used (^{13}C, ^{1}H, ^{15}N, etc.) depending upon the information required. Carbon-13 (^{13}C) NMR is particularly useful for the structural analysis of polyurethane adhesives. For instance, if one was interested in determining the number and position of carbon atoms in a sample solution, ^{13}C NMR may be used (Balci 2005). ^{13}C NMR was employed to probe the molecular structure of the commercial moisture cure polyurethane adhesive used in this research, as well as to track substantial changes in its chemistry over time.

2.2.2 Dynamic Mechanical Analysis

Dynamic Mechanical Analysis (DMA) has become an increasingly common tool in the laboratory for analyzing the material properties of polymers. This method measures a polymer material's response to an oscillatory force. The applied force is a sinusoidal stress (σ) and the material's response is in the form of a sinusoidal strain (ε) (Menard 1999). By analyzing the deformation of the sample, as well as the phase lag between the applied sinusoidal stress and resulting strain waves, material properties such as modulus, damping, and viscosity can be calculated (Menard 1999). By increasing the temperature while simultaneously applying stress, one can probe the thermomechanical behavior of the material. The impact of frequency and shear rate on the sample can be investigated in a similar manner (Menard 1999).

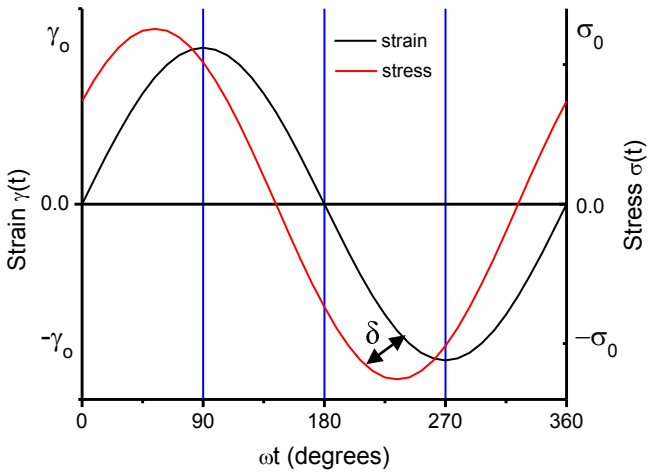

Figure 2-5. Association of applied stress, resulting strain, and phase lag in DMA.

Using the material's response to the stress sine wave one can calculate three particular material properties that are important to this research: the storage modulus(E'), loss modulus (E"), and tan δ (Mark et al. 2002). To calculate these values one must understand that at any one point on the stress curve, the stress applied is calculated as:

$$\sigma = \sigma_0 \sin\omega t$$ [Equation 2-4]

where σ is the stress at time t, σ_0 is the maximum stress at the peak of the sinusoidal curve, ω is the frequency of oscillation, and t is time. The resulting strain at any one point can then be defined as:

$$\varepsilon = \varepsilon_0 \sin(\omega t + \delta)$$ [Equation 2-5]

where ε is the strain at time t, ε_0 is the maximum strain, ω is the frequency of oscillation, t is time, and δ is the phase lag that occurs between the applied sinusoidal stress and resulting strain curve (see Figure 2-5) (Ward and Sweeney 2004).

DMA does not simply produce E' and E" using this data, however. It yields a complex modulus, which can be broken down into two components: a component that is in phase with the strain (elastic modulus), and one that is 90° out of phase with the strain (loss modulus) (Ward and Sweeney 2004). The stress-strain relationship is therefore defined by E', which is in phase with the strain, and E", which is 90° out of phase with the strain:

$$\sigma = \varepsilon_0 E' sin\omega t + \varepsilon_0 E" cos\omega t$$ [Equation 2-6]

where

$$E' = \frac{\sigma_0}{\varepsilon_0 cos\delta}$$ [Equation 2-7] and $$E'' = \frac{\sigma_0}{\varepsilon_0 sin\delta}$$ [Equation 2-8]

Figure 2-6 represents how equations 2-7 and 2-8 combine to produce a complex modulus, E* (Equation 2-9). If $\sigma = \sigma_0 \exp(i\omega t)$, then $\varepsilon = \varepsilon_0 \exp[i(\omega t+\delta)]$, so that:

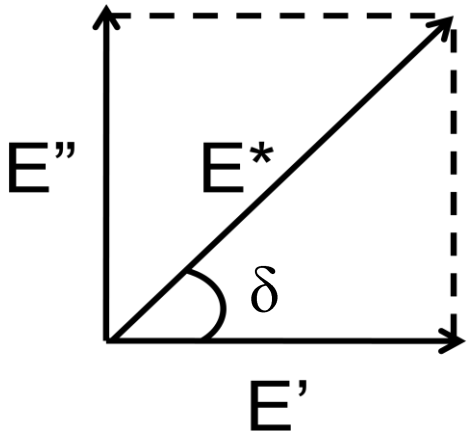

Figure 2-6. Complex modulus E* = E’ + E” and phase lag tan δ = E”/E’

$$E* = \frac{\sigma}{\varepsilon} = \frac{\sigma_0}{\varepsilon_0 exp(i\delta)}$$

$$E* = \frac{\sigma_0}{\varepsilon_0(cos\delta + isin\delta)}$$

$$E* = E' + E'' \qquad \text{[Equation 2-9]}$$

where E’ defines the storage modulus, which represents the amount of energy stored in the sample due to applied stress, and E” defines the loss modulus, or the amount of energy dissipated from the sample. Tanδ represents the ability of the material to dissipate energy, and is simply the ratio of E” to E’. The term δ represents the phase lag between the stress and strain sine waves, and for viscoelastic materials it is between 0°-90° (completely elastic and inelastic materials have phase angles of 0° and 90°, respectively) (Ward and Sweeney 2004). Tanδ is calculated using the following simple equation:

$$Tan\delta = \frac{E''}{E'} \qquad \text{[Equation 2-10]}$$

It is important to note that the complex modulus calculated in equation 2-9 assumes that the sample is tested within the linear viscoealastic response (LVR) region, where the resultant strain sine wave is the same frequency as the applied stress sine wave (Cowie 1991). In other words, the viscoelastic properties observed in this region are independent of imposed stress (Rubinstein and Colby 2003). This ensures that any observations depict the relationship between molecular structure and viscoelastic behavior, and are not due to stress-dependent structural deformation. In light of this, all DMA tests performed in this research were conducted within the specimen LVR region.

2.2.2.1 Applications of DMA

DMA is a very common tool for measuring polymer thermal transitions. Its greater sensitivity often reveals transitions undetectable by other means, such as differential scanning calorimetry or thermomechanical analysis. By testing over a range of temperatures at a fixed frequency it is possible to investigate the relaxation processes of a polymer (Menard 2008).

In this research, a primary softening relaxation known as the glass transition is of major importance. This temperature (T_g) is characteristic of a polymer where within a narrow range of temperature, significant changes in physical properties such as hardness, stiffness, and volume are observed; it marks the transition of the material from a hard, glassy state to a rubbery state (Menard 2008). Several testing parameters can impact the T_g, including the applied stress/strain, heating rate, and frequency used.

A number of inherent polymer properties influence a polymer's T_g as well, including chain flexibility, molecular structure (steric effects), molar mass, branching, and crosslinking (Cowie 1991). The flexibility of a chain reflects its ability to rotate about constituent chain

bonds; flexible chains exhibit a low T_g. The insertion of specific chemical groups, for instance poly(p-phenylene), can effectively stiffen a polymer chain by impeding rotation, thereby raising its T_g (Cowie 1991). Additionally, a plasticizer may be added to a polymer to increase its free volume, causing polymer chains to flow at lower temperatures (Wilkes et al. 2005). Of particular importance to this research is the impact of crosslinking on the glass transition temperature. Crosslinking in a polymer increases its density and decreases free volume, thereby restricting molecular motion and raising the T_g (Cowie 1991).

The T_g of a polymer tested in DMA is commonly identified as the temperature at the peak of its tan δ curve (Menard 2008). Tan δ, or the loss tangent, is a measure of the ratio of energy lost to energy stored during a sinusoidal oscillation (Equation 2-10). The loss tangent determines several macroscopic properties including the damping of free vibrations, the attenuation of propagated waves, and the frequency width of a resonance response (Ferry 1980).

2.2.2.2 Wood DMA

DMA has been used to probe the organization and properties of *in situ* wood polymers since the early 1960's. Norimoto and Yamada (Norimoto and Yamada 1966) and Becker and Noack (Becker and Noack 1968) were the first to do so, using the torsional pendulum apparatus to investigate the viscoelastic response of wood. Becker and Noack discovered an inherent relationship between the moisture content of beech wood and its temperature at maximum damping (T_g). As moisture content increased from 0% to fiber saturation, the T_g dropped significantly (~140°C-78°C).

In 1982, Back and Salmen (Back and Salmen 1982) argued that the T_g of wood polymers occur at rather high temperatures (cellulose 200°C-250°C, hemicelluloses 140°C-220°C, and lignin

~205°C) where thermal degradation is occurring. This obstructed visualization of individual wood polymer softening temperatures when they are heated *in situ* in DMA. In an effort to resolve these transitions, Salmen (Salmen 1984) tested spruce wood in water-saturated conditions. The wood T_g was found to drastically reduce from ~200°C in dry wood to 70°C-100°C, depending on frequency. This T_g was believed to be that of lignin; Olsson and Salmen (Olsson and Salmen 1997) concluded that this high temperature transition viewed in water-swelled wood changed significantly depending on the wood specimen lignin composition. This implied that the T_g viewed by Becker and Noack (Becker and Noack 1968) in 1968 was that of lignin.

Kelley et al. (Kelley et al. 1987) later studied the viscoelastic properties of wood at varied moisture contents and a wide temperature range (-150°C to 150°C). They observed two distinct transitions which they attributed to the glass transitions of lignin and hemicellulose. This pointed to the existence of a phase-separated morphology of the amorphous polymers in the cell wall; however since the authors did not employ moisture control, their measurements could have been complicated by mechano-sorption effects. They further examined the plasticization effect of water and other diluents on wood, observing depressed T_g values as diluent content increased. These plasticizer effects were found to fit the Kwei model used for predicting glass transition temperatures.

Sadoh (Sadoh 1981) used DMA to study the impact of a variety of plasticizers on wood polymer properties. He found formamide plasticization to drastically reduce the lignin T_g (~48°C), while glycol plasticization resulted in T_g values similar to that observed in water-plasticized wood (~100°C). Ishimaru et al. (Ishimaru et al. 2001) investigated a variety of organic liquids, including glycols, diols, and cellosolves for use as wood plasticizers. Liquids

with a molar volume larger than 100 ml/mol were found to exceed the swelling induced by water; it had previously been thought that liquids of this molar volume could not swell wood. Softening temperatures between 40°C-60°C were observed in several of the organic liquids.

Sugiyama and Norimoto (Sugiyama and Norimoto 1998) investigated the effect of chemical treatments on the viscoelastic properties of wood. A chemical treatment of polyethylene glycol (PEG) with a molecular weight of 1,000 was found to plasticize the cell wall polymer matrix, suggesting large molecules of this order were capable of penetrating the cell wall.

Marcinko et al. (Marcinko et al. 1998; Marcinko et al. 1999) used DMA to investigate the impact of pMDI and UF adhesives on the molecular properties of *in situ* cell wall polymers. The pMDI coating was found to penetrate into wood and intimately associate with the cell wall polymers; it resulted in a broader tan δ peak and a depression of the lignin T_g.

Olsson and Salmen (Salmen and Olsson 1998) utilized controlled isothermal humidity scans to determine how hemicelluloses (xylan and glucomannan) are oriented in the cell wall polymer matrix. By testing isolated xylan, delignified wood, and native wood, the researchers suggested that xylan is likely closely associated with lignin while glucomannan is more associated with cellulose (Salmen and Olsson 1998).

The natural anisotropy of wood has been shown to reveal itself through grain orientation effects in DMA. Salmen (Salmen 1984) showed a T_g dependence on fiber orientation (along grain vs. across grain) in spruce wood. Backman and Lindberg (Backman and Lindberg 2001) expanded this effect to include T_g and modulus differences between the radial and tangential direction of scots pine tested in tension. The elastic modulus was found to be much lower in

tangential than the radial direction, with the radial direction being almost twice as stiff (Backman and Lindberg 2001).

Laborie et al. (Laborie et al. 2004) used cooperativity analysis to investigate the *in situ* lignin glass transition of ethylene glycol-swelled wood. Cooperativity analysis was validated as a way of characterizing *in situ* lignin softening temperatures of softwood and hardwood species, and as a novel tool for probing molecular changes in wood due to physical or chemical treatment.

Sun et al. (Sun et al. 2007) recently conducted DMA of dry wood to investigate its linear viscoelastic region (LVR) response, as well as the effects of minor moisture content changes. It was observed that the LVR of dried wood was a function of grain orientation and temperature. The effects of small moisture content changes below 1% MC were found to primarily impact the low-temperature secondary relaxations.

Most recently Jiang and Lu (Jiang and Lu 2009) investigated all three grain orientations (radial, tangential, and longitudinal) in two different modes of testing (tension and bending) and with different thermal treatments. The researchers concluded stiffness to be greatest in the longitudinal and lowest in the tangential direction; tension test specimens produced higher modulus values than bending; and a heat pretreatment increased the modulus and decreased damping while a freeze pretreatment decreased modulus and increased damping (Jiang and Lu 2009).

2.2.3 Mode-I Fracture

2.2.3.1 Introduction

Three independent fracture modes exist for all materials (see Figure 2-7): open/cleaveage (I), forward shear (II), and transverse shear (III). Failure generally occurs at the lowest energy in Mode-I fracture, making this the critical fracture mode (Scoville 2001; Yoshihara and Kawamura 2006). Mode-I fracture testing is primarily conducted using dual cantilever beam (DCB) specimens. DCBs are rectangular specimens of uniform thickness, with a crack initiated on the end to be loaded (Yoshihara and Kawamura 2006). Pinholes located on the upper and lower cantilever in the DCB specimen (see Figure 2-8) allow it to be loaded through application of a crosshead displacement rate (mm/min). This displacement input from the test frame results in a tensile load; at peak load, the initiated crack begins to extend and the compliance increases. Using the following equations one can calculate the fracture toughness of the material (Boeman et al. 1999; Gagliano and Frazier 2001):

$$G_{Ic} = \frac{P_c^2}{2b}\frac{dC}{da} \qquad \text{[Equation 2-11]} \qquad G_{Ia} = \frac{P_a^2}{2b}\frac{dC}{da} \qquad \text{[Equation 2-12]}$$

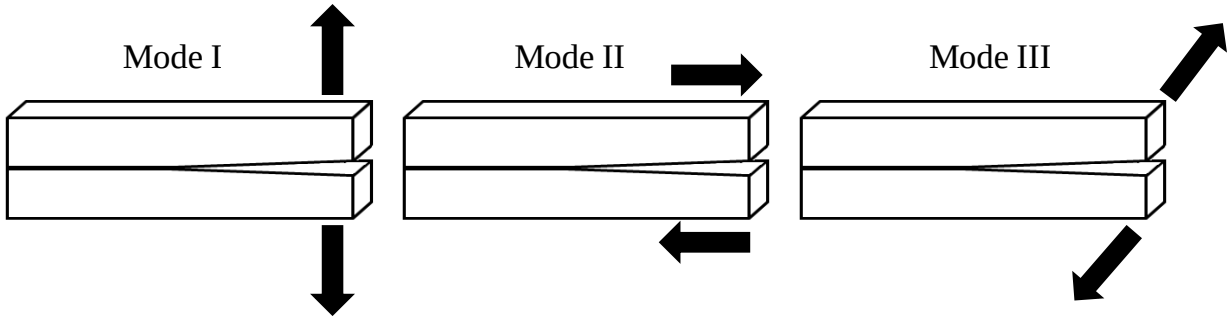

Figure 2-7. Modes of fracture: opening/cleavage (I), forward shear (II), and transverse shear (III).

where G_{Ic} is the critical fracture energy, or the energy required to initiate crack propagation; G_{Ia} is the arrest fracture energy, or the energy required to stop crack propagation; P_c is the critical load required to extend crack; P_a is the load after quasi-stabilization; dC/da is the change in compliance (C) over the change in crack length (a); and b is the width of the DCB specimen.

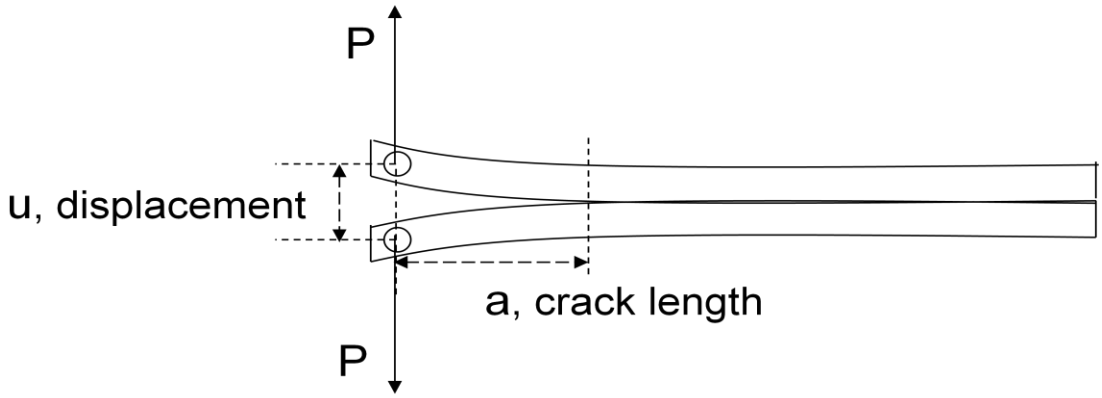

Figure 2-8. Mode-I fracture test and DCB specimen.

Compliance, or simply the reciprocal of slope of the load vs. displacement curve, can be calculated as (Gagliano and Frazier 2001):

$$\boldsymbol{C = \frac{2a^3}{3EI}} \qquad \text{[Equation 2-13]}$$

Where E represents the flexural modulus of the cantilever beams, and I is the moment of inertia of one of these cantilevers. Rewriting this equation in a form which is useful for calculating the fracture energies:

$$\boldsymbol{\frac{dC}{da} = \frac{2a^2}{EI}} \qquad \text{[Equation 2-14]}$$

Combining equation 2-14 with equations 2-11 and 2-12:

$$G_{Ic} = \frac{P_c^2 a^2}{bEI}$$ [Equation 2-15] $$G_{Ia} = \frac{P_a^2 a^2}{bEI}$$ [Equation 2-16]

The low shear moduli of substrates such as fiber-composites and wood can result in rotations and deflections at the crack tip which are ignored using simple beam analysis (Blackman et al. 1991; Hashemi et al. 1990). Therefore, a shear corrected compliance method was developed; the fracture toughness equation corrected for shear effects is shown below:

$$G_{Ic} = \frac{Pc^2(a+x)^2}{b(EI)_{eff}}$$ [Equation 2-17] $$G_{Ia} = \frac{Pa^2(a+x)^2}{b(EI)_{eff}}$$ [Equation 2-18]

where $(EI)_{eff}$ represents the effective flexural rigidity of the DCB specimen, and x is the shear correction factor. These variables are derived from the slope (m) and y-intercept (b) of the measured compliance ($C^{1/3}$) versus crack length (a) curve. An example plot is shown below in Figure 2-9, where m = 0.293 and b = 0.004.

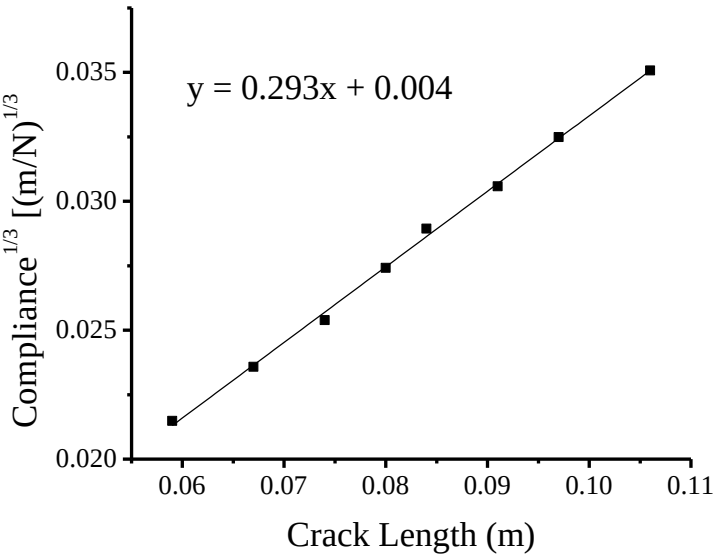

Figure 2-9. Example of measured compliance ($C^{1/3}$) vs. crack length (a) plot.

To calculate $(EI)_{eff}$ the following equation is used:

$$(EI)_{eff} = \frac{2}{3m^3}$$ [Equation 2-19]

The shear correction factor x can be measured experimentally by simply identifying the x-intercept of the measured compliance versus crack length plot (Blackman et al. 1991). It represents the crack length offset, and can be derived mathematically by dividing the y-intercept of the linear fit line in the compliance plot by the slope (Gagliano and Frazier 2001):

$$x = \frac{b}{m}$$ [Equation 2-20]

2.2.3.2 Mode-I Fracture in Wood Composite Applications

One of the most important mechanical properties of any composite is its resistance to delamination (Hashemi et al. 1990). Mode-I fracture can be used to measure the toughness of a composite bondline, which is a very good representation of its delamination resistance. Because adhesive bondlines are integral to all wood composite products, this method has been thoroughly researched using wood as the primary substrate.

Ebewele, River, Koutsky, and Mijovic have extensively studied bonded wood in mode-I fracture using a contoured dual cantilever beam (CDCB) specimen. In these works Ebewele et al. and Mijovic studied composite variables such as: bondline thickness (Ebewele et al. 1979); wood grain angle (Ebewele et al. 1979; Mijovic and Koutsky 1979), surface roughness ; surface aging (Ebewele et al. 1980); resin constitution (Ebewele et al. 1982); and phenolic adhesive chemistry (Ebewele et al. 1986) on fracture toughness. These studies clearly show fracture testing to be sensitive to adhesive and adhesive bondline properties.

The CDCB specimen (see Figure 2-10 adapted from (Ebewele et al. 1979)) used by Ebewele and his colleagues was adapted from ASTM D 3433 (1993), a method for fracture testing adhesively bonded metal joints. A primary benefit of the CDCB over the previously-used

uniform dual cantilever beam (UDCB) geometry is that by carefully contouring the loading-end of the beam to ensures that compliance changes linearly with crack length, the testing procedure is simplified (Ebewele et al. 1979). When dC/da is held constant, measuring crack propagation is not necessary; fracture toughness can be measured simply by measuring the critical and arrest load (refer to equations 2-11 and 2-12). While this geometry indeed simplified the test, preparation of the specimens was both laborious and time-consuming.

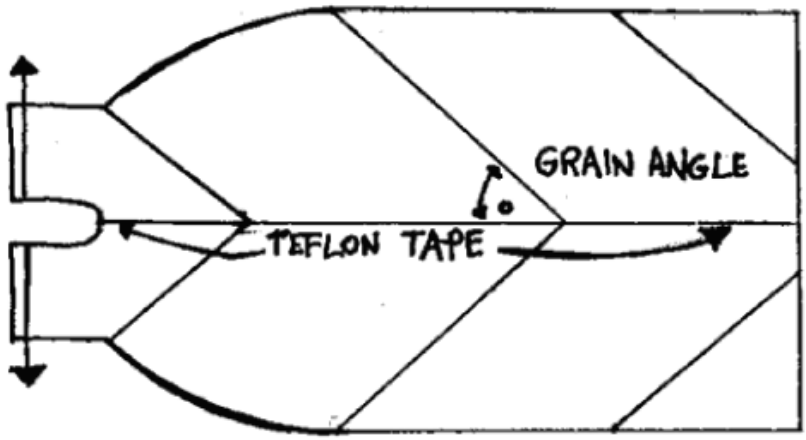

Figure 2-10. Solid wood CDCB geometry, adapted from (Ebewele et al. 1979).

In 1989, River et al. (River et al. 1989) introduced a new fracture geometry by adhesively bonding a solid wood laminate to aluminum contoured beams; this design was further investigated by Scott et al. (Scott et al. 1992) in 1992. It was found that accurate bond toughness measurements could be made for thin wood specimens as long as necessary conditions were met: the contoured metal beams must be calibrated so that dC/da is known, and wood lamina properties (species, grain angle, width, and height) must also be known (Scott et al. 1992). This geometry was simpler: flat wood laminates could be used instead of contoured; recording crack length was unnecessary as long as contoured metal beams were calibrated; and the contoured aluminum backings could be reused. There were several disadvantages of this aluminum-wood

specimen, however. It was found to yield less data than solid wood CDCBs due to crack length-compliance uniformity in only the first 90 mm of the beam; after allowing for nontypical behavior at the start of the crack, data was only retrievable from 40-50 mm of the bondline (River and Okkonen 1993). The specimen preparation was still time-consuming, as the aluminum beams needed to be etched prior to bonding with the wood laminate, and needed to be cleared of wood after each test.

In 1993, River and Okkonen introduced a fracture geometry which utilized oriented strandboard (OSB) instead of aluminum for the contoured beam backing. The contoured OSB beams could be manufactured very simply, did not require special etching for bonding, and could potentially hold dC/da uniform for a longer portion of the bondline by adjusting the taper (River and Okkonen 1993). By experimenting with a concave contour, River and Okkonen increased compliance-crack length uniformity up to the first 200 mm of the beam, essentially doubling the useful data range.

This tapered dual cantilever beam method was subsequently validated by Davalos et al. (Davalos et al. 1997) in 1997; laminated strand lumber (LSL) was used as the DCB backing to investigate the fracture of hybrid materials in mode-I fracture. But this composite CDCB specimen geometry was still demanding: calibration of the composite backing, intricate specimen preparation, and careful wood selection were still required.

In 2001, Gagliano and Frazier (Gagliano and Frazier 2001) presented an improved method for testing the flat wood DCB specimen geometry (see Figure 2-11). This specimen was previously regarded as inefficient and difficult to use because the compliance-crack length relationship was not uniform across the beam, meaning crack lengths needed be measured at the

critical load as the crack propagated. However, Gagliano and Frazier utilized improvements in optical technology to very accurately and simply visualize this crack extension.

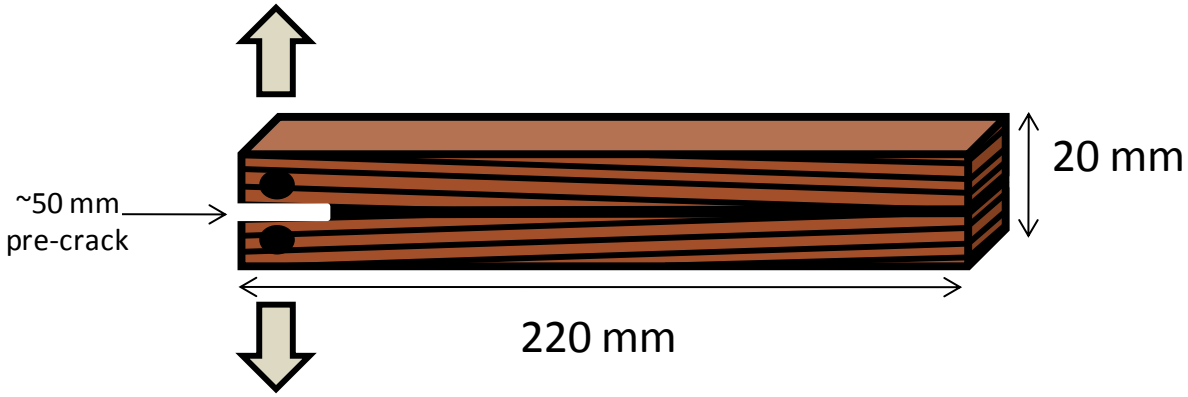

Figure 2-11. Flat DCB geometry.

Toughness measurements were also improved by utilizing a shear correction factor (x) developed by Hashemi et al. (Hashemi et al. 1990) to compensate for substrates with low shear moduli such as fiber-polymer composites and wood (for application and computation of this factor see equations 2-17 and 2-20). These improvements, coupled with the flat DCB's simple sample preparation, made mode-I fracture testing of adhesively-bonded wood more accessible to industrial applications.

2.3 References

Rheology solutions: determining the linear viscoelastic region in polymers. TA Instruments, New Castle, DE. RS-23

D 3433-93 (1993) Standard test method for fracture strength in cleavage of adhesives in bonded metal joints. ASTM International, West Conshohocken, PA. 15.06

D 1101-97a (1997) Standard test methods for integrity of glue joints in structural laminated wood products for exterior use. ASTM International, West Conshohocken, PA. 15.06

D 2559-04 (2004) Standard specification for adhesives for structural laminated wood products for use under exterior (wet use) exposure conditions. ASTM International, West Conshohocken, PA. 15.06

D 5155-07 (2007) Standard test methods for polyurethane raw materials: determination of the isocyanate content of aromatic isocyanates. ASTM International, West Conshohocken, PA. 8.03

Back, E. L. and L. Salmen. (1982) Glass Transitions of Wood Components Hold Implications for Molding and Pulping Processes. *Tappi*, 65, 107-110.

Backman, A. C. and K. A. H. Lindberg. (2001) Differences in wood material responses for radial and tangential direction as measured by dynamic mechanical thermal analysis. *J. Mater. Sci.,* J. Mater. Sci. 36, 3777-3783.

Balci, M. Basic 1H-13C-NMR Spectroscopy. Elsevier B.V., Amsterdam, The Netherlands,2005

Barnes, H. A. A Handbook of Elementary Rheology. University of Wales Institute of Non-Newtonian Fluid Mechanics, Wales,2000

Becker, H. and D. Noack. (1968) Studies on the dynamic torsional viscoelasticity of wood. *Wood Science and Technology*, 2, 213-230.

Blackman, B., J. P. Dear, A. J. Kinloch and S. Osiyemi. (1991) The calculation of adhesive fracture energies from double-cantilever beam test specimens. *Journal of Materials Science Letters,* 10, 253-256.

Boeman, R. G., D. Erdman, L. Klett and R. Lomax. 1999: A practical test method for mode I fracture toughness of adhesive joints with dissimilar substrates. In Energy, D. o., editor, Oak Ridge, TN.

Christiansen, A. W. (2000) Resorcinol-formaldehyde reactions in dilute solution observed by carbon-13 NMR spectroscopy. *Journal of Applied Polymer Science,* 75, 1760-1768.

Christiansen, A. W. (2005) Chemical and mechanical aspects of HMR primer in relationship to wood bonding. *For. Prod. J.,* 55, 73-78.

Christiansen, A. W. and A. H. Conner. (1995) Hydroxymethylated resorcinol coupling agent for enhanced adhesion of epoxy and other thermosetting adhesives to wood. *Proceedings of a symposium sponsored by USDA Forest Service Forest Products Laboratory and The Forest Products Society,* Proceedings no. 7296, 47-55.

Christiansen, A. W. and E. A. Okkonen. (2003) Improvements to hydroxymethylated resorcinol coupling agent for durable bonding to wood. *For. Prod. J.,* 53, 81-84.

Christiansen, A. W., C. B. Vick and E. A. Okkonen. 2000: A Novolak-based hydroxymethylated resorcinol coupling agent for wood bonding. *Wood Adhesives 2000,* Lake Tahoe, NV, 245-250.

Cowie, J. M. G. Polymers: chemistry and physics of modern materials. Chapman and Hall, New York,1991

Dagher, H. J., T. E. Kimball, S. M. Shaler and B. Abdel-Magid. 1996: Effect of FRP reinforcement on low grade eastern hemlock glulams. *National conference on wood transportation structures,* Madison, WI, 207-214.

Davalos, J. F., P. Madabhusi-Raman and P. Qiao. (1997) Characterization of mode-I fracture of hybrid material interface bonds by contoured DCB specimens. *Engineered Fracture Mechanics,* 58, 173-192.

Ebewele, R., B. H. River and J. A. Koutsky. (1979) Tapered double cantilever beam fracture tests of phenolic-wood adhesive joints. Part 1. Development of specimen geometry; effects of bondline thickness, wood anisotropy and cure time on fracture energy. *Wood and Fiber Science,* 11, 197-213.

Ebewele, R., B. H. River and J. A. Koutsky. (1980) Tapered double cantilever beam fracture tests of phenolic-wood adhesive joints. Part 2. effects of surface roughness, the nature of surface roughness, and surface aging on joint fracture *Wood and Fiber Science,* 12, 40-64.

Ebewele, R., B. H. River and J. A. Koutsky. (1982) Relationship between phenolic adhesive chemistry, cure and joint performance, part I. Effects of base resin constitution and hardener on fracture energy and thermal effects during cure. *The Journal of Adhesion,* 14, 189-217.

Ebewele, R., B. H. River and J. A. Koutsky. (1986) Relationship between phenolic adhesive chemistry and adhesive joint performance; effect of filler type on fraction energy. *Journal of Applied Polymer Science,* 31, 2275-2302.

Eisenheld, L. and D. J. Gardner. (2005) Developing an industrial friendly process for hydroxymethyl resorcinol (HMR) priming of wood using a novolak-based HMR. *For. Prod. J.,* 55, 61-66.

Ferry, J. D. Viscoelastic properties of polymers. John Wiley & Sons, Inc., New York,1980

Follrich, J., C. Hansmann, A. Teischinger and U. Muller. (2007) Tensile strength of a softwood butt end joints. Part 2: Improvement of bond strength by a hydroxymethylated resorcinol primer. *Wood Material Science and Engineering,* 2, 90-95.

Gagliano, J. M. and C. E. Frazier. (2001) Improvements in the fracture cleavage testing of adhesively-bonded wood. *Wood and Fiber Science,* 33, 377-385.

Gardner, D. J., C. E. Frazier and A. W. Christiansen. 2005: Characteristics of the wood adhesion bonding mechanism using hydroxymethyl resorcinol. In Frihart, C. R., editor, *Wood Adhesives 2005,* San Diego, CA: Forest Products Society, 93-97.

Gardner, D. J., W. T. Tze and S. Q. Shi. 2000: Adhesive wettability of hydroxymethyl resorcinol (HMR) treated wood., *Wood Adhesives,* Madison, WI, 321-327.

Gupta, R. K. Polymer and Composite Rheology. Marcel Dekker, Inc., New York, NY,2000

Hashemi, S., A. J. Kinloch and T. G. Williams. (1990) The analysis of interlaminar fracture in uniaxial fibre-polymer composites. *Proceedings of the Royal Society of London. Series A,* 427, 173-199.

Ishimaru, Y., S. Narimoto and I. Iida. (2001) Mechanical properties of wood swollen in organic liquids with two or more functional groups for hydrogen bonding in a molecule. *Journal of Wood Science,* 47, 171-177.

Jiang, J. L. and J. X. Lu. (2009) Anisotropic characteristics of wood dynamic viscoelastic properties. *For. Prod. J.,* For. Prod. J. 59, 59-64.

Kelley, S. S., T. G. Rials and W. G. Glasser. (1987) Relaxation behavior of the amorphous components of wood. *J. Mater. Sci.,* 22, 617-624.

Kurt, R., A. Krause, H. Militz and C. Mai. (2008) Hydroxymethylated resorcinol (HMR) priming agent for improved bondability of wax-treated wood. *Holz Roh Werkst,* 66, 333-338.

Laborie, M. P. G., L. Salmen and C. E. Frazier. (2004) Cooperativity analysis of the in situ lignin glass transition. *Holzforschung,* Holzforschung. 58, 129-133.

Lopez-Anido, R., D. J. Gardner and J. L. Hensley. (2000) Adhesive bonding of eastern hemlock gluelam panels with e-glass/vinyl ester reinforcement. *For. Prod. J.,* 50, 43-47.

Lorenz, L. F. and C. R. Frihart. (2006) Adhesive bonding of wood treated with ACQ and copper azole preservatives. *For. Prod. J.,* 56, 90-93.

Marcinko, J. J., S. Devathala, P. L. Rinaldi and S. Bao. (1998) Investigating the molecular and bulk dynamics of pMDI/wood and UF/wood composites. *For. Prod. J.,* 48, 81-84.

Marcinko, J. J., P. L. Rinaldi and S. Bao. (1999) Exploring the physicochemical nature of pMDI/wood structural composite adhesion. *For. Prod. J.,* 49, 75-84.

Mark, R. E., J. Habeger, C.C., J. Borch and M. B. Lyne, editors. 2002: *Handbook of physical testing of paper*. New York, NY: Marcel Dekker, Inc.

Meier-Westhues, U. Polyurethanes: adhesives, coatings, and sealants. Vincentz, Hannover, Germany,2007

Menard, K. P. Dynamic Mechanical Analysis: A Practical Introduction. CRC Press,1999

Menard, K. P. Dynamic mechanical analysis: a practical introduction. CRC Press LLC, Boca Raton, FL,2008

Mijovic, J. S. and J. A. Koutsky (1979) Effect of wood grain angle on fracture properties and fracture morphology of wood-epoxy joints. *Wood Science,* 11, 164-168.

Norimoto, M. and T. Yamada. (1966) Dynamic torsional viscoelasticity of wood. *Wood Research,* 38, 32-39.

Olsson, A.-M. and L. Salmen. (1997) The effect of lignin composition on the wiscoelastic properties of wood. *Nordic Pulp and Paper Research Journal,* 3, 140-144.

Pirvu, A., D. J. Gardner and R. Lopez-Anido. (2004) Carbon fiber-vinyl ester composite reinforcement of wood using the VARTM/SCRIMP fabrication process. *Composites: Part A,* 35, 1257-1265.

Randall, D. and S. Lee, editors. 2002: *The polyurethanes book*. John Wiley and Sons, LTD.

Rath, S. K., A. M. Ishack, U. G. Suryavansi, L. Chandrasekhar and M. Patri. (2008) Phase morphology and surface properties of moisture cured polyurethane-urea (MCPU) coatings: effect of catalysts. *Progress in Organic Coatings,* 62, 393-399.

River, B. H. and E. A. Okkonen. (1993) Contoured wood double cantilever beam specimen for adhesive joint fracture tests. *Journal of Testing and Evaluation*, 21-28.

River, B. H., C. T. Scott and J. A. Koutsky. (1989) Adhesive joint fracture behavior during setting and aging. *For. Prod. J.,* 39, 23-28.

Rogers, M. E. and T. E. Long. Synthetic methods in step-growth polymers. John Wiley & Sons, Ltd.,2003

Rubinstein, M. and R. H. Colby. Polymer Physics. Oxford University Press,2003

Sadoh, T. (1981) Viscoelastic properties of wood in swelling systems. *Wood Science and Technology,* 15, 57-66.

Salmen, L. (1984) Viscoelastic properties of *in situ* lignin under water-saturated conditions. *J. Mater. Sci.,* 19, 3090-3096.

Salmen, L. and A.-M. Olsson. (1998) Interaction between hemicelluloses, lignin, and cellulose: Structure-propert relationships. *Journal of Pulp and Paper Science,* 24, 99-103.

Scott, T. C., B. H. River and J. A. Koutsky. (1992) Fracture testing wood adhesives with composite cantilever beams. *American Society for Testing and Materials*, 259-264.

Scoville, C. Characterizing the durability of PF and pMDI adhesive wood composites through fracture testing. 2001. Virginia Tech, Blacksburg

Sebenik, U. and M. Krajnc. (2007) Influence of the soft segment length and content on the synthesis and properties of isocyanate-terminated urethane prepolymers. *Int. J. Adhes. Adhes.*, 27, 527-535.

Son, J. and D. J. Gardner. (2004) Dimensional stability measurements of thin wood veneers using the Wilhelmy plate technique. *Wood and Fiber Science,* 36, 98-106.

Son, J., W. T. Tze and D. J. Gardner. (2005) Thermal behavior of hydroxymethylated resorcinol (HMR)-treated maple veneer. *Wood and Fiber Science,* 37, 220-231.

Sprung, M. M. (1941) Reactivity of phenols towards paraformaldehyde. *Journal of the American Chemical Society,* 63, 334-343.

Sugiyama, M. and M. Norimoto. (1998) Viscoelastic properties of the matrix substance of chemically treated wood. *J. Mater. Sci.,* 33, 3505-3510.

Sun, N. and C. E. Frazier. (2005) Probing the hydroxymethylated resorcinol coupling mechanism with stress relaxation analysis. . *Wood and Fiber Science,* 37, 673-681.

Sun, N. J., S. Das and C. E. Frazier. (2007) Dynamic mechanical analysis of dry wood: Linear viscoelastic response region and effects of minor moisture changes. *Holzforschung,* 61, 28-33.

Swarbick, J., editor. 2004: *Encyclopedia of Pharmaceutical Technology*. New York, NY: Marcel Dekker, Inc.

Szycher, M. Szycher's handbook of polyurethanes. CRC Press LLC., Boca Raton, FL,1999

Tze, W. T., G. Bernhardt, D. J. Gardner and A. W. Christiansen. (2005) X-ray photoelectron spectroscopy of wood treated with hydroxymethyalted resorcinol. *International Journal of Adhesion & Adhesives,* 26, 550-554.

Vick, C. B., A. W. Christiansen and E. A. Okkonen. (1998) Reactivity of hydroxymethylated resorcinol coupling agent as it affects durability of epoxy bonds to douglas-fir. *Wood and Fiber Science,* 30, 312-322.

Vick, C. B., R. L. Geimer and J. Wood, J. E. (1996a) Flakeboards from recycled CCA-treated southern pine lumber. *For. Prod. J.,* 46, 89-91.

Vick, C. B. and E. A. Okkonen. (2000) Durability of one-part polyurethane bonds to wood improved by HMR coupling agent. *For. Prod. J.,* 50, 69-75.

Vick, C. B., K. Richter and B. H. River. 1996b: Hydroxymethylated resorcinol coupling agent and method for bonding wood. United States: The United States of America as represented by the Secretary of Agriculture, Washington, D.C., 1-17.

Vick, C. B., K. Richter, B. H. River and A. R. Fried. (1995) Hydroxymethylated resorcinol coupling agent for enhanced durability of bisphenol-A epoxy bonds to sitka spruce *Wood and Fiber Science,* 27, 2-12.

Ward, I. M. and J. Sweeney. An Introduction to the Mechanical Properties of Solid Polymers. John Wiley & Sons, Ltd.,2004

Wilkes, C. E., J. W. Summers and C. A. Daniels, editors. 2005: *PVC handbook*. Cincinnati, OH: Hanser Gardner Publications, Inc.

Wipf, T. J., M. A. Ritter and D. L. Wood. 1999: Evaluation and testing of timber highway bridges. In Walford, G. B. and Gaunt, D. J., editors, *Pacific Timber Engineering Conference*, Rotorua, New Zealand, 333-340.

Yoshihara, H. and T. Kawamura. (2006) Mode I Fracture toughness estimation of wood by DCB test. *Composites. Part A: Applied science and manufacturing,* 37, 2105-2113.

3 Adhesive Characterization

3.1 Introduction

A commercial moisture-cure polyurethane adhesive (Gorilla Glue®) was used over the course of this study. As a class of adhesives, moisture-cure polyurethanes have become more significant in the forest products industry; a good example is for the web-to-flange connection in composite I-beams. Applications such as for composite I-beams require structural certification. The adhesive used in this study is not certified as a structural wood adhesive, but it is quite similar to certified polyurethanes. Furthermore, moisture-cure polyurethanes are a class of adhesives shown to benefit from the HMR primer (Vick and Okkonen 2000). A variety of analytical techniques were employed in an effort to document adhesive properties, and how certain properties changed during this study. This chapter summarizes the analytical characteristics of the adhesive used in this study.

3.2 Experimental

3.2.1 Materials

Dibutylamine (DBA), toluene, 1.0 N hydrochloric acid (HCl), 1,2,4-trichlorobenzene (TCB), molecular sieves (4Å), deuterated chloroform ($CDCl_3$, 99.8% atom d), and tetramethylsilane (TMS) were obtained from commercial suppliers and used as received. One bottle ofcommercial moisture cure polyurethane adhesive, Gorilla Glue®, was obtained from a local hardware store and used as received. During the use of the adhesive, special care was exerted to prevent and/or minimize adhesive exposure to atmospheric moisture. After opening the adhesive, the container was always subjected to a stream of dry N_2 gas to remove any moisture; after closure the

adhesive container was placed in a desiccator over P_2O_5 and the entire vessel was flushed with N_2 gas.

3.2.2 Analytical Techniques

3.2.2.1 Isocyanate Determination

The isocyanate (NCO) content of the commercial moisture-cure polyurethane adhesive was measured using test method C of the ASTM D 5155-07 standard. All glassware was cleaned with soap and water, rinsed with acetone, and then dried (80°C, 24 hours) prior to testing. All transfers were performed under N_2. DBA (52 g) was combined with toluene (200ml) in a 500 ml flask over Type 4Å molecular sieves for 24 hours.

TCB (25 ml) was added to a 250 ml beaker, followed by the dry DBA/toluene solution (20 ml). Assuming a 17% NCO content, adhesive (4.94 g) was added to the TCB/DBA/toluene solution; the reaction flask was covered and stirred (20-25 min, room temperature) and then anhydrous methanol (110ml) was added to facilitate pH measurement. This solution was then titrated (1.0 N HCl) to the endpoint (pH ~ 4 to 4.4). Blanks containing no adhesive were also prepared and tested as above. The NCO content was calculated as follows:

$$\%\,\boldsymbol{NCO} = \boldsymbol{4.202(B-S)N/W} \qquad \text{[Equation 3-1]}$$

Where B represents the HCl volume (ml) for blank titration; S is the HCl volume (ml) for adhesive titration; N is the HCl normality; W is the sample mass (g); and 4.202 is a constant.

3.2.2.2 Concentric Cylinder Viscometry

Steady-state viscometric flow curves were obtained (25°C) using a concentric-cylinder geometry (conical rotor: 14 mm radius, 42 mm height; cup: 15 mm radius) on a TA Instruments

AR G2 rheometer that was enclosed in a clear box purged with dry air. Approximately 20 ml of adhesive was added to the sample cup and the rotor was lowered to a 5920 μm gap. The specimen was conditioned (25°C, 2 min) and then ramped over a shear rate range of $0.01s^{-1}$ to 1000 s^{-1}. Average curves were created using OriginPro software, version 8.0.63; the "Average multiple curves" function was used with a tolerance of about 0.1 s^{-1}.

3.2.2.3 ^{13}C Solution State Nuclear Magnetic Resonance (NMR)

Solution ^{13}C NMR experiments were performed on a Varian Unity 400 NMR spectrometer at 9.39 T magnetic field, corresponding to ^{13}C Larmor frequency of 100.58 MHz. The adhesive and 0.75 ml of deuterated chloroform ($CDCl_3$) were combined in a 5 ml glass vial to achieve a sample concentration of 61-62% (adhesive mass/solvent volume). 2-3 drops of TMS were added to the solution before an adequate sample quantity was transferred to a standard 5 mm NMR glass tube for testing with the following parameters: acquisition time = 1.2 s, relaxation delay = 2s, spectral width = 30 KHz, number of scans per sample = 368. Spectra were referenced to TMS and normalized to highest peaks (value=1).

Spectra were normalized (highest peak intensity = 1) and manual integration of peaks for calculation of area were performed using MestReNOVA software, version 6.1.0-6224.

3.3 Results and Discussion

3.3.1 Viscosity Measurements

Viscosity measurements were conducted on four separate occasions: At the beginning of the experiment (September 2009), one month later (October 2009), five months later (February 2010), and then near the end of the study (April 2010). Average viscosity curves for these measurements can be found in Figure 3-1 below.

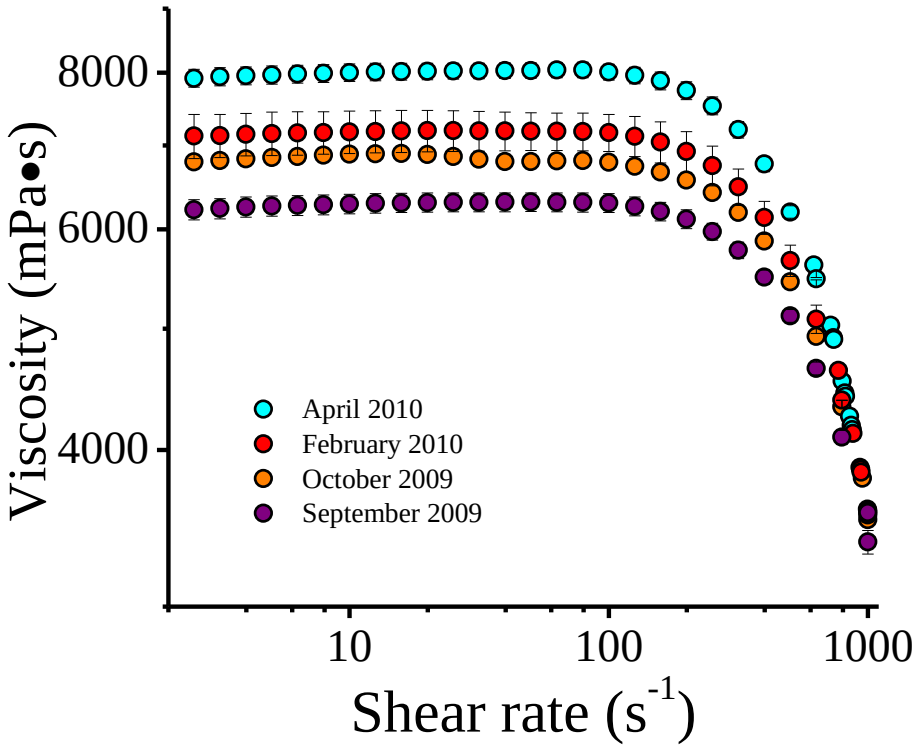

Figure 3-1. Viscosity measurements (October: n=1, all others: n=3) for moisture-cure polyurethane adhesive over 8 month period (error bars represent one standard deviation).

Figure 3-1 shows that the adhesive displays a non-newtonian response, shear-thinning at shear rates beyond 150 - 200 s^{-1}. The figure also demonstrates that the viscosity of the adhesive increased over the period of this study (from 6,200 to 8,000 mPa•s; 29%). While care was taken to store the adhesive under strictly anhydrous conditions (in desiccator under nitrogen, over P_2O_5) over the course of this experiment, it is still possible that some ambient moisture reacted with the adhesive, resulting in molecular weight increase through urea formation. Such reactions with atmospheric moisture could elevate viscosity through increased molecular weight and also through intermolecular interactions by urea hydrogens (hydrogen bonding).

3.3.2 Isocyanate Content Measurement

Isocyanate content measurements were conducted on four separate occasions: at the beginning of the experiment (September 2009), two months later (November 2010), five months later (February 2010), and then near the end of the study (May 2010). Graphical representation of the data is shown below in Figure 3-2; numerical results can be found in Table 3-1.

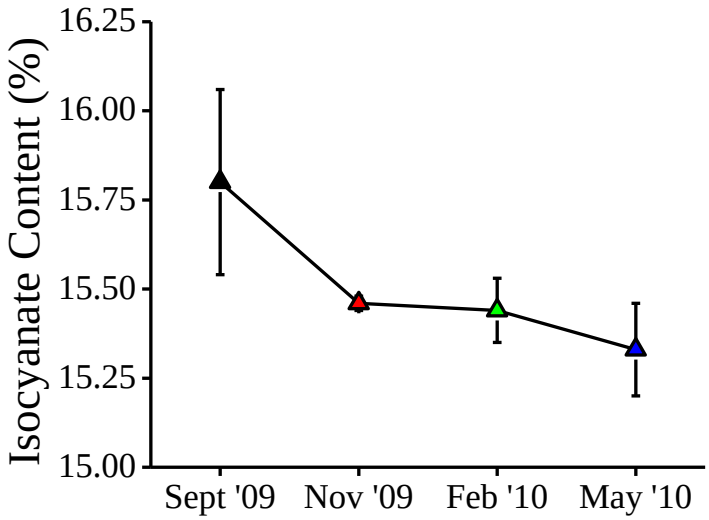

Figure 3-2. Average isocyanate content (n=3) measurements of moisture-cure polyurethane adhesive over 8-month period (error bars represent one standard deviation).

Figure 3-2 illustrates that a 3.07% reduction in isocyanate content is observed over the course of this study, from 15.8% to 15.33%. While standard deviations are starkly different across time periods, it is clear that the %NCO of the adhesive measured in September 2009 is statistically different (ANOVA $p = 0.032$) from that measured in May 2010. This result agrees with the change in viscosity observed in Figure 3-1, and is further evidence of the adhesive changing over time.

Table 3-1. Average isocyanate content (n=3) measurements of moisture cure polyurethane adhesive over 8-month period.

Month	Isocyanate Content (%)
Sept '09	15.80 ±0.26
Nov '09	15.46 ±0.02
Feb '10	15.44 ±0.09
May '10	15.33 ±0.13

3.3.3 Carbon-13 Nuclear Magnetic Resonance (^{13}C NMR)

^{13}C NMR spectroscopy was employed at the start of this study in an effort to characterize the molecular structure of the adhesive. As the study progressed, ^{13}C NMR was utilized to track substantial changes in the adhesive molecular structure. If the formation of urea groups was detected, this would suggest the reaction with moisture over time. If a reduction in NCO groups was observed, as indicated by the titration results, this would support the broader conclusion that the adhesive is changing.

Figure 3-3 shows a ^{13}C NMR spectrum of the moisture-cure polyurethane adhesive used in this study. Based on peak values documented in the literature, the two primary components of the adhesive were identified as polymeric methylenebis(phenylisocyanate) (pMDI) and poly(propylene oxide) (PPO). The measured peak values, along with values documented in the literature, are presented in Table 3-2.

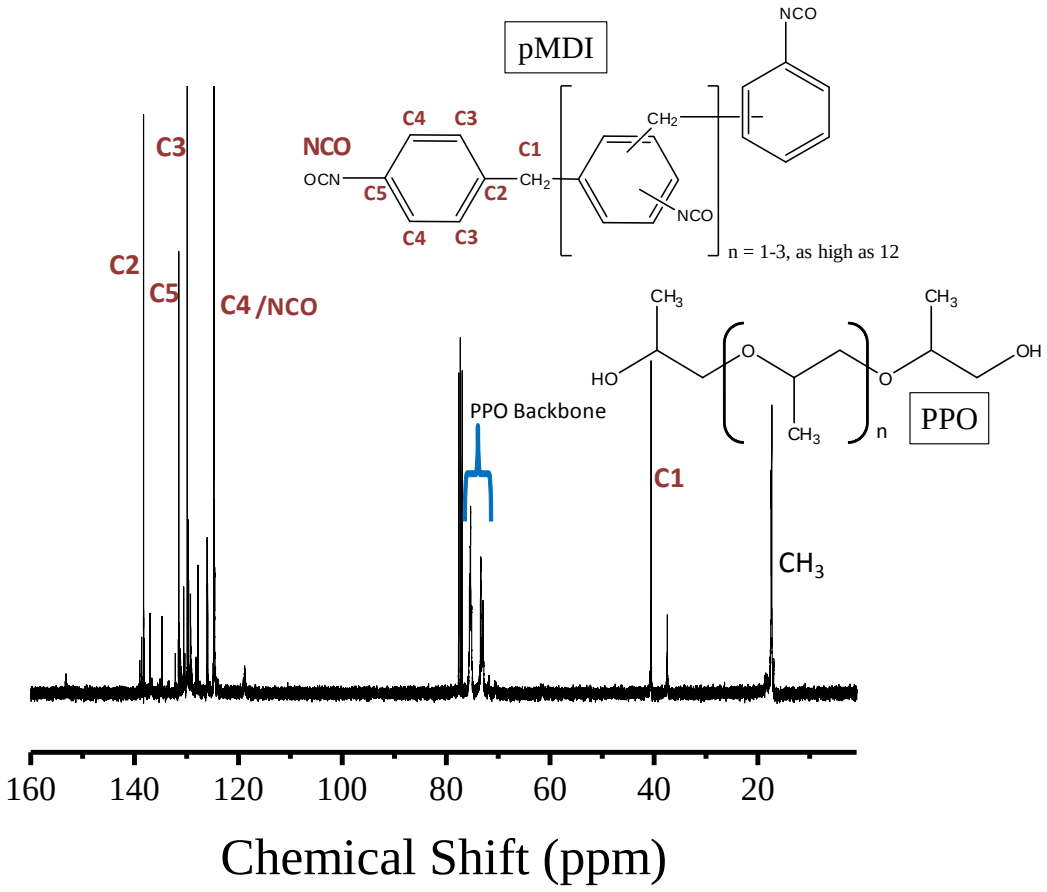

Figure 3-3. ^{13}C NMR spectrum of moisture-cure polyurethane adhesive in $CDCl_3$ solvent (77.23 ppm). Parameters: 368 scans, 1.2 s acquisition time, 2 s relaxation delay, 30 khz spectral width.

Upon close inspection of Figure 3-3 a small peak is observed at 153.2 ppm. Aromatic urethane groups are commonly located between 153 - 154 ppm (Delides and Pethrick 1981), suggesting this peak represents the urethane linkage between pMDI and PPO chains; additionally, urea linkages may also be found in this region. This initial test was performed in December 2009, when the adhesive was relatively new. To gain insight on changes in NCO groups over the period of study, a second specimen was prepared and tested in July 2010 using the same parameters and approximate adhesive wt./solvent vol. concentration (61-62%) as the first test. Figure 3-4 displays the urethane/urea resonance regions for both the old and new

adhesive specimens. A second peak appeared to form in the July 2010 test at ~153.3 ppm, which may be that of urea; while the signal:noise ratio is poor, this observation would be consistent with the reaction of ambient moisture with isocyanate groups in the adhesive.

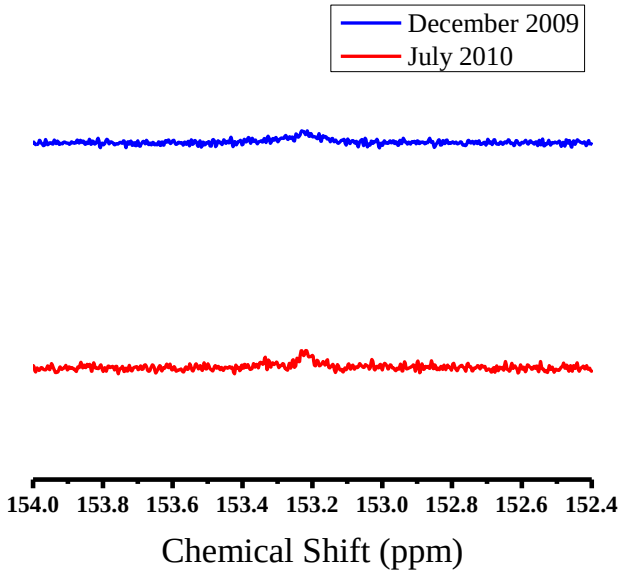

Figure 3-4. ^{13}C NMR spectra of moisture-cure polyurethane adhesive in $CDCl_3$ solvent (December 2009 and July 2010): ureathane/urea region. Parameters: 368 scans, 1.2 s acquisition time, 2 s relaxation delay, 30 khz spectral width.

The signal:noise ratio is likely poor because the parameters of this experiment were not optimized to view and quantify carbonyls; this is because the primary concern of the initial ^{13}C NMR experiment run in December 2009 was to identify the base components of the adhesive, which required a relatively small number of scans. A short acquisition time (1.2 s) and relaxation delay (2 s) were also used; it is good practice to determine the spin lattice relaxation time (T1) prior to testing, and ensure the relaxation time used is five times greater than T1 for quantitative measurements. This was not done in this research, however Delides and Pethrick

(Delides and Pethrick 1981) predicted T1 values greater than 1 second for carbonyl groups in polyurethane prepolymers; this indicates the test parameters set in this study were not adequate for accurately viewing or quantifying carbonyl peak areas or intensities.

Table 3-2. Observed chemical shift (ppm) values of pMDI and PPO in moisture-cure polyurethane adhesive, compared to documented ppm values for neat pMDI and PPO. pMDI carbons C1-C6 represent those shown in Figure 3-3.

Polymeric methylenebis(phenylisocyanate)		
Carbon	**Observed**	**Documented[a]**
C1	40.59	40.69
C2	138.28	138.2
C3	129.88	129.8
C4	124.75	124.7
C5	131.48	131.5
NCO	124.75	124.7
Poly(propylene oxide)		
Carbon	**Observed**	**Documented[b]**
methyl group	~17	~17
backbone	73-76	73-76

[a](Delides and Pethrick 1981)
[b](Schilling and Tonelli 1986)

In an effort to learn more about changes in NCO content, peak integration was performed on the pMDI aromatic (C5) and PPO methyl peaks of each spectrum to obtain peak areas; the areas of each peak in the same spectrum were then compared to obtain C5:methyl ratios. Due to the proximity of C5 to the isocyanate group in the pMDI molecule, changes in NCO content should impact the chemical shift of C5. Using the isocyanate resonance itself would have been ideal, but as Figure 3-3 shows, it is unavailable as its peak overlaps with another aromatic carbon (C4). The methyl group was chosen for comparison to the C5 carbon because it should remain

relatively stable over time. Figure 3-5 below shows the stacked ^{13}C NMR spectra of the old and new tests with a focus on the aromatic carbon C5 and methyl group chemical shift region.

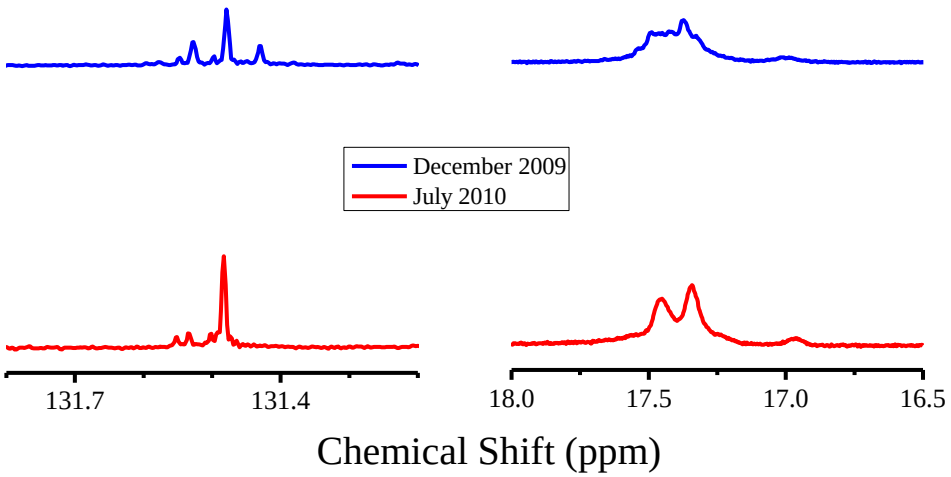

Figure 3-5. Stacked ^{13}C NMR spectra of moisture-cure polyurethane adhesive in $CDCl_3$ solvent (December 2009 and July 2010). Left: aromatic carbon (C5) group region; Right: PPO methyl group region. Parameters: 368 scans, 1.2 s acquisition time, 2 s relaxation delay, 30 khz spectral width.

All peaks observed in the range of 131.4 – 131.6 ppm were assumed to be related to C5 resonance. Moreover, all peaks observed between 16.75 and 17.75 ppm were assumed to be related to the PPO methyl peak. Areas from peak integrations and ratios for each spectrum are displayed below in Table 3-3. The ratios of C5:methyl groups were 0.12:1 and 0.10:1 for the old and new test, respectively. This result implies a reduction in NCO content of ~17% over the course of this study; this is in contrast to the isocyanate content measurement, which demonstrated only a 3% reduction.

But it is clear by comparing the spectra in Figure 3-5 that fundamental differences in the test results exist; for example, well-defined peaks observed in the C5 region of the December 2009 spectrum are not present in July 2010. In contrast, well-defined methyl peaks appear in the July 2010 spectra where there was only an ill-resolved multiplet in December 2009. These differences suggest there may have been error in the tuning and shimming of the spectrometer, and therefore there is less confidence in the peak integration results. Furthermore, a 17% reduction in NCO content as suggested by peak integration would likely have resulted in significant production of urea linkages, which is not supported by the July 2010 spectrum. In any case, there is great confidence in the isocyanate content measurements discussed previously, which showed a slight 3% reduction in NCO content. While minor, this reduction in NCO content appears to have dramatically increased adhesive viscosity (~29%) over the course of the study.

Table 3-3. Peak areas and ratios for December 2009 and July 2010 ^{13}C NMR spectra.

Specimen	Area		C5:Methyl
	C5 Group	Methyl Group	
December 2009	1.83	15.35	0.119:1
July 2010	1.89	19.26	0.098:1

3.4 Conclusions

The moisture-cure polyurethane adhesive used in this study changes over the time of storage. The adhesive's viscosity steadily increased, which is believed to be a result of ambient moisture reacting with a portion of the isocyanate groups to form urea linkages; urea linkages could increase the molecular weight of the adhesive and participate in secondary interactions. The isocyanate content measurements supported this conclusion, showing a slight 3% reduction in %NCO. While the ^{13}C NMR spectroscopy performed in this study was not optimized for

carbonyl visualization or quantification, the observation of a small peak at ~153.3 ppm in the adhesive specimen tested at the end of this study suggests the formation of urea linkages.

3.5 References

Delides, C. and R. A. Pethrick. (1981) Characterization of polyurethane elastomers by 13C n.m.r. spectroscopy. *Polymer,* 22, 1205-1210.

Schilling, F. C. and A. E. Tonelli. (1986) Carbon-13 NMR determination of poly(propylene oxide) microstructure. *Macromolecules,* 19, 1337-1343.

Vick, C. B. and E. A. Okkonen. (2000) Durability of one-part polyurethane bonds to wood improved by HMR coupling agent. *For. Prod. J.,* 50, 69-75.

4 Mode-I Fracture: Investigating the Impact of Wood Primer Treatments on Adhesive Bond Toughness

4.1 Introduction

The purpose of this study was to investigate the impact of HMR and two variations of the HMR primer on mode-I fracture toughness, and the associated durability against simulated weathering. Three wood primers were selected: 1) HMR, which is proven to be an effective wood primer, 2) alkyl-HMR (a-HMR), which is analogous to HMR but where 30% of the resorcinol is replaced with 2-methylresorcinol, and 3) polymeric methylenebis(phenylisocyanate) dissolved in N-methylpyrrolidone (known as "pMDI" or "pMDI treatment"), a novel treatment devised to mimic HMR. Christiansen (2005) discovered that a-HMR improves epoxy adhesion to southern pine (compared to unprimed wood), but that a-HMR did not equal HMR; a-HMR treatment would not meet the criterion required to pass the ASTM D 2559 delamination test (Christiansen 2005). Consequently, Christiansen (2005) concluded that difunctional 2-methylresorcinol impairs HMR action by reducing crosslink density below some required minimum. The third primer, pMDI, was novel with unknown wood priming potential. A 5 wt% solution of pMDI in NMP, this system was intended to mimic HMR (HMR is a reactive mixture of monomers, oligomers, and polymers dissolved in alkaline water). HMR monomers can penetrate the wood cell wall, and this is likely facilitated by alkaline water, an effective wood swelling agent. Qualitatively similar, pMDI is a reactive, isocyanate functional, mixture of monomers, oligomers, and polymers. Likewise, NMP is a powerful wood swelling agent, but nonreactive with pMDI.

4.2 Experimental

4.2.1 Sample Preparation

4.2.1.1 Materials

A commercial moisture-cure polyurethane adhesive (Gorilla Glue®) was obtained from a local hardware store and used as received. Materials used for primer synthesis are described in Chapter 5.

4.2.1.2 Lumber Machining

Red oak lumber was cut to rough rectangular dimensions (200-250mm longitudinal x 125mm tangential x 50mm radial) on a radial arm saw. The radial surfaces were edged on a joiner to reveal grain orientation. Laminates were cut on a bandsaw to attain a grain angle of approximately 3° between the radial grain pattern and the longitudinal axis of the lumber. Each rough-cut piece of lumber yielded 2-3 15mm thick laminae which were subsequently planed to ~11 mm and placed in an environmental chamber (65% RH, 20°C, ~2 weeks).

4.2.1.3 Laminate/Dual Cantilever Beam Preparation

Laminae were planed to a final thickness of 10 mm immediately prior to bonding. Two laminae were paired so that the 3° grain angles converged to a "V" shape at the bonding surface. A debond area extending 25.4 mm from the open side of the "V" was drawn using a paraffin-wax crayon. The adhesive was applied (172 g/m^2) in front of the debond area of one lamina; the paired lamina was placed on top. Laminates were interspaced with Teflon sheets to prevent self-adhesion and then cold-pressed between two steel caul plates (120 psi, 24 hours). After pressing, 10 mm-wide strips were removed from both sides of the bonded laminates using a table saw and subsequently ripped to final dimensions (20 mm x 20 mm x 220 mm); each laminate produced 5

dual cantilever beam (DCB) specimens. All specimens were re-equilibrated (65% RH, 20°C, ~2 weeks) to ~10% MC prior to testing. The DCB was secured in a vice grip and a 50 mm pre-crack was initiated at the loading end of the DCBs using a hammer and chisel. Two holes (4.4 mm diameter) were drilled into the DCBs for attachment to the test grips. A schematic of the resulting DCB test specimen is shown in Figure 4-1.

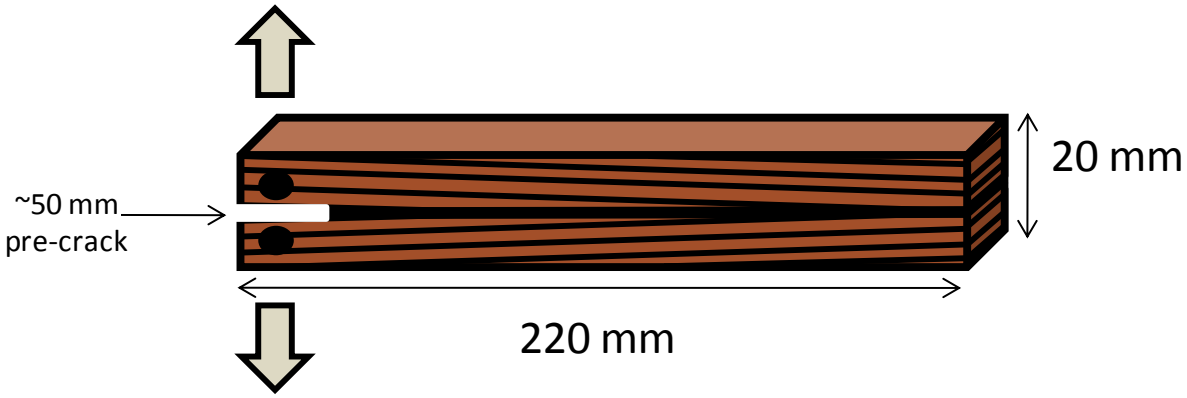

Figure 4-1. Schematic of DCB test specimen.

4.2.1.4 Primer Application

HMR, pMDI, and a-HMR primer systems were prepared as described in the primer synthesis section found in Chapter 5. After planing to final thickness, laminae were brushed with primer treatment on both sides so that the exposed surfaces were lightly saturated and then air-dried (atmospheric conditions, ~24 hours) prior to bonding. The pMDI-treated laminae were wiped with a brush 20 minutes after application to blend in pMDI globules that had formed on the wood surface. Recall from Chapter 3 that primer-treated DMA specimens were post-cured at 150˚C to eliminate curing effects from the observed rheological response. No such post-cure was applied to the primer-treated specimens used for fracture testing.

4.2.1.5 DCB Weathering Procedure

DCB specimens were saturated in water, vacuum-soaked (~25 mmHg, 1.5 hr), allowed to soak at atmospheric pressure (room temperature, 2 hr), and then dried (60°C, 48 hr). Initially, a more severe drying step (100°C for 24 hr) was applied, but it resulted in complete delamination of untreated DCBs; the procedure was adjusted to provide intact specimens. Specimens were equilibrated to ~10% MC in the environmental chamber (65% RH, 20°C, ~2 weeks) prior to testing.

4.2.2 Mode-I Fracture Test Method

The procedure was adapted from the method described by Gagliano (Gagliano 2001). Mode-I fracture testing was performed on a screw-driven MTS Systems, Syntec 10/GL in displacement control. TestWorks 4™ software was used to acquire data and control the testing procedure. A CCD camera with 10x magnification was used to monitor crack length during testing. A video monitor connected to the camera allowed for instantaneous crack length measurements. The camera was mounted on a movable track, providing a means to observe crack initiation and growth. A white typographic correction fluid was applied to the specimen bondline in order to provide a brittle contrast coating, allowing for simple crack viewing. A white paper ruler with millimeter divisions was attached to the bottom cantilever and crack lengths were recorded from the point of loading.

Prior to testing, a pre-load (~10 N) was applied to the DCB specimen, after which the crosshead displacement was zeroed. A 1mm/min displacement rate was employed in the initial fracture cycle. When the load versus displacement plot deviated from linearity, the crosshead displacement was halted; the crosshead position remained fixed for 40 seconds, during which time the crack extended until the load stabilized; thereafter the crosshead was returned to its

starting position, thus completing one fracture cycle. Subsequent fracture cycles were obtained by repeating this process in cyclic fashion until either the crack length extended beyond the useable data range (50mm from the end of the DCB), or until the specimen failed catastrophically. The displacement rate was increased with each subsequent cycle to maintain crack propagation on the order of 1 minute from the beginning of each loading cycle. This stipulation ensured the crack tip strain rate was approximately constant for all cycles. Each specific displacement rate was calculated for each cycle as the maximum displacement recorded in the previous cycle divided by one minute.

During testing, the crack length was manually recorded and no data was taken within 50 mm of the loading point, nor from within 50 mm of the end of the DCB specimen. From each loading cycle, the reciprocal slope (compliance) was measured, as were the critical crack initiation and crack arrest loads.

4.2.2.1 Data Analysis

The corrected compliance method (Hashemi et al. 1990) was applied in the calculation of fracture energies. Using this method, the following equations can be used to calculate these energies (Blackman et al. 1991):

$$G_{Ic} = \frac{Pc^2(a+x)^2}{b(EI)_{eff}} \quad \text{[Equation 4-1]} \qquad G_{Ia} = \frac{Pa^2(a+x)^2}{b(EI)_{eff}} \quad \text{[Equation 4-2]}$$

Where $(EI)_{eff}$ represents the effective flexural rigidity of the DCB specimen, and x is the crack length correction factor. These variables are derived from the slope (m) and y-intercept (b) of the measured compliance ($C^{1/3}$) versus crack length (a) curve. An example plot is shown below in Figure 4-2.

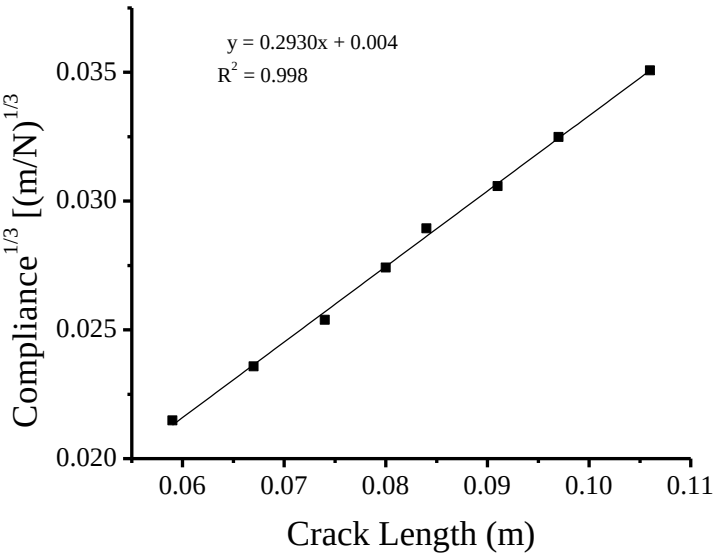

Figure 4-2. Example compliance ($C^{1/3}$) vs. crack length (a) plot.

$$(\boldsymbol{EI})_{\boldsymbol{eff}} = \frac{\boldsymbol{2}}{\boldsymbol{3m^3}}$$ [Equation 4-3]

The crack correction factor, x, is determined by simply identifying the x-intercept of the measured compliance versus crack length plot (Blackman et al. 1991). It represents the crack length offset, and can be obtained by dividing the y-intercept of the linear fit line in the compliance plot by the slope (Gagliano and Frazier 2001):

$$\boldsymbol{x} = \frac{\boldsymbol{b}}{\boldsymbol{m}}$$ [Equation 4-4]

In this study, two separate criteria for data validity were applied. First regarding fracture testing, a compliance plot (Figure 4-2) criterion was applied where a specimen was considered invalid if its compliance plot correlation coefficient (R^2, for the least squares fit) was less than 0.99. The second criterion addressed the survival of the simulated weathering procedure; "failed specimens" were those that after weathering delaminated outright, or that sustained fewer than 3 fracture test cycles, or that exhibited a degree of delamination that prevented reliable crack

length measurement. The number of failed specimens was recorded and used to calculate the "survival ratio," discussed below. Keep in mind that a specimen could meet the survival criterion, but perhaps not meet the compliance plot criterion.

4.2.2.2 Statistical Analysis

Critical and arrest energy values of individual sample groups were subjected to a Shapiro-Wilk normality test to check whether the dataset was drawn from a normal distribution; a majority of sample groups were not. However, a majority of sample groups also had a sample size $n \geq 30$ fracture cycles. It was therefore deemed acceptable to use a parametric test to compare their means, as the central limit theorem states as a rule of thumb that when $n \geq 30$, it is acceptable to assume normality of the sample mean distribution (Crowe and Feinberg 2001). For mean comparisons which involved non-normal sample groups with $n < 30$ fracture cycles, a non-parametric Mann-Whitney test was conducted in concert with a t-test, and both results were reported; when n is close to 30, and the distribution is close to normal, a t-test comparison of means can be acceptable (Crowe and Feinberg 2001). T-tests and Mann-Whitney tests (α=0.05) were performed separately for critical and arrest energy groups between 1) unweathered and weathered samples of the same primer treatment, and 2) a primer treatment and its appropriate control.

4.3 Results and Discussion

The adhesive used in this study was commercially available moisture-cure polyurethane (PUR). Even though the adhesive was stored under anhydrous conditions, it was determined that significant adhesive changes were occurring during the course of this study (Chapter 3). Consequently, separately bonded control specimens were prepared for the analysis of each primer system. The HMR primer system was bonded first, followed by the pMDI treatment, and

lastly the a-HMR treatment; when the a-HMR-treated laminates were prepared, several HMR-treated and pMDI-treated laminates were prepared as well to enable direct comparison of the primer systems (hereafter referred to as the "concurrently-bonded" laminates).

4.3.1 Hydroxymethyl Resorcinol (HMR)

Figure 4-3 shows the average critical and arrest energies for unweathered and weathered HMR-treated specimens compared to untreated specimens. When considering the baseline performance defined by "dry" (unweathered) specimens, the HMR treatment has a dramatically positive effect; respectively, unweathered critical and arrest energies are increased 69% and 72% over that seen in untreated specimens. This is significant, as HMR is primarily known for improving the weather durability of an adhesive bond (Christiansen and Conner 1995; Lopez-Anido et al. 2000; Lorenz and Frihart 2006; Pirvu et al. 2004; Vick et al. 1996; Vick and Okkonen 2000; Vick et al. 1995). However, more recently HMR has been found to enhance the dry strength of adhesive bonds (Follrich et al. 2007; Kurt et al. 2008), which suggests HMR may have a significant impact on adhesion overall. The results of this study are therefore consistent with the findings in the literature.

Relative to the control group, the weathering procedure does not significantly alter bond toughness (critical energy: $p = 0.722$; arrest energy: $p = 0.518$). The HMR treatment is negatively impacted by weathering (critical energy: $p = \sim0.000$; arrest energy: $p = \sim0.000$), but significantly enhances bond durability compared to the control (critical energy: $p = 0.037$; arrest energy: $p = 0.036$). Note that Figure 4-3 is misleading because the data suggests that untreated specimens suffered no effects from weathering; but this reflects the specimens that survived the weathering process. Table 4-2 demonstrates that untreated specimens exhibit a survival ratio of 5/10 (50% survival), whereas HMR treated specimens exhibit a survival ratio of 11/12 (92%

survival). Summarizing HMR effects on adhesive performance, HMR significantly improved bondline toughness in unweathered specimens. Regarding durability, HMR treatment again had a positive impact; in fact, weathered HMR-treated specimens exhibited greater toughness that that found in unweathered, untreated specimens. Finally in terms of the survival ratio, HMR treatment caused a significant increase in bondline durability.

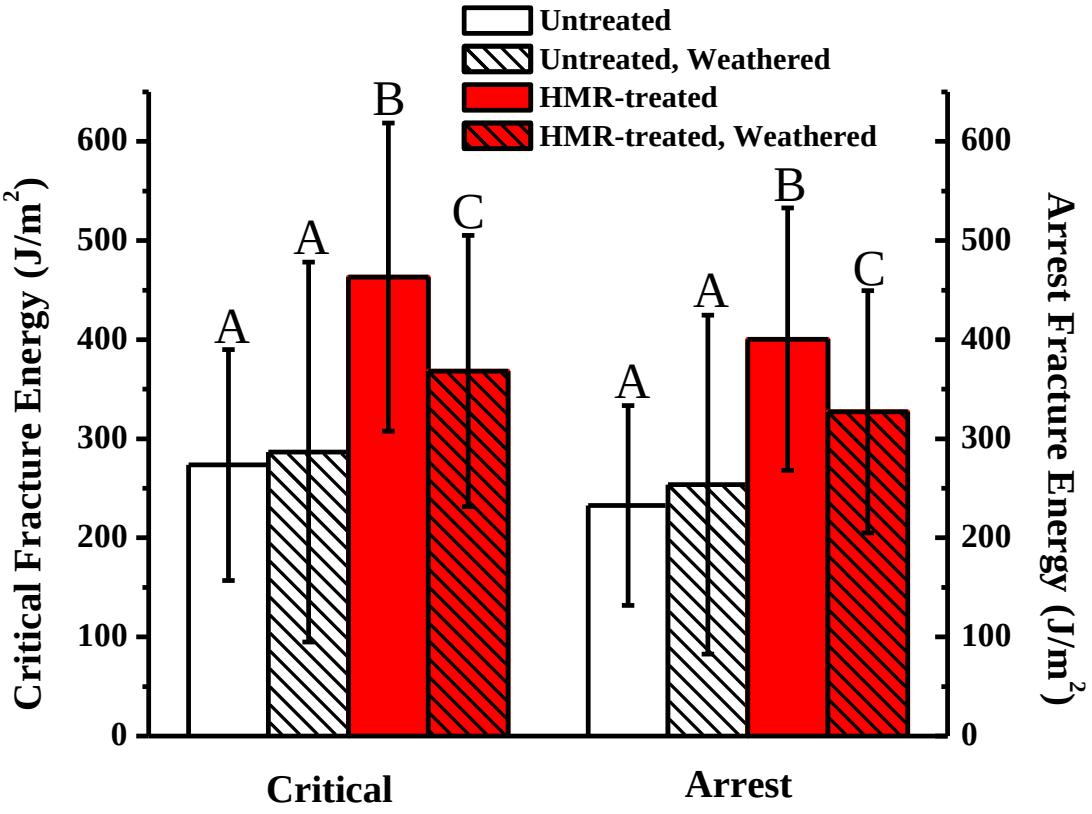

Figure 4-3. Average critical and arrest energy values for unweathered and weathered HMR-treated samples compared to untreated (error bars represent ±1 standard deviation). Sample averages connected by letters in same energy group (critical/arrest) may not be significantly different (α-value = 0.05). Average critical and arrest energies for unweathered and weathered HMR-treated and untreated sample groups.

Table 4-1. Average critical and arrest energies for unweathered and weathered HMR-treated and untreated sample groups.

	Critical Fracture Energy (J/m^2)		Arrest Fracture Energy (J/m^2)	
Treatment	Unweathered	Weathered	Unweathered	Weathered
Untreated	273.5 ± 116.4	286.6 ± 191.8	232.7 ± 100.9	253.9 ± 171
HMR	463.1 ± 155.5	368.4 ± 137	400.5 ± 132.3	327.3 ± 122.2

Table 4-2. Fraction of valid tests and number of fracture cycles produced for unweathered and weathered HMR-treated and untreated specimens.

	Unweathered		Weathered	
Treatment	Number of successfully tested specimens	Number of Fracture Cycles	Survival Ratio	Number of Fracture Cycles
Untreated	11/11	119	5/10	30
HMR	12/12	139	11/12	90

4.3.2 Alkyl Hydroxymethyl Resorcinol (a-HMR)

Figure 4-4, and Table 4-3 and Table 4-4 show the influence of a-HMR treatment on adhesive performance and durability. First note that a-HMR dramatically increases the baseline performance seen in unweathered specimens; respectively, unweathered critical and arrest energies are increased 139% and 143% over that seen in untreated specimens. Regarding baseline performance, this is a far greater enhancement than was seen from HMR treatment, described above (also notice that overall energies are greater for the HMR study [Figure 5-3], probably reflecting changes in the adhesive, as mentioned previously). Additionally, weathering causes no toughness loss in a-HMR treated specimens (critical energy: $p = 0.355$; arrest energy: $p = 0.104$); nor does weathering reduce the toughness of untreated specimens (critical energy: $p = 0.380$; arrest energy: $p = 0.110$). Curiously however, both a-HMR treated and untreated

specimens exhibit perfect survival ratios (100% survival in both cases). Summarizing the effects of a-HMR treatment, the baseline performance was dramatically improved, and no durability loss was observed. Relative to the HMR treatment previously discussed, it appears that a-HMR might be considered as the superior adhesion primer. However, the respective data sets are not easily compared because adhesive changes are known to have occurred during the intervening period. Later, the "concurrently-bonded" specimens will provide a direct comparison, and it will be shown that HMR and a-HMR provide the same performance enhancement.

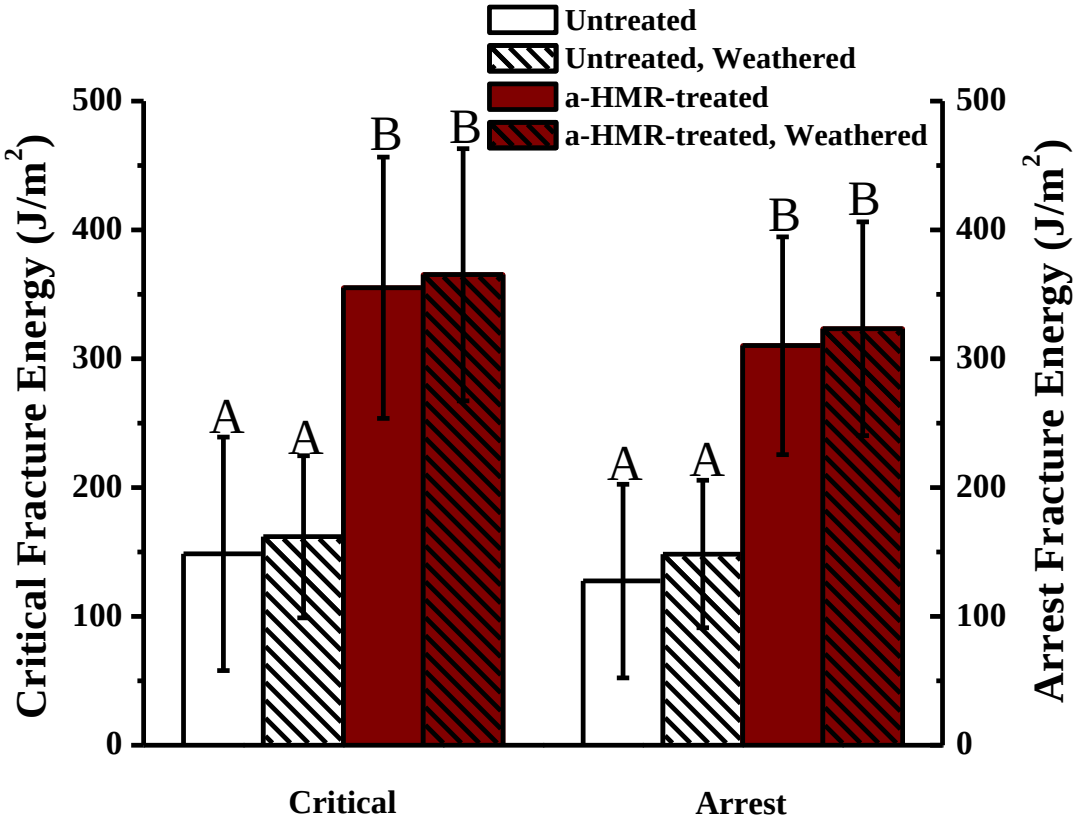

Figure 4-4. Average critical and arrest energy values for unweathered and weathered a-HMR-treated samples compared to untreated (error bars represent ±1 standard deviation). Sample averages connected by letters of the same energy (critical/arrest) may not be significantly different (α-value = 0.05).

Regarding the a-HMR treatment, recall Christiansen's (Christiansen 2005) report that a-HMR was significantly less effective than HMR. Be reminded that Christiansen's results indicated that a-HMR provided significant improvements over unprimed specimens, but that a-HMR did not quite match the performance seen with HMR treatment. In this regard, the findings presented here are consistent with those of Christiansen. Again later, the discussion of concurrently bonded specimens will demonstrate that mode-I fracture cannot distinguish the effects of a-HMR from those of HMR. Relative to mode-I fracture, perhaps the delamination test (ASTM D2559) is better suited to judge the effects of wood primers. The respective adhesion test methods differ dramatically. In the future, it would be interesting to directly compare the delamination (ASTM D2559) and fracture test methods.

Table 4-3. Average critical and arrest energies for unweathered and weathered a-HMR-treated and untreated samples.

	Critical Fracture Energy (J/m2)		**Arrest Fracture Energy (J/m2)**	
Treatment	Unweathered	Weathered	Unweathered	Weathered
Untreated	148.6 ± 90.6	161.8 ± 62.9	127.5 ± 75.1	148.4 ± 57.2
a-HMR	355.1 ± 101.5	365.2 ± 98	310.1 ± 84.4	323.2 ± 83

Table 4-4. Fraction of valid tests and number of fracture cycles produced for weathered and unweathered a-HMR-treated and untreated samples.

	Unweathered		**Weathered**	
Treatment	Number of Tested Specimens	Number of Fracture Cycles	Survival Ratio	Number of Fracture Cycles
Untreated	3/3	57	5/5	51
a-HMR	11/11	208	11/11	223

4.3.3 Polymeric Methylenebis(phenylisocyanate) in N-methylpyrrolidone ("pMDI")

Figure 4-5 (and Table 4-5) shows the average critical and arrest energies for unweathered and weathered pMDI-treated samples compared to untreated specimens. Note that in this section, p-values obtained from mann-whitney tests are in parenthesis following p-values from t-tests. It is clear that the pMDI treatment decreases the baseline performance of unweathered specimens (critical: p = ~0.000 (~0.000); arrest: p = ~0.000 (~0.000)); unweathered critical and arrest energies are reduced by 29% and 34%, respectively, compared to untreated specimens. Curiously, weathering causes no toughness loss in pMDI treated specimens (critical: p = 0.215 (0.788); arrest: p = 0.537 (0.912)), while weathering does reduce bond toughness of untreated specimens (critical: p = ~0.000 (0.002); arrest: p = ~0.000 (~0.000)). While no reduction in bond toughness is shown, the pMDI treated specimens are clearly affected by weathering: the treatment reduces the survival ratio from 100% to 27% (Table 4-6). To summarize, the pMDI treatment causes a reduction in baseline performance and a negative impact on bondline durability with regards to the survival ratio; while not observed in these specimens, the "concurrently-bonded" pMDI treated DCBs actually exhibit a significant reduction in weathered bond toughness.

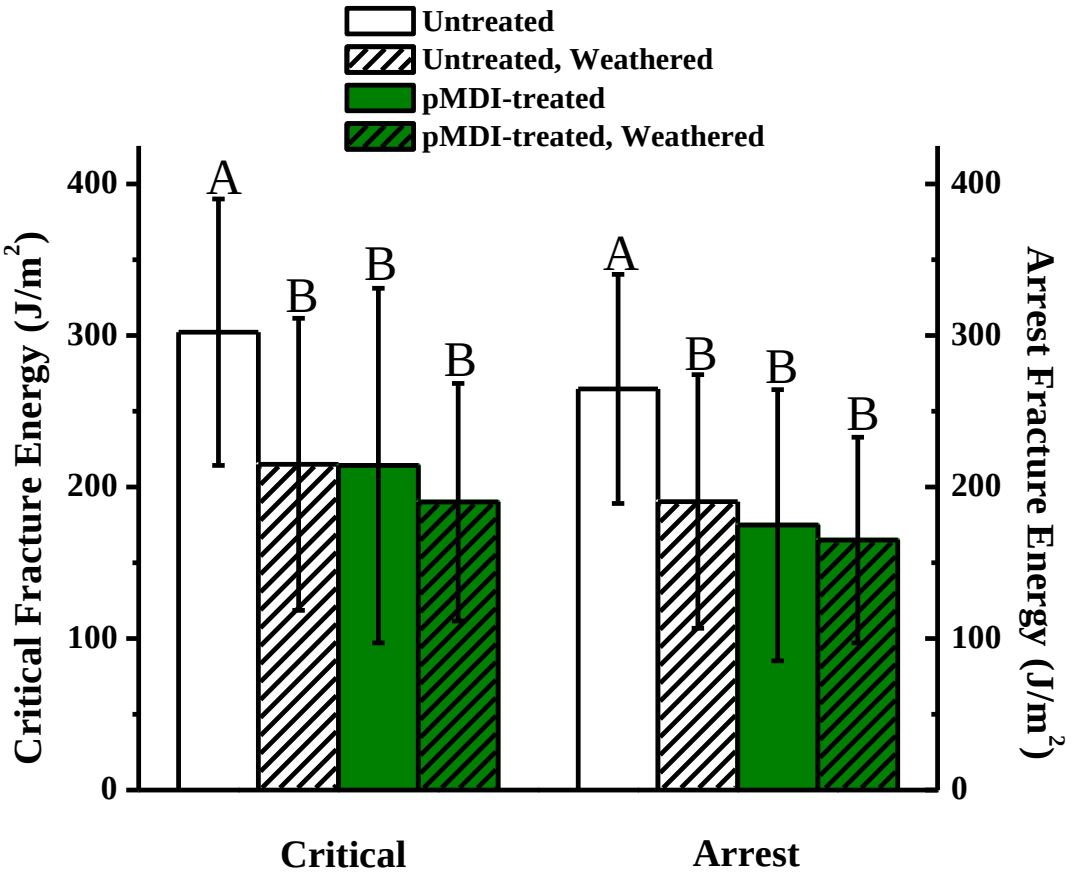

Figure 4-5. Average critical and arrest energy values for unweathered and weathered pMDI-treated samples compared to untreated (error bars represent ±1 standard deviation). Sample averages connected by letters of same energy (critical/arrest) may not be significantly different (α-value = 0.05).

Table 4-5. Average critical and arrest energies for unweathered and weathered pMDI-treated and untreated samples.

	Critical Fracture Energy (J/m2)		Arrest Fracture Energy (J/m2)	
Treatment	Unweathered	Weathered	Unweathered	Weathered
Untreated	302.1 ± 88	215 ± 96.3	264.6 ± 75.6	190.4 ± 83.7
pMDI	214.1 ± 116.9	190 ± 78.4	174.8 ± 89.5	164.9 ± 67.9

Table 4-6. Fraction of valid tests and number of fracture cycles produced for unweathered and weathered pMDI-treated and untreated samples.

	Unweathered		Weathered	
Treatment	**Number of successfully tested specimens**	**Number of Fracture Cycles**	**Survival Ratio**	**Number of Fracture Cycles**
Untreated	2/2	26	3/3	33
pMDI	7/7	90	3/11	28

A photograph of the bonding surfaces of an untreated and pMDI-treated DCB is shown in Figure 4-6. The untreated bonding surface is representative of the control group, as well as the HMR and a-HMR treatment; it is characterized by a very thin, translucent, shiny adhesive layer. The pMDI treatment results in a unique interfacial delamination at the bondline, evidenced by a "flaky" appearance of the adhesive. Furthermore, an unusually thick adhesive layer was observed on the bonding surface, suggesting it was not able to penetrate fully.

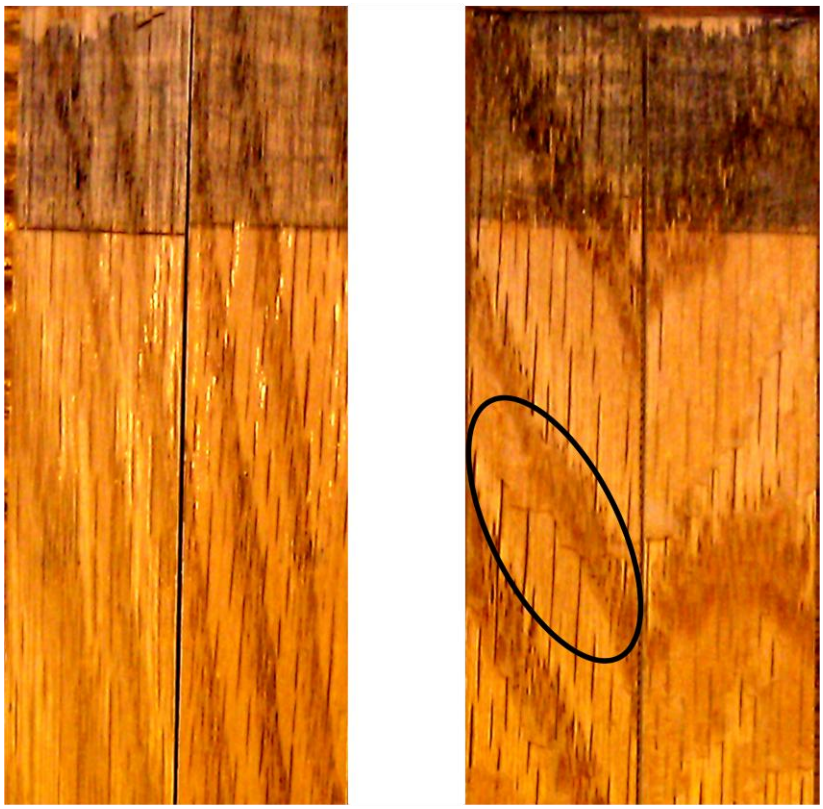

Figure 4-6. Comparison of representative untreated (left) and pMDI-treated (right) DCB bonding surfaces after testing; evidence of flaking is marked on right image.

It is known from Chapter 3 that pMDI was one of the primary components of the PUR adhesive; it is possible the pMDI in the pMDI treatment interfered with the PURs natural adhesion mechanism, thereby inhibiting its penetration and effectiveness. Moreover, the pMDI treatment may negatively impact wood surface chemistry and wetting. More research is necessary to determine why the adhesive layer is altered so significantly, but in terms of this experiment it is most important to note that the pMDI treatment reduces dry bond toughness, and that it does not significantly impact weathered bond toughness.

4.3.4 Primer Treatment Comparisons – Concurrently-Bonded

The following results are for primer-treated DCBs with no difference in adhesive age, as all laminates were bonded up concurrently. Figure 4-7, Table 4-7, and Table 4-8 shows the impact of HMR, a-HMR, and pMDI treatment on bond performance and durability.

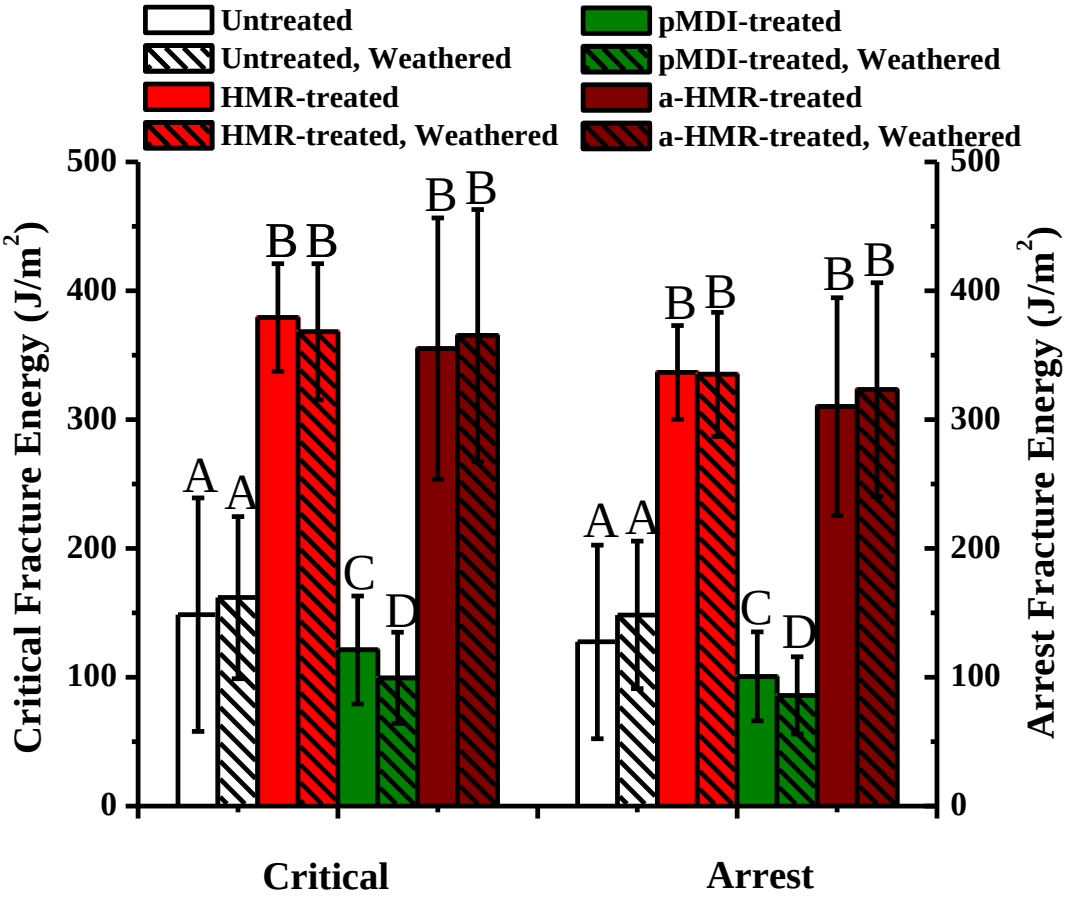

Figure 4-7. Average critical and arrest energy values for all primer-treated sample groups compared to untreated (error bars represent ±1 standard deviation). Sample averages connected by letters of the same energy (critical/arrest) may not be significantly different (α-value = 0.05).

In this case, the HMR treatment causes dramatic bond toughness enhancement in both baseline and weathered performance over that observed in Figure 4-3. In fact, with no difference in adhesive age, the effects of HMR and a-HMR treatments are essentially indistinguishable from each other; both primer systems enhance bond toughness on the order of 140-165% compared to untreated specimens, regardless of weathering (Table 4-9, Table 4-10). Regarding the pMDI treatment, recall that weathering did not impact bond toughness of the specimens in Figure 4-5; in the concurrently bonded specimens, pMDI treated DCBs are negatively impacted by weathering (critical: $p = 0.001$; arrest: $p = 0.006$), including when they are compared to the untreated specimens (critical: $p = \sim 0.000$; arrest: $p = \sim 0.000$). Considering the survival ratios (Table 4-8), only the pMDI treatment exhibits a reduced bondline durability (64%). To summarize, the HMR and a-HMR treatments caused a substantial improvement in baseline performance, and exhibited no reduction in bond durability. Alternatively, the pMDI treatment actually negatively affected bond performance; a reduction in both baseline toughness and weather durability was observed.

With regards to a-HMR treatment, the extent to which the primer enhanced bond performance was unexpected. Recall that the primer system was analogous to HMR, only with 30 mole% of its resorcinol replaced with 2-methylresorcinol; with 30% of its reactive aromatic monomers now having 2 reactive sites instead of 3, a-HMR's ability to form crosslinked networks inside the cell wall was reduced. This was predicted to decrease the cured primer's strength and stiffness, thereby reducing its overall mechanical integrity (Christiansen 2005). The delamination test (ASTM D 2559) showed a-HMR to reduce bond durability compared to HMR (Christiansen 2005); this was not the case in mode-I fracture. Therefore, it is possible the amount of crosslink density achievable by a-HMR is enough to enhance wood adhesion using

this test method. Furthermore, it may be that HMR effectiveness is not related to its ability to form a highly crosslinked synthetic network itself, but instead to its ability to form HMR chains with reduced branching spanning between amorphous wood polymers.

Table 4-7. Average critical and arrest fracture energies for unweathered and weathered concurrently-bonded untreated, HMR-, a-HMR-, and pMDI-treated sample groups.

	Critical Fracture Energy (J/m2)		**Arrest Fracture Energy (J/m2)**	
Treatment	Unweathered	Weathered	Unweathered	Weathered
Untreated	148.6 ± 90.6	161.8 ± 62.9	127.5 ±75.1	148.4 ± 57.2
HMR	379.3 ± 41.7	368.2 ± 52.9	336.7 ±36.3	335.1 ± 48.1
a-HMR	355.1 ± 101.5	365.2 ± 98	310.1 ±84.4	323.2 ± 83
pMDI	121.2 ± 42	99.5 ± 35.4	100.6 ±34.5	85.9 ± 29.9

Table 4-8. Fraction of valid tests and number of fracture cycles produced for each primer treatment and condition.

	Unweathered		**Weathered**	
Treatment	**Number of successfully tested specimens**	**Number of Fracture Cycles**	**Survival Ratio**	**Number of Fracture Cycles**
Untreated	4/4	57	5/5	51
HMR	5/5	98	5/5	111
a-HMR	12/12	208	12/12	223
pMDI	11/11	115	7/11	52

With regards to the adhesive, it is clear that chemical changes occurring over the course of this work are shown to impact overall toughness, weather survivability, and variability. Tables 4-1 through Table 4-8 show that the control group exhibits a ~50% reduction in critical energy (~300 J/m^2 to 150 J/m^2) between the beginning and end of the study; the HMR and pMDI treated specimens exhibit similar toughness reductions. In contrast, the survival ratio of the control group increases from 50% to 100% as the adhesive ages. Lastly, variability in the form

of standard deviation is clearly reduced across primer treatments as the study progresses. It is unclear why changes in the adhesive might impact variability or survivability, but a reduction in the number of reactive isocyanate groups (Chapter 3) may be expected to reduce overall bond toughness.

While adhesive aging shows an impact on bond performance, the comprehensive effects of the primer systems are clear: HMR and a-HMR dramatically enhance baseline performance and weather durability, while the pMDI treatment does not.

Table 4-9. Percent increase/decrease in critical fracture energy for each primer treatment and condition, compared to respective control group. N/S = no significant difference; N/A = not available.

	HMR		pMDI		a-HMR	
	Dry	**Weathered**	**Dry**	**Weathered**	**Dry**	**Weathered**
Individually bonded	+69%	+29%	-29%	N/S	N/A	N/A
Concurrently bonded	+155%	+128%	-18%	-39%	139%	126%

Table 4-10. Percent increase/decrease in arrest fracture energy for each primer treatment and condition, compared to respective control group. N/S = no significant difference; N/A = not available.

	HMR		pMDI		a-HMR	
	Dry	**Weathered**	**Dry**	**Weathered**	**Dry**	**Weathered**
Individually Bonded	+72%	+29%	-34%	N/S	N/A	N/A
Concurrently Bonded	+164%	+126%	-21%	-42%	+143%	+118%

4.4 Conclusions

Substantial changes in the moisture-cure polyurethane adhesive appear to positively impact weather survivability and variability, while simultaneously reduce overall bond performance. Nevertheless, the effects of the primer treatments are clear: the HMR treatment significantly enhances both baseline and weathered bond performance, suggesting its effectiveness as a wood primer may extend beyond its reputation as a durability promoter. The a-HMR treatment demonstrates a substantial enhancement of wood adhesion, in essentially an indistinguishable manner to HMR. This finding suggests the amount of crosslink density achievable by a-HMR is enough to enhance wood adhesion in the mode-I fracture test. Furthermore, it could be that HMR effectiveness is more dependent on its ability to form an effective network between amorphous polymer chains, rather than its ability to form a highly crosslinked synthetic network itself. In any event, a-HMR performs very well as a wood primer. The pMDI treatment exhibited no enhancement of bond performance, and actually exhibited a reduction in dry and weathered bond toughness in the concurrently-bonded specimens.

4.5 References

Blackman, B., J. P. Dear, A. J. Kinloch and S. Osiyemi. (1991) The calculation of adhesive fracture energies from double-cantilever beam test specimens. *Journal of Materials Science Letters,* 10, 253-256.

Chowdhury, S., J. Fabiyi and C. E. Frazier. (2010a) Compressive-torsion wood DMA advancing the dynamic mechanical analysis of biomass: comparison of tensile-torsion and compressive-torsion wood DMA. *Holzforschung,* In Press.

Chowdhury, S., J. Fabiyi and C. E. Frazier. 2010b: Small specimen wood rheology: a novel tool to investigate the HMR coupling mechanism. *International conference on wood adhesives*, Lake Tahoe, CA.

Christiansen, A. W. (2005) Chemical and mechanical aspects of HMR primer in relationship to wood bonding. *For. Prod. J.,* 55, 73-78.

Christiansen, A. W. and A. H. Conner. (1995) Hydroxymethylated resorcinol coupling agent for enhanced adhesion of epoxy and other thermosetting adhesives to wood. *Proceedings of a symposium sponsored by USDA Forest Service Forest Products Laboratory and The Forest Products Society,* Proceedings no. 7296, 47-55.

Crowe, D. and A. Feinberg, editors. 2001: *Design for reliability*. Boca Raton, FL: CRC Press LLC.

Fengel, D. and G. Wegener. Wood: chemistry, ultrastructure, reactions. Walter de Gruyter, Berlin,2003

Follrich, J., C. Hansmann, A. Teischinger and U. Muller. (2007) Tensile strength of a softwood butt end joints. Part 2: Improvement of bond strength by a hydroxymethylated resorcinol primer. *Wood Material Science and Engineering,* 2, 90-95.

Gagliano, J. M. An improved method for the fracture cleavage testing of adhesively-bonded wood. 2001. Virginia Tech, Blacksburg, VA

Gagliano, J. M. and C. E. Frazier. (2001) Improvements in the fracture cleavage testing of adhesively-bonded wood. *Wood and Fiber Science,* 33, 377-385.

Green, D. W., J. E. Winandy and D. E. Kretschman. Wood Handbook: wood as an engineering material. USDA Forest Products laboratory, Madison, WI,1999

Hashemi, S., A. J. Kinloch and T. G. Williams. (1990) The analysis of interlaminar fracture in uniaxial fibre-polymer composites. *Proceedings of the Royal Society of London. Series A,* 427, 173-199.

Heitner, C. and D. Atack. (1984) Dynamic mechanical properties of sulfite-treated aspen. *Paperi Puu,* 66, 84-89.

Kurt, R., A. Krause, H. Militz and C. Mai. (2008) Hydroxymethylated resorcinol (HMR) priming agent for improved bondability of wax-treated wood. *Holz Roh Werkst,* 66, 333-338.

Lopez-Anido, R., D. J. Gardner and J. L. Hensley. (2000) Adhesive bonding of eastern hemlock gluelam panels with e-glass/vinyl ester reinforcement. *For. Prod. J.,* 50, 43-47.

Lorenz, L. F. and C. R. Frihart. (2006) Adhesive bonding of wood treated with ACQ and copper azole preservatives. *For. Prod. J.,* 56, 90-93.

Pirvu, A., D. J. Gardner and R. Lopez-Anido. (2004) Carbon fiber-vinyl ester composite reinforcement of wood using the VARTM/SCRIMP fabrication process. *Composites: Part A,* 35, 1257-1265.

Sadoh, T. (1981) Viscoelastic properties of wood in swelling systems. *Wood Science and Technology,* 15, 57-66.

Sadoh, T. and E. Yamaguchi. (1968) The swelling of wood in amines and the rigidity of wood swollen with amines. *Bull. Kyoto Univ. Forest,* 40.

Salmen, L. (1984) Viscoelastic properties of *in situ* lignin under water-saturated conditions. *J. Mater. Sci.,* 19, 3090-3096.

Salmen, L. (1995) Influence of ionic groups and their counterions on the softening properties of wood materials. *Journal of Pulp and Paper Science,* 21, J310-J315.

Stamm, A. J. Wood and cellulose science. The Ronald Press, New York,1964

Tshabalala, M. A., P. Kingshott, M. R. VanLandingham and D. Plackett. (2003) Surface chemistry and moisture sorption properties of wood coated with multifunctional alkoxysilanes by sol-gel process. *Journal of Applied Polymer Science,* 88, 2828-2841.

Vick, C. B., R. L. Geimer and J. Wood, J. E. (1996) Flakeboards from recycled CCA-treated southern pine lumber. *For. Prod. J.,* 46, 89-91.

Vick, C. B. and E. A. Okkonen. (2000) Durability of one-part polyurethane bonds to wood improved by HMR coupling agent. *For. Prod. J.,* 50, 69-75.

Vick, C. B., K. Richter, B. H. River and A. R. Fried. (1995) Hydroxymethylated resorcinol coupling agent for enhanced durability of bisphenol-A epoxy bonds to sitka spruce *Wood and Fiber Science,* 27, 2-12.

5 Dynamic Mechanical Analysis of Primer-treated Red Oak

5.1 Introduction

The purpose of this study was to investigate the impact of HMR and two variations of the HMR primer on the *in situ* lignin glass transition (T_g) of red oak (*Quercus rubra*). Dynamic mechanical analysis (DMA) was employed while specimens were immersed in a wood plasticizing solvent. This submersion-mode DMA reduces the T_g to lower temperatures that avoid wood thermal decomposition. The DMA stress mode was torsion where the specimen was compressively clamped between parallel-plates. Compressive-torsion wood DMA was recently introduced and compared to the classic pendulum-torsion (or tensile-torsion) analysis (Chowdhury et al. 2010a). Compressive-torsion DMA imposes a complex stress state and produces responses that slightly differ from other more common DMA stress modes (Chowdhury et al. 2010b) During the development of compressive-torsion DMA it was discovered that HMR alters the rheological properties of southern pine (*Pinus spp*.); stiffness is enhanced, damping (peak tan δ intensity) is reduced, and the lignin T_g is significantly increased, however detection of these effects was solvent dependent (Chowdhury et al. 2010a). The HMR effect was minor in ethylene glycol, but it was very significant when dimethylformamide (DMF) was the analytical medium. Considering these observations, this work was devised to study the HMR effect in DMF plasticized red oak. Furthermore, since HMR is an effective wood primer and because it has a specific impact on the rheological properties of wood, another objective was to determine if wood primers could be more simply screened using compressive-torsion DMA in DMF. In other words, if an experimental primer elicits a wood rheological response as HMR does, will this wood treatment also enhance adhesion? This chapter addresses how the three primers impact the rheological properties of red oak.

5.2 Experimental

5.2.1 Materials

Anhydrous N-methylpyrrolidone (NMP), N,N-dimethylformamide (DMF), sodium hydroxide, resorcinol, 2-methylresorcinol, and formaldehyde (37%) were obtained from commercial suppliers and used as received. Commercial pMDI resin (Rubinate® M from Hunstman Polyurethanes, 31.2% NCO) was used as received. Knot-free red oak (*Quercus rubra*) flat-sawn, 51 mm thick, lumber was obtained from a local commercial supplier.

5.2.2 Methods

5.2.2.1 Sample Preparation

Compressive-torsion disc specimens (8 mm dia., 6mm thick) were tested in parallel-plate torsion such that the cylinder axis (thickness direction) was parallel to the torsional axis and the cylinder ends were in contact with the parallel plates. Three grain orientations were defined as RT, TR, and XL; the first letter indicates the wood surface contacting the parallel plates, perpendicular to the torsional axis (T-tangential, R-radial and X-cross sectional); the second letter indicates the grain direction parallel to the torsional axis (T-tangential, R-radial and L-longitudinal).

Control, HMR, and a-HMR treated specimens were vacuum dried (0.01-0.1 mmHg,>24 hr, room temperature) and stored in a desiccator over P_2O_5 for at least 48 hours. pMDI/NMP and corresponding control specimens were instead equilibrated to 9% moisture content by equilibration over a saturated ammonium nitrate solution (62-65% relative humidity). Prior to analysis, all DMA specimens were saturated in DMF, vacuum soaked (~5 mmHg, 30 min), followed by soaking at atmospheric pressure (room temperature, ~ 24 hours).

5.2.2.2 Primer Synthesis and Sample treatment

5.2.2.2.1 Hydroxymethyl Resorcinol (HMR)

HMR synthesis followed the literature (Vick et al. 1995) using the ingredients shown in Table 5-1. In the following order, reagents were added to a clean 250ml Erlenmeyer flask: 1) Resorcinol (3.34 g, 0.0303 moles); 2) NaOH (3M, 2.44g, 0.061 moles); 3) water (45.2 g, 2.5 moles); 4) 37% aqueous formaldehyde (3.79g, 0.047 moles); and to rinse 5) water (45.2 g, 2.5 moles). The formaldehyde to resorcinol equivalent ratio (F/R) (formaldehyde = 2 equivalents; resorcinol = 3 equivalents) was 1.03. This mixture was stirred for 4 hours (room temperature), and the resulting pH was ~8.34.

Table 5-1. Ingredients list for hydroxymethyl resorcinol synthesis.

Ingredient	% by weight	equivalents	F/R equivalent ratio
Water, distilled	90.43		1.03
Formaldehyde, 37%	3.79	(f=2) = .094	
Resorcinol	3.34	(f=3) = .0909	
3M NaOH	2.44		

Disc specimens (8 for each grain orientation) were saturated in the freshly prepared HMR solution, vacuum soaked (~0.15 mmHg, 30 min), followed by soaking at atmospheric pressure (room temperature, 5 min). The specimens were then removed from solution and allowed to air-dry under ambient conditions (16-24 hours), after which they were thoroughly cured (150°C, 1 hour). The percent weight gain due to HMR treatment was found to be ~1.5% of the original dry wood mass. Two types of control specimens were prepared: 1) "untreated" specimens, which were simply heat-treated (150°C, 1 hour) to match the thermal history of HMR specimens, and 2) "NaOH-treated" specimens, which were impregnated with aqueous NaOH (pH ~8.34) and thermally treated, all as described above for HMR treatment.

5.2.2.2.2 Alkyl Hydroxymethyl Resorcinol (a-HMR)

Alkyl HMR was prepared as described above however resorcinol was replaced with 2-methylresorcinol, 33% by mass and 30 mole %. The formaldehyde to aromatic equivalent ratio (F/(R+MeR))(2-methylresorcinol = 2 equivalents) was 1.002. As above, the mixture was stirred for 4 hours (room temperature), and the resulting pH was 8.43; this was slightly higher than the pH ~8.34 stated for HMR, but the same NaOH control treatment (pH ~8.34) was used. This could be a source of error in the results, but a ~0.09 increase in pH is not expected to significantly alter the overall impact of a-HMR.

Table 5-2. Ingredients list for alkyl hydroxymethyl resorcinol synthesis.

Ingredient	% by weight	Equivalents	F/(R+MeR) Equivalent Ratio
Water	90.43		1.002
Resorcinol	2.33	(f=3) = .0636	
2-Methylresorcinol	1.13	(f=2) = .0182	
Formaldehyde, 37%	3.33	(f=2) = .082	
3M NaOH	2.44		

Disc specimens (8 for each grain orientation) were saturated and cured as described above. The percent weight gain due to a-HMR treatment was found to be ~1.75% of the original dry wood mass. The two controls prepared for HMR comparison (untreated and NaOH-treated) were also used in a-HMR comparison.

5.2.2.2.3 Polymeric methylenebis (phenylisocyanate) in N-methylpyrrolidone

A 5 wt% solution of pMDI in NMP was prepared under anhydrous conditions using clean glassware that was flamed prior to use. Using cannulae and N_2, anhydrous NMP and pMDI were measured into graduated cylinders fitted with rubber septa. The liquids were cannula transferred

into a 250ml round bottom flask for mixing, and the solution was subsequently transferred to another 250ml round bottom flask containing the wood specimens (previously equilibrated to 9% moisture; see above). The specimens were vacuum-soaked (~0.15 mmHg, 20-30 min, room temperature), after which soaking continued at atmospheric pressure for 5 minutes. The saturated specimens were then air-dried at ambient conditions for 16-24 hours, and subsequently cured (150°C, 1 hour). Residual NMP was then removed under vacuum (0.15 mmHg, 60°C, 24 hours). The percent weight gain due to the pMDI/NMP treatment (henceforth referred to as "pMDI" or "pMDI treatment") was found to be between 9%-10% of the dry wood mass. Two types of control specimens were prepared: 1) "untreated" specimens as described above and 2) "NMP-treated" specimens were saturated in neat NMP, heated, and vacuum dried as described for the pMDI/NMP treatment. Weight change for the NMP treated specimens was not measured.

5.2.2.3 Solvent-Submersion Dynamic Mechanical Analysis

Prior to analysis, all DMA specimens were saturated in DMF, vacuum soaked (~5 mmHg, 30 min), followed by soaking at atmospheric pressure (room temperature, ~ 24 hours). DMF was used as the plasticizing solvent due to its excellent wood swelling properties; Sadoh (Sadoh 1981) previously found formamide to drastically reduce the lignin T_g (~48°C) observed using the torsion pendulum apparatus. Formamides are especially well-suited for investigating the amorphous regions of wood, as they do not cause intracellular swelling of cellulose microfibrils (Sadoh and Yamaguchi 1968).

The melting and boiling points of DMF are -61°C and 153°C, respectively. A conservative temperature range of -10°C to 80°C was therefore employed for all DMA tests – prolonged exposure to 80°C did not significantly evaporate the solvent. The flash point of DMF

is 58°C; the testing chamber was consequently purged with pure N_2 gas to prevent ignition by the exposed heating elements in the DMA oven.

Compression-torsion DMA was conducted with specimens immersed in DMF using a TA Instruments AR-2000 rheometer that was fitted with 8mm dia. parallel-plates and a stainless steel solvent cup to maintain specimen immersion. All tests were performed under anhydrous N_2 gas (flow rate 10L/min); liquid N2 was used to control temperature. Required to prevent plate slippage during analysis, specimens were maintained under a 20 N compressive force; this represents a stress of about 1.6% and 9% of red oak green compression strength parallel and perpendicular to grain, respectively (Green et al. 1999).

5.2.2.4 Determination of Linear Viscoelastic Response (LVR) limit

The LVR limit was determined using a dynamic stress sweep (10,000-70,000 Pa, 5 Hz) for all sample types (2 for each treatment/grain combination). Specimens used for LVR determination were not used for any other purpose. LVR measurements were conducted at the temperature extremes used in DMA (-10 and 80°C) as follows: 1) equilibrate -10˚C. 3 min., 2) stress sweep, 3) heat to 80˚C (3˚C/min), 3) equilibrate 80˚C. 1 min., 4) stress sweep, 5) equilibrate 80˚C, 20 min., 6) stress sweep, 7) cool to -10˚C (3˚C/min), 8) equilibrate -10˚C., 1 min., 9) stress sweep. Linear stress/strain plots were created, and the LVR limit was defined as the highest stress level that maintained the plot's correlation coefficient (r^2, for the least squares fit) above or equal to 0.9995; see Figure 5-1 for example. The static compressive load caused no interference in the LVR determination; the associated stress/strain plots were all highly linear. The lowest LVR stress limit recorded for a sample class was taken as the maximum allowable stress during temperature scans for that sample class; but an oscillation stress slightly lower than this value was generally used.

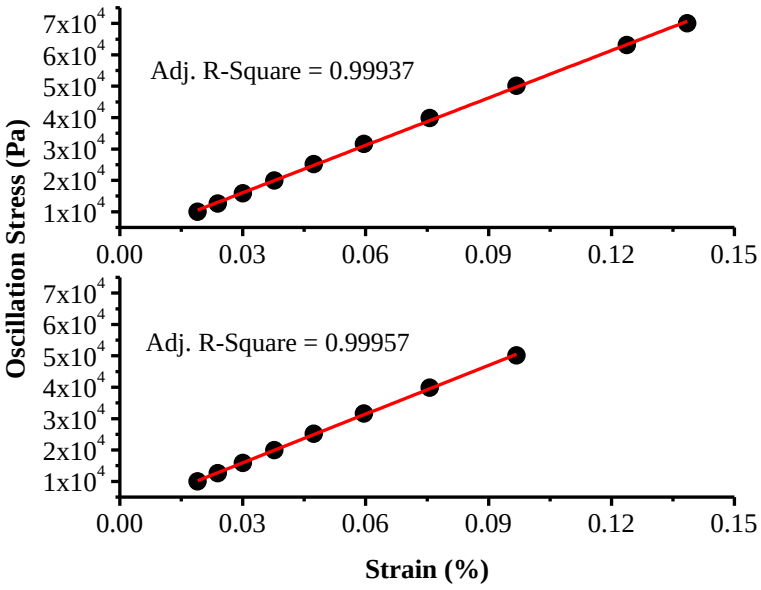

Figure 5-1. Example of LVR determination from one isothermal (80°C) stress sweep. Top: the R^2 value of the linear fit line was less than 0.9995, meaning an oscillation stress of 70,000 Pa was beyond the LVR region; Bottom: upper stress values were removed and an LVR limit was identified at 50,000 Pa.

5.2.2.5 Temperature Ramp Procedure

Specimens were subjected to sequential heating and cooling at 5 Hz (a smaller number of specimens were subjected to sequential heat/cool/heat) as follows: 1) equilibrate -10°C (2 min.), 2) heat to 80°C (3°/min), 3) equilibrate 80°C (20 min.), 4) cool to -10°C (3°/min), 5) for some specimens equilibrate -10°C (2 min.), 6) heat to 80°C (3°/min). Oscillation stresses ranged from 31,000 Pa to 70,000 Pa depending on primer treatment and grain orientation; complete documentation of the stresses and resulting percent strains for each sample group can be found in appendix D.

5.2.2.6 Data Analysis

The glass transition temperature (T_g) was defined as the maximum in the tan δ curve, and this was determined using Rheology Advantage Data Analysis (TA Instruments Ltd.) software. A light smoothing technique was employed when T_g values could not be easily discerned. Smoothed data was not used for creating average curves (see below). Average storage modulus and tan δ were created using OriginPro software, version 8.0.63; the "Average multiple curves" function was used with a tolerance of 0.5 - 3°C (1°C most commonly).

5.2.2.7 Statistical Analysis

Results obtained from all sample groups were assumed to come from normal populations. A one-way analysis of variance (ANOVA) with a significance cut-off p-value (α) of 0.10 was performed on the recorded lignin T_g values. Employing the Bonferroni method for multiple comparisons, ANOVA tests were conducted separately for each grain orientation, as well as for the same treatment across grain orientations.

5.3 Results and Discussion

Figure 5-2 shows sequential heat/cool/heat scans of a NaOH-treated specimen immersed in DMF. The first heat exhibits a softening that spans nearly one decade of storage modulus; and at a maximum temperature of 80˚C, a rubbery plateau modulus is not quite achieved. Upon cooling, the specimen exhibits a slight stiffening beyond the initial state; this has been attributed to densification under the compressive clamping force (Chowdhury et al. 2010a). The second heat generally follows the cooling response, meaning that reversibility is achieved after the first heat. This softening transition is attributed to lignin (Salmen 1984), and in this work the temperature associated with the tan δ maximum is defined as the glass transition temperature, T_g. Regarding the tan δ curve, the first heat exhibits an asymmetric peak covering the full 90˚C

temperature range. The subsequent cool exhibits a slightly narrowed transition with a significantly reduced damping intensity. Relative to the first heat, the cooling-mode T_g is 4-6˚C lower, and this is probably due to the increased swelling that occurs upon heating through the glass transition (Chowdhury et al. 2010a). The second heat tan δ closely resembles the first cool, where the T_gs differ by 1-2˚C because of kinetic effects (Chowdhury et al. 2010a). It should be pointed out that the first heat tan δ trace exhibits a faint shoulder (~10-20˚C) to the left of the tan δ maximum. Such a first-heat shoulder is often more prominent in other plasticizers such as water and ethylene glycol (Chowdhury et al. 2010a). Consistent with Chowdhury et al. (Chowdhury et al. 2010a), this first-heat shoulder is not seen in the subsequent scan, and it would perhaps reappear if the specimen were extracted to remove DMF, dried, and then reexamined using the same procedure depicted in Figure 5-2.

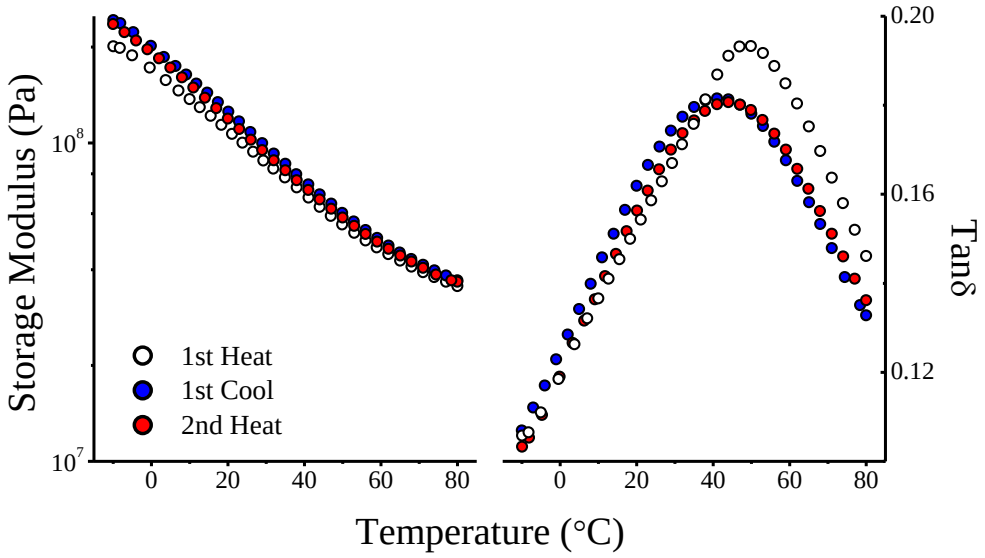

Figure 5-2. Representative DMA scans of a NaOH-treated, DMF-plasticized red oak specimen, RT orientation (3°C/min, 5Hz).

Figure 5-2 demonstrates that the red oak, lignin glass/rubber transition is clearly and easily studied in DMF. Also, apparent thermal history effects indicate that the first heat response is different from that seen in the subsequent cool and heat. Consequently, the first cool scan is optimal for studying the experimental treatments used in this work, and only the first cool data will be discussed from this point onward. The following discussion will employ first cool scans for analysis of the experimental treatments. However, all first heat curves (and when available, second heat curves) for all treatments and grain orientations can be found in appendix D.

5.3.1 Hydroxymethyl Resorcinol (HMR)

For all grain orientations, Figure 5-3 shows average DMA cooling scans for HMR-treated red oak specimens, and two controls: 1) "NaOH" treated specimens impregnated with aqueous NaOH (pH~ 8.34, as for HMR solution) and subjected to a 1hour, 150˚C thermal treatment, and 2) "untreated" specimens receiving only the 1hour, 150˚C thermal treatment, mimicking the cure imposed on HMR specimens. Considering the storage modulus as a function of grain orientation, on average it appears that HMR treatment causes a slight modulus increase, whereas the NaOH treatment causes a slight reduction. A minor grain dependency is observed, where modulus effects are more easily discerned in TR and XL specimens.

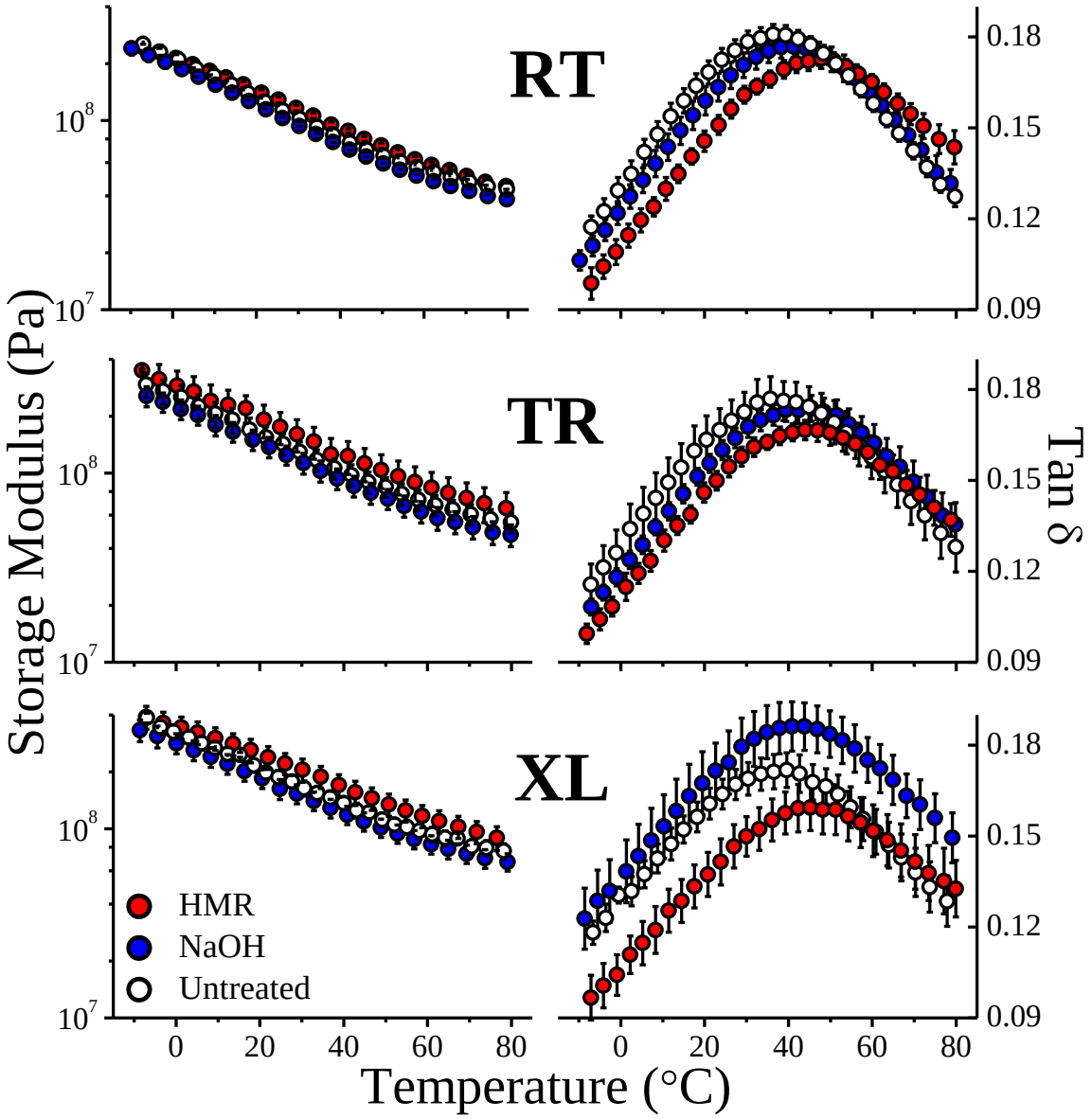

Figure 5-3. From top to bottom: Average DMA scans of HMR-treated (n=4), NaOH-treated (n=4), and untreated (n=6) RT red oak specimens; HMR-treated (n=3), NaOH-treated (n=4), and untreated (n=6) TR red oak samples; and HMR-treated (n=5), NaOH-treated (n=3), and untreated (n=5) XL red oak samples immersed in DMF (3°C/min, 5 hz; error bars represent ±1 standard deviation).

The grain dependency of HMR effects is more significant when considering the tan δ response, Figure 5-3. Regarding the tan δ intensities (damping), HMR treatment appears to reduce damping, and the effect is most significant in XL specimens. In contrast, NaOH treatment causes little or no damping change in RT and TR specimens; but in XL specimens the damping is increased relative to untreated specimens. Recall from the experimental section that these measurements were rigorously conducted within the linear response region, meaning that the damping differences are real, and are caused by chemical treatment and not by excessive stress. Figure 5-3 demonstrates that HMR and also NaOH treatments impact the lignin T_g. The mean Tgs are summarized in Figure 5-4 and also in Table 5-3. First notice that T_gs in the untreated specimens exhibit little or no grain dependency (The observation of T_g grain dependency has been highly variable, minor in some reports and significant in others (Chowdhury et al. 2010a)). After NaOH treatment, red oak specimens show no evidence of T_g grain dependency, and NaOH treatment causes a T_g increase of about 4.5˚C. After HMR treatment, red oak specimens exhibit T_gs with a clear grain dependency; and HMR treatment causes a T_g increase of about 5 – 10˚C, relative to the untreated specimens. Finally, careful inspection of Figure 5-3 reveals that HMR treatment slightly increases the breadth of the tan δ signal, and this is most noticeable in the RT specimens. In contrast, NaOH treatment appears not to impact the breadth of the tan δ response in RT or TR; but a slight broadening is apparent on the high temperature side of the XL transition. Figure 5-3 and Figure 5-4 demonstrate that HMR alters the red oak cell wall such that the storage modulus is slightly increased, the damping (tan δ intensity) is reduced, the breadth of the glass/rubber transition is slightly increased, and the T_g is significantly increased. These findings are consistent with those of Chowdhury et al. (Chowdhury et al. 2010b) using southern yellow pine, but analyzed only in one grain orientation.

However, the effects were more significant in pine, and Chowdhury's results were replicated in this study (Appendix A). Because the HMR primer is network forming, and because red oak structural polymers contain electrophiles and nucleophiles that are compatible with HMR reactivity, it seems that two or three scenarios could explain how HMR alters the DMA response. HMR monomers and dimers could penetrate the cell wall and subsequently polymerize into a network that interpenetrates amorphous wood polymers. Likewise, all wood polymers could react to form covalent attachments, although lignin is perhaps most reactive. It is also possible that both network interpenetration and covalent attachment could occur. Any of these three possibilities could be expected to reduce amorphous wood polymer flexibility such that the storage modulus and the lignin T_g are increased. While it is clear that HMR treatment impacts the red oak cell wall, associated effects not specific to methylolated resorcinol must also be considered; in this case, the alkalinity of the HMR solution deserves consideration.

The HMR solution is weakly alkaline, and alkaline water is known to have specific, and sometimes damaging effects on wood. For instance, near and above pH=8 wood swells to a degree in excess of the swelling seen at or below pH=7 (Stamm 1964). Furthermore, aqueous alkali disrupts and may dissolve hardwood xylans (Fengel and Wegener 2003); and alkaline water can cause significant strength reductions in hardwoods (Stamm 1964). However, the xylan solvation and strength reductions mentioned here are associated with high alkali levels, far in excess of that seen in HMR solutions. Nevertheless, Figure 5-3 and Figure 5-4 clearly demonstrate that the red oak cell wall is altered by aqueous NaOH (pH= 8.34, followed by heat treatment, 150˚C, 1hr). On one hand, some degree of degradation is perhaps evident in the minor stiffness loss, Figure 5-3. On the other hand, NaOH treatment causes a T_g increase, but there is little reduction in damping, and damping is actually increased in the XL specimens. Treatment

with pH=8.34 water is not expected to cause significant lignin phenol ionization; in aqueous media, phenol ionization seems to reduce the T_g (Heitner and Atack 1984; Salmen 1995) which was confirmed by Fabiyi and Frazier (2010, unpublished results). If lignin phenols were significantly ionized, it is perhaps conceivable that a T_g increase might be observed when the plasticizing medium is DMF, where phenolate solvation would be less favorable; but again phenol ionization is probably not very significant in this case. NaOH treatment could also cause saponification of ester groups on xylan, and of those between lignin and xylan; but these effects might be expected to cause a T_g reduction. It is also possible such a weakly alkaline solution could cleave both the alpha and beta-aryl ether bonds in lignin, as these are most quickly and easily cleaved during delignification using the soda (caustic) pulping process, regardless of the alkali concentration used (Fengel and Wegener 2003). However, this may be expected to lower the lignin T_g as well. In other words, it is unclear how NaOH treatment causes a T_g increase, but it seems reasonable to assume that the NaOH effects are related to the 150˚C thermal treatment that was imposed after NaOH treatment. Appendix A indicates that the NaOH treatment causes a slight T_g reduction in southern pine. Consequently, the NaOH treatment effects seen in red oak might be related to differences in lignin structure and/or the greater xylan content in red oak. In any event, the effects caused by NaOH treatment complicate the understanding of the HMR effects seen here. For instance in the TR and XL specimens, HMR treatment causes a T_g increase that is not significantly different from that seen in NaOH treated specimens (TR, $p = 0.82$; XL, $p = 0.28$). A significant difference is seen in RT specimens ($p = 0.000$, Figure 5-3), and so it seems that the grain dependency of the respective treatments is the most significant difference. Regarding T_g increases, HMR treatment shows a clear grain dependency, whereas NaOH treatment does not. Finally, recall that the HMR treatment resulted in a ~1.5% weight

gain based on the original dry wood mass, whereas the NaOH treatment caused ~0.7% weight loss. The nature of weight loss from NaOH treatment is unknown, but it is perhaps related to extractives loss as opposed to alkaline catalyzed hydrolysis - as mentioned the alkaline treatment was rather mild. Appendix D shows all pair-wise comparisons resulting from ANOVA tests.

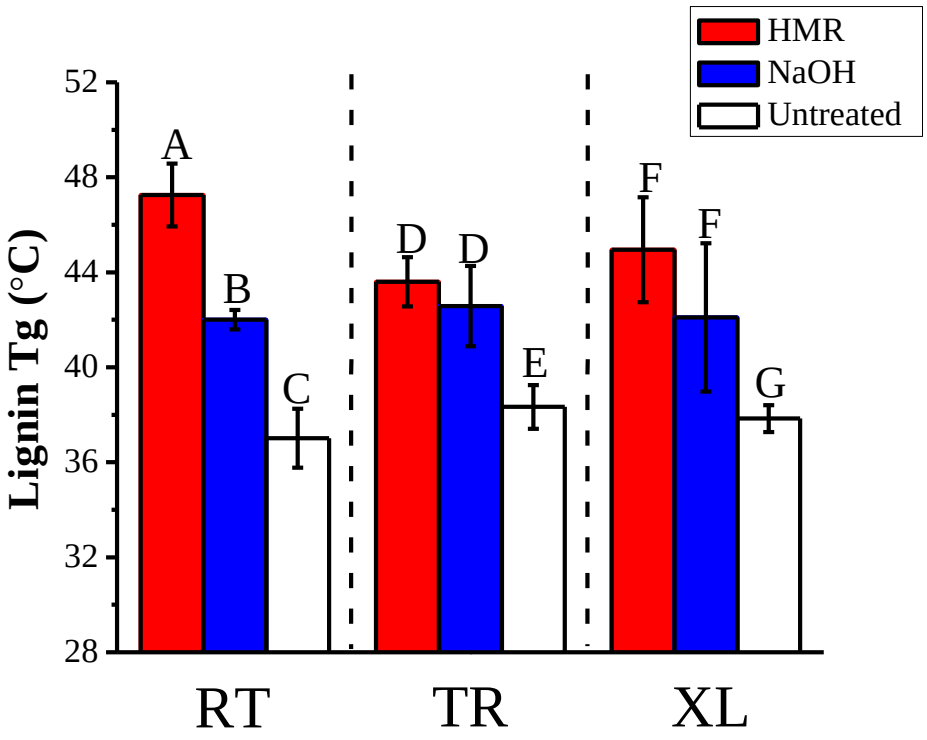

Figure 5-4. Average lignin T_g values for HMR-treated, NaOH-treated, and Untreated DMA specimens in each grain orientation (error bars represent ±1 standard deviation). Averages connected by the same letter in same grain orientation may not be significantly different (ANOVA test α=0.10).

Table 5-3. Average Lignin T_g values (°C) for HMR-treated, NaOH-treated, and untreated red oak samples in RT, TR, and XL grain orientations (± standard deviation).

Treatment	RT	TR	XL
HMR	47.3 ±1.3	43.6 ±0.5	45.0 ±1.9
NaOH	42.0 ±0.4	42.6 ±1.7	42.1 ±3.1
Untreated	37.0 ±1.2	38.3 ±0.9	37.8 ±0.6

5.3.2 Alkyl Hydroxymethyl Resorcinol (a-HMR)

For all grain orientations, Figure 5-5 shows average DMA cooling scans for alkyl HMR (a-HMR) treated red oak specimens, and two controls: NaOH treated and untreated (identical to those discussed for HMR, above). Considering the storage modulus as a function of grain orientation, a-HMR shows some impact on stiffness when compared to the untreated control, but this effect is governed by specimen orientation; a slight stiffening effect may be observed in RT and TR, while no impact is seen in the XL orientation. The NaOH treatment causes a slight reduction in stiffness across all grain orientations, as mentioned previously.

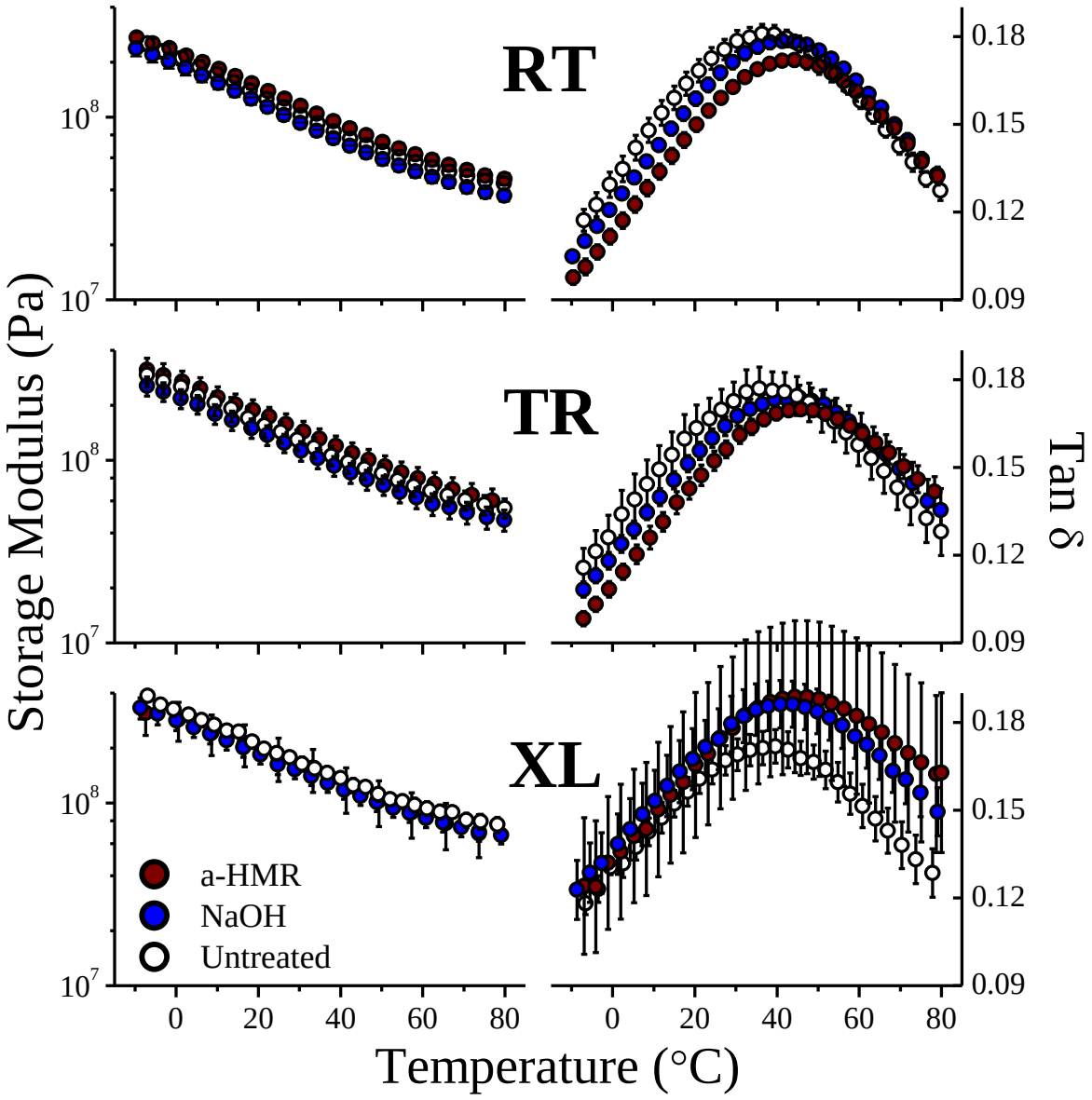

Figure 5-5. From top to bottom: Average DMA tan δ and storage modulus curves of a-HMR-treated (n=6), NaOH-treated (n=4), and untreated (n=5) RT red oak samples; a-HMR-treated (n=3), NaOH-treated (n=4), and untreated (n=6) TR red oak samples; and a-HMR-treated (n=4), NaOH-treated (n=3), and untreated (n=5) XL red oak samples immersed in DMF (3°C/min, 5 hz; error bars represent ±1 standard deviation).

The grain dependency of a-HMR effects is also observed when considering the tan δ response displayed in Figure 5-5. In RT and TR the peak tan δ intensity is reduced compared to untreated specimens; conversely, in the XL orientation the intensity is significantly increased. Additionally, a very slight broadening of the tan δ transition may be observed for a-HMR in RT and TR, while the broadening effect is very significant in XL. Recall the NaOH treatment shows little to no impact on peak intensity or breadth of transition (except in XL) in the tan δ response. Figure 5-5 also demonstrates that a-HMR impacts the lignin T_g. The mean T_gs can be found in Figure 5-6 and also in Table 5-4. Recall that HMR treatment exhibited lignin T_g grain dependency while both of the control treatments (untreated and NaOH) did not. The a-HMR treatment did not elicit a clear T_g grain dependency, but it did cause a lignin T_g increase of 6-8°C, relative to untreated specimens; this is in comparison to the ~4.5°C increase observed for the NaOH treatment.

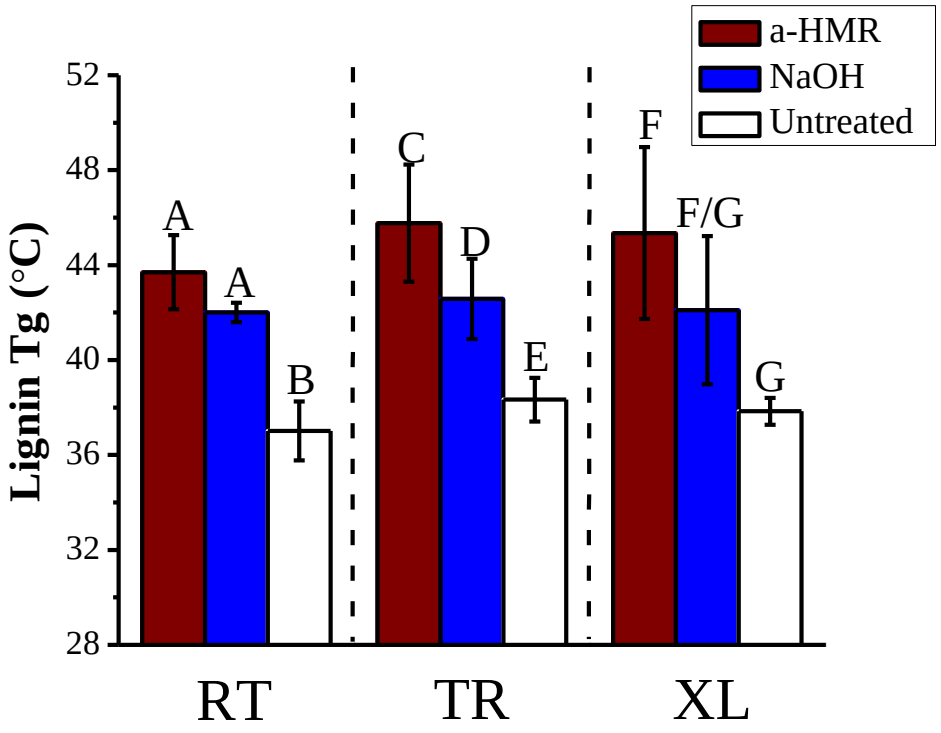

Figure 5-6. Average lignin T_g values for a-HMR-treated, NaOH-treated, and Untreated DMA specimens in each grain orientation (error bars represent ±1 standard deviation). Averages connected by the same letter in same grain orientation may not be significantly different (ANOVA test α=0.10).

Table 5-4. Average Lignin T_g values (°C) for a-HMR-treated, NaOH-treated, and untreated red oak samples in RT, TR, and XL grain orientations (± standard deviation).

Treatment	RT	TR	XL
a-HMR	43.7 ± 1.6	45.8 ± 2.5	45.4 ± 3.6
NaOH	42.0 ± 0.4	42.6 ± 1.7	42.1 ± 3.1
Untreated	37.0 ± 1.2	38.3 ± 0.9	37.8 ± 0.6

Figure 5-5 and Figure 5-6 demonstrate that a-HMR impacts the red oak cell wall such that the storage modulus is slightly increased and tan δ damping is reduced in the RT and TR orientation; the breadth of the glass transition is slightly increased, displaying the greatest effect in XL; and the T_g is significantly increased. Overall, these results were similar to those observed for the HMR treatment. The a-HMR treatment may be impeding cell wall polymer mobility through covalent bonding with wood, or through molecular interpenetration, or through both effects as described previously. However, as was done for the HMR treatment, the inherent effect of solution alkalinity must be considered. The a-HMR treatment only shows a significant increase in T_g over the NaOH treatment in the TR orientation ($p = 0.074$); recall HMR exhibited a significant increase in T_g over NaOH in the RT orientation. This further demonstrates how the alkalinity of the HMR and a-HMR treatments complicates the observed impact on T_g in red oak. When directly comparing the effects of HMR and a-HMR treatment shown in Figure 5-3 and Figure 5-5, respectively, it is observed that the tan δ responses exhibit very similar peak intensities in the RT and TR orientations (identical at 0.172 in RT; 0.170 for a-HMR compared to 0.167 for HMR in TR); in contrast, the a-HMR treatment shows a significant increase in damping in the XL orientation, while HMR shows a reduction. The T_g increase for the respective treatments is comparable, but slightly greater for HMR; a-HMR exhibits a 6-8°C T_g increase over that of untreated specimens, compared to a 5-10°C increase for HMR. So while there are similarities between the impact of HMR and a-HMR treatments in DMA, there are also points of difference, as mentioned above. These changes in rheology may be related to the difference in crosslink densities between the two treatments.

Recall that the 30% replacement of resorcinol with 2-methylresorcinol was found to reduce the effectiveness of HMR as a wood primer in the ASTM D 2559 delamination test, and

this was attributed to a reduction in crosslink density (Christiansen 2005). It is important to note, however, that the reduction in HMR effectiveness documented by Christiansen (Christiansen 2005) was not very dramatic; the HMR treatment reduced percent delamination of the wood-adhesive laminate samples to below 5%, while a-HMR yielded delamination values of 6-8% (down from 50% observed in unprimed wood (Christiansen 2005)). In other words, the a-HMR treatment is clearly beneficial to bond performance, indicating that a-HMR treatment could also be expected to cause a change in the wood rheological response.

5.3.3 Polymeric methylenebis(phenylisocyanate) in N-methylpyrrolidone ("pMDI")

For all grain orientations, Figure 5-7 shows average DMA cooling scans for pMDI treated red oak specimens, and two controls: 1) "NMP" treated specimens impregnated with NMP and subjected to a thermal treatment (150°C, 1 hr, followed by 0.15 mmHg, 60°C, 24 hours); and 2) "untreated" specimens receiving only the 150˚C thermal treatment. Considering the storage modulus, the pMDI treatment appears to have no significant impact on stiffness. This is surprising, as recall the pMDI treated specimens showed a 9-10% increase in weight compared to dry wood weight, compared to 1.5% and 1.8% for HMR and a-HMR treatments, respectively. With this large mass increase, one might expect the pMDI monomers, dimers, and some oligomers to have fully penetrated and reacted within the cell wall, resulting in some form of stiffness enhancement. Moreover, the NMP, XL control specimens exhibit a stiffness increase that is not observed in the pMDI sample group. This is perplexing, as NMP has no crosslinking capabilities.

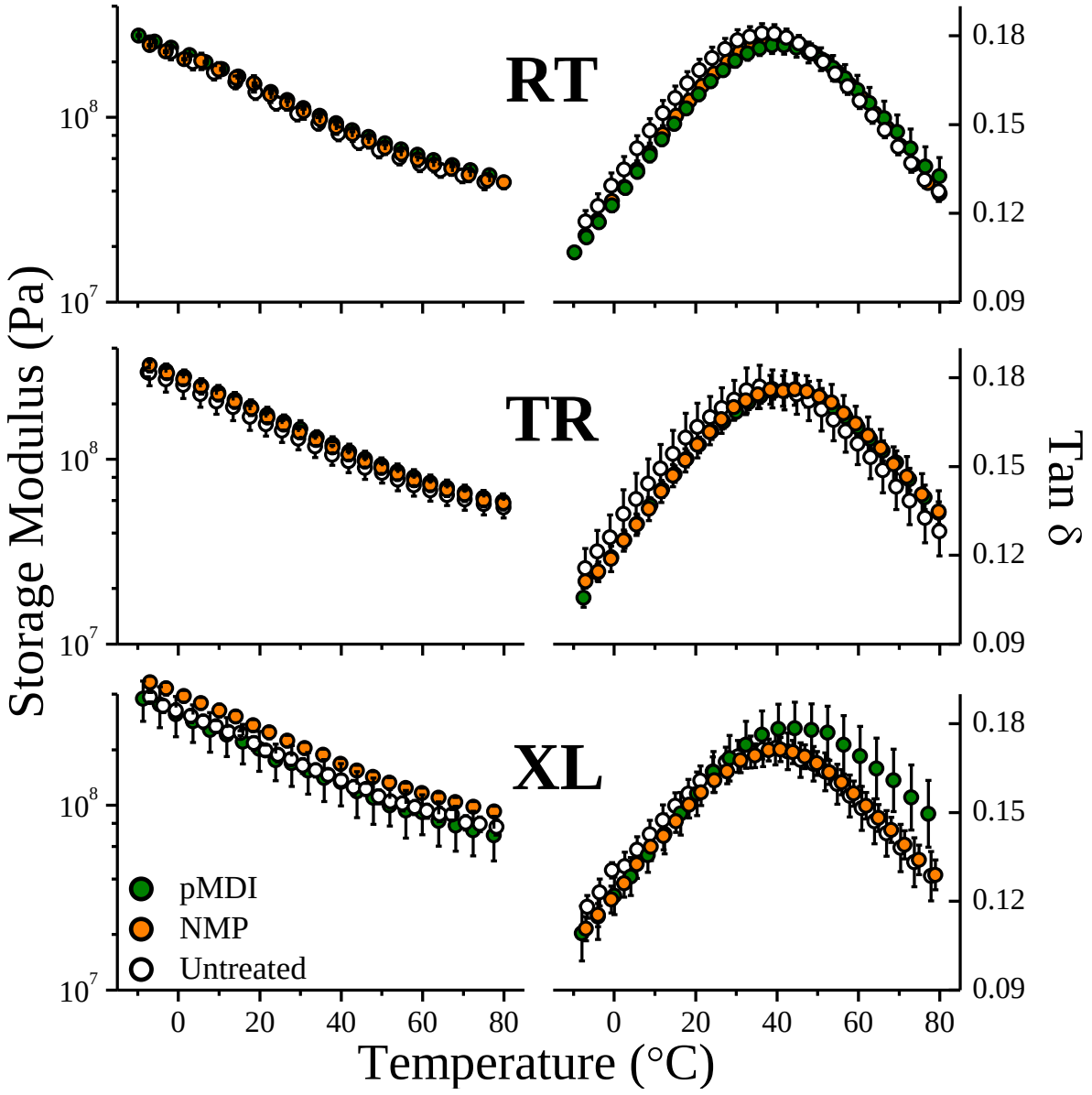

Figure 5-7. From top the bottom: Average DMA tan δ and storage modulus curves of pMDI-treated (n=3), NMP-treated (n=5), and untreated (n=6) RT red oak samples; pMDI-treated (n=4), NMP-treated (n=5), and untreated (n=6) TR red oak samples; and pMDI-treated (n=4), NMP-treated (n=3), and untreated (n=5) XL red oak samples immersed in DMF (3°C/min, 5 hz; error bars represent ±1 standard deviation).

The pMDI treatment causes grain dependency effects as illustrated by the tan δ response displayed in Figure 5-5. For RT specimens, both the pMDI and neat NMP treatments slightly reduce the peak tan δ intensity compared to untreated specimens. Also for RT and TR specimens, pMDI and neat NMP treatments result in tan δ curves that are essentially identical, and which are slightly different from those seen in untreated specimens. In contrast, pMDI and neat NMP treatments elicit clearly different responses in the XL orientation; neat NMP causes a minor overall change, while pMDI treatment significantly increases the T_g and also broadens the relaxation. Figure 5-7 demonstrates that both the pMDI and neat NMP treatments impact the lignin T_g. The mean T_gs are summarized in Figure 5-8 and also in Table 5-5. First recall that the untreated specimens exhibited no T_g grain dependency; after NMP treatment, a 2-4°C T_g increase occurs and this exhibits grain dependency. The pMDI treatment caused a 4-6°C T_g increase also with grain dependency (but grain effects differ from those seen in the neat NMP treatment). Lastly, recall that both HMR and a-HMR treatments caused a slight increase in the breadth of the glass transition viewed in the tan δ curve. Neither the PMDI nor NMP treatment appears to impact the breadth of the transition in the RT or TR orientations; the pMDI treatment broadens the transition in the XL orientation.

Figure 5-7 and Figure 5-8 demonstrate that the pMDI treatment has a complex effect on the red oak cell wall polymers: the treatment does not significantly impact specimen storage modulus, it has a slight impact on the peak tan δ intensity and breadth of transition, and it significantly increases the lignin T_g. However, the impact of pMDI itself can be elucidated further by considering the effect of the neat NMP treatment. The NMP treatment is found to significantly increase the lignin T_g in all grain orientations; this complicates interpretation of the pMDI treatment results. For instance, RT and TR specimens exhibit similar T_g increases

resulting from both pMDI and neat NMP treatments. In the XL orientation, however, the pMDI treatment demonstrates a T_g increase beyond that resulting from the neat NMP treatment ($p = 0.010$). Regarding the NMP treatment, it is unclear why such T_g increases would occur. However, it is known that NMP is capable of dissolving organic wood extractives, as well as some carbohydrates and polyhydroxy compounds (Tshabalala et al. 2003); a loss in storage modulus or reduction in lignin T_g might therefore be predicted, but neither is observed. Alternatively, the removal of extractives and other non-structural polymers may introduce void space, allowing amorphous wood polymers to more thoroughly compact and associate during the 150°C heat treatment, during which time the polymers are mobile. Ultimately, it is unclear why NMP treatment causes these effects, but this certainly prevents the simple interpretation of the pMDI treatment results.

In comparison to the HMR treatment, the pMDI treatment demonstrates little similarity in changes in rheological properties. pMDI demonstrates a consistently higher peak tan δ intensity across all grain orientations, no impact on stiffness, and little to no impact on breadth of transition. The magnitude of T_g increase is also different: pMDI shows a 4-6°C increase, while HMR shows a 5-10°C compared to untreated specimens.

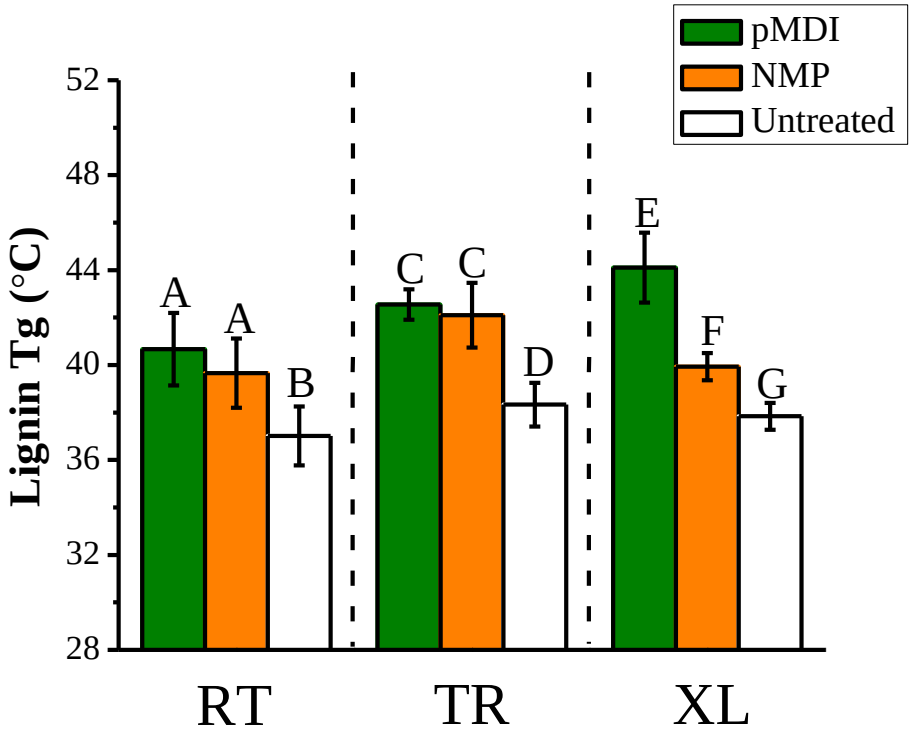

Figure 5-8. Average lignin T_g values for pMDI-treated, NMP-treated, and Untreated DMA specimens in each grain orientation (error bars represent ±1 standard deviation). Averages connected by the same letter in same orientation may not be significantly different (ANOVA test α=0.10).

Table 5-5. Average Lignin T_g values (°C) for pMDI-treated, NMP-treated, and untreated red oak samples in RT, TR, and XL grain orientations (± standard deviation).

Treatment	RT	TR	XL
pMDI	40.7 ± 1.5	42.6 ± 0.6	44.1 ± 1.5
NMP	39.7 ± 1.5	42.1 ± 1.4	39.9 ± 0.6
Untreated	37.0 ± 1.2	38.3 ± 0.9	37.8 ± 0.6

Table 5-6 shows the average increase in T_g due to primer/control treatments (compared to the untreated control group) across grain orientations. Averaged across all grain orientations, HMR and a-HMR both cause a significant T_g increase (~ 7°C), which is greater than the average T_g increase resulting from the NaOH treatment (< 5°C). Furthermore, neat NMP and pMDI treatments cause a modest average T_g increase (also less than 5°C). In chapter 4 it was shown that both HMR and a-HMR improved wood adhesion, whereas pMDI treatment did not. Consequently, it might be feasible to screen for effective wood primers by testing for average T_g increases that exceed 5°C. However, perhaps such a screening process is cumbersome if it requires the analysis of every grain orientation. It would be far simpler if a single grain orientation could be employed to screen for effective wood primers. For instance, the RT orientation is most sensitive according to HMR treatment results, but not so for a-HMR. Perhaps an effective screening criterion could be a T_g increase of 5°C or more in either RT or TR grain orientations. Likewise, perhaps XL specimens should not be used for screening since the pMDI treatment causes a 6°C increase for these specimens; and as demonstrated in Figure 5-3, Figure 5-5, and Figure 5-7, XL specimens exhibit the greatest degree of DMA response variation. Another screening criterion could be a significant reduction in peak tan δ intensity in RT or TR; both HMR and a-HMR exhibit very similar, decreased peak tan d intensities in these grain orientations. More testing may be needed to further develop the primer screening criteria. In any event, it seems that red oak does not lend itself to a clear and definitive procedure for screening priming agents. In contrast, it seems that the screening process might be easier for softwoods like southern pine - recall that Appendix A shows that NaOH treatment has little effect on the southern pine T_g, while the HMR treatment exhibits a tremendous increase (>30°C).

Table 5-6. Change in T_g (°C) due to primer/control treatments for each grain orientation.

Orientation	NaOH	HMR	a-HMR	NMP	pMDI
RT	+5	+10.3	+6.7	+2.7	+3.7
TR	+4.3	+5.3	+7.5	+3.8	+4.3
XL	+4.3	+7.2	+7.6	+2.1	+6.3
Average	**+4.5**	**+7.6**	**+7.3**	**+2.9**	**+4.8**

5.4 Conclusions

HMR appears to alter the red oak cell wall such that the stiffness of the material is increased, the peak tan δ intensity (damping) is reduced, the breadth of the transition is slightly broadened, and the lignin T_g is significantly increased. These findings are consistent with those of Chowdhury et al. (Chowdhury et al. 2010b) using southern yellow pine, although they are less acute. These findings indicate that HMR restricts amorphous cell wall polymer mobility; it is hypothesized that the small HMR molecules penetrate the cell wall and either 1) covalently bond with the amorphous wood polymers; 2) form an interpenetrating network; or 3) participate in both effects. The NaOH control complicates the T_g effect observed in red oak; even so, HMR is shown to significantly increase T_g over that of the NaOH treatment in the RT grain orientation.

The a-HMR treatment displays similar changes in rheological properties compared to HMR, but the effects are not the same; this may be related to a-HMR's reduction in crosslink density. As in HMR, the NaOH treatment complicates the impact of a-HMR treatment on T_g; a significant increase in T_g over the NaOH treatment was only observed in TR. Additionally, the magnitude of T_g increase for a-HMR treatment is similar to that of the HMR treatment (6-8°C compared to 5-10°C, respectively).

The pMDI treatment causes subtle changes in rheological properties; these are significantly complicated by the neat NMP control treatment, as a significant increase in T_g over

NMP is only observed in XL; additionally, the NMP treatment appears to dominate the DMA response in both RT and TR. With respect to magnitude of T_g increase, the pMDI treatment exhibits a consistently lower impact across grain orientations (4°C-6°C).

Lastly, an effective criterion for screening potential wood primers in DMA was proposed: a chemical treatment which causes a reduction in peak tan δ intensity and an increase in T_g (>5°C) in either the RT or TR grain orientation may enhance wood adhesion.

5.5 References

Chowdhury, S., J. Fabiyi and C. E. Frazier. (2010a) Compressive-torsion wood DMA advancing the dynamic mechanical analysis of biomass: comparison of tensile-torsion and compressive-torsion wood DMA. *Holzforschung,* In Press.

Chowdhury, S., J. Fabiyi and C. E. Frazier. 2010b: Small specimen wood rheology: a novel tool to investigate the HMR coupling mechanism. *International conference on wood adhesives*, Lake Tahoe, CA.

Christiansen, A. W. (2005) Chemical and mechanical aspects of HMR primer in relationship to wood bonding. *For. Prod. J.,* 55, 73-78.

Fengel, D. and G. Wegener. Wood: chemistry, ultrastructure, reactions. Walter de Gruyter, Berlin,2003

Green, D. W., J. E. Winandy and D. E. Kretschman. Wood Handbook: wood as an engineering material. USDA Forest Products laboratory, Madison, WI,1999

Heitner, C. and D. Atack. (1984) Dynamic mechanical properties of sulfite-treated aspen. *Paperi Puu,* 66, 84-89.

Sadoh, T. (1981) Viscoelastic properties of wood in swelling systems. *Wood Science and Technology,* 15, 57-66.

Sadoh, T. and E. Yamaguchi. (1968) The swelling of wood in amines and the rigidity of wood swollen with amines. *Bull. Kyoto Univ. Forest,* 40.

Salmen, L. (1984) Viscoelastic properties of *in situ* lignin under water-saturated conditions. *J. Mater. Sci.,* 19, 3090-3096.

Salmen, L. (1995) Influence of ionic groups and their counterions on the softening properties of wood materials. *Journal of Pulp and Paper Science,* 21, J310-J315.

Stamm, A. J. Wood and cellulose science. The Ronald Press, New York,1964

Tshabalala, M. A., P. Kingshott, M. R. VanLandingham and D. Plackett. (2003) Surface chemistry and moisture sorption properties of wood coated with multifunctional alkoxysilanes by sol-gel process. *Journal of Applied Polymer Science,* 88, 2828-2841.

Vick, C. B., K. Richter, B. H. River and A. R. Fried. (1995) Hydroxymethylated resorcinol coupling agent for enhanced durability of bisphenol-A epoxy bonds to sitka spruce *Wood and Fiber Science,* 27, 2-12.

6 Correlation of DMA and Mode-I Fracture Results

In chapter 5 it was shown that each of the primer treatments (HMR, a-HMR, pMDI) exhibited a specific rheological impact on red oak; stiffness, breadth of tan δ transition, peak tan δ intensity (damping) and lignin T_g were generally found to be grain dependent. In Chapter 4 it was shown that both the HMR and a-HMR treatments dramatically improved wood adhesion; conversely, the pMDI treatment resulted in a reduction in bond performance. HMR and a-HMR therefore behaved as effective wood primers, while the pMDI treatment did not.

Using this information, criteria were developed to relate primer efficacy to how a primer alters wood rheology; these were based on rheological changes which were observed in HMR and a-HMR treated specimens, but not in either control (NaOH, NMP) or pMDI treatment. Two effective criteria for the screening of potential wood primers using DMA were thus proposed: if a chemical treatment causes a >5°C increase in lignin T_g and a reduction in peak tan δ intensity in the RT and TR grain orientation, it may act as an effective wood primer. The two rheological properties mentioned previously, stiffness and breadth of transition, may also play a role in the screening process; but with the current primers and wood species evaluated, a clear correlation to bond performance was not observed.

7 Conclusions

In DMA, a correlation was found based on rheological data that peak tan δ intensity (damping) and lignin T_g were the most sensitive to primer effects. However, these properties were grain dependent: for HMR treatment, the change in lignin T_g (ΔT_g) was much greater in RT than either TR or XL. For a-HMR, grain dependency was not observed for ΔT_g, but damping was reduced in TR and RT while increased in the XL grain orientation. For the pMDI treatment, both properties increased dramatically in XL. Based on this information, a correlation could be made between a primer treatment's response in DMA and its impact on bond toughness measured in mode-I fracture. HMR and a-HMR treatment were found to dramatically improve fracture performance overall, enhancing both baseline (unweathered) and weathered bond toughness; alternatively, the pMDI treatment was found to negatively impact wood adhesion. Comparing these results to each primer's DMA response, it was observed that only HMR and a-HMR treatmentscaused a 5°C increase in ΔT_g and a reduction in damping in both RT and TR grain orientations; these observations were thus suggested as criteria for screening potential wood primers in DMA.

The results from DMA suggest that HMR is restricting amorphous wood polymer mobility; the small reactive HMR molecules are likely penetrating into the wood cell wall and either 1) covalently bonding; 2) forming an interpenetrating network; or 3) participating in both effects with the amorphous wood polymers. a-HMR is likely participating in these same effects, however at a lower crosslink density; but this is clearly not inhibiting its ability to enhance wood adhesion. This suggests that the level of crosslink density is not very important for HMR effectiveness as observed in the mode-I fracture test; its impact is likely related to its general ability to form a crosslinked network and/or react with amorphous wood polymers inside the cell

wall. While not seen in fracture performance, this difference in crosslink density appears to be observed in DMA: the treatments exhibit similar effects in RT and TR, but differences in XL are clear. Additionally, ΔT_g differences between RT and TR further suggest a crosslink density effect.

8 Suggested Future Work

- The NaOH and NMP treatments uniquely impacted wood rheology; these treatments should be tested as wood primers using the mode-I fracture test, and their results compared to those of the HMR, a-HMR, and pMDI treatments.
- Develop and study potential wood primers in DMA and mode-I fracture to further investigate relationship between test methods;
- Use southern pine for these investigations, as HMR exhibits a clearer difference in rheological response compared to NaOH control in this wood species.
- Investigate correlation between ASTM D 2559 delamination test and mode-I fracture test by testing DCBs weathered with the ASTM delamination test, or designing delamination specimens to match DCB grain orientation;
- It is within the ASTM standard guidelines to bond laminates with a 3° grain angle, forming a "V" shape along the bondline, as in the mode-I fracture specimens;
- Further correlation between mode-I fracture and the delamination test may be elucidated by running both tests side by side.
- Use alternative reagents to resorcinol such as 4-methylresorcinol (the 4-position on the resorcinol monomer is substantially more reactive than the 2-position) or phenol (a substantially less reactive and less expensive reagent than resorcinol) to further investigate effect of crosslink density in HMR;
- If effective, phenol substitution would also aid in economizing the HMR treatment.

9 APPENDICES

Appendix A

Species Dependence of HMR treatment in DMA

The effect of HMR treatment on southern yellow pine (*Pinus spp.*) was studied using compression-torsion DMA while specimens were submersed in DMF.

Materials

SYP lumber was obtained from a local softwood distributor and used as received. Materials related to HMR primer synthesis were used in this study and are documented in Chapter 5.

Method

Sample preparation

SYP compressive-torsion disc specimens (8 mm dia., 6mm thick, RT grain orientation) were prepared and tested as outlined in Chapter 5.

HMR, sodium hydroxide (pH = ~8.34) and untreated sample groups were prepared as described in Chapter 5.

Temperature Ramp Procedure

SYP specimens were subjected to sequential heating, cooling, and second heating at 5 Hz as follows: 1) equilibrate -10°C (2 min.), 2) heat to 80°C (3°/min), 3) equilibrate 80°C (20 min.), 4) cool to -10°C (3°/min), 5) equilibrate -10°C (2 min.), 6) heat to 80°C (3°/min). The oscillation stress used for all specimens was 50,000 Pa.

Determination of Linear Viscoelastic Region (LVR)

The LVR limit was determined using a dynamic stress sweep (5,000-200,000 Pa, 5 Hz) for HMR and Untreated specimens. Specimens used for LVR determination were not used for any other purpose. LVR measurements were conducted at the temperature extremes used in DMA (-10 and 80°C), as well as at an intermediate temperature (50°C), as follows: 1) equilibrate -10˚C. 3 min., 2) stress sweep, 3) heat to 50˚C, unregulated 4) equilibrate 50˚C. 3 min., 5) stress sweep, 6) heat to 80˚C, unregulated 7) stress sweep, 8) equilibrated 80˚C. 3 min., 9.) stress sweep, 10.) equilibrate 80˚C. 20 min., 11.) stress sweep, 12.) cool to 50˚C, unregulated 13) equilibrate 50˚C. 3 min., 14) stress sweep, 15) cool to -10˚C, unregulated 16) equilibrate -10˚C. 3 min., 17) stress sweep. Linear stress/strain plots were created, and the LVR limit was defined as the highest stress level that maintained the plot's correlation coefficient (r^2, for the least squares fit) above or equal to 0.9995.

Due to such high stress values (200,000 Pa) used in the LVR procedure, the specimen was likely stressed outside of its LVR region in the first stress sweep, invalidating the results of subsequent sweeps. Additionally, only one HMR-treated and untreated specimen was tested, not 2 or 3 as in Chapter 5; no NaOH-treated specimens were tested. Previous work found oscillation stresses of 30,000-40,000 Pa to be in the LVR range for HMR-treated, NaOH-treated, and untreated RT-oriented SYP specimens submersed in DMF (Chowdhury et al. 2010). However, the findings of this study correlate well with those documented by Chowdhury, suggesting the 50,000 Pa oscillation stress used in this study may still be within the LVR region, or only slightly outside of it.

Results

Figure 9-1 shows the average cooling scans of HMR-treated, NaOH-treated, and untreated RT-oriented SYP specimens in DMA (first and second heat scans can be found at the end of this appendix). The HMR treatment significantly increases the lignin glass transition (T_g), defined as the peak in the tan δ curve, in SYP. The HMR-treated specimens do not reach lignin T_g within the temperature range (>80˚C), while the NaOH-treated and untreated specimens show average lignin T_gs of 46.2˚C ± 2˚C and 51.4˚C ± 1.5˚C, respectively. This ~30˚C increase in lignin T_g as a result of HMR treatment is in sharp contrast to the ~5-10˚C increase observed in red oak. Additionally, this ~5°C drop in T_g due to NaOH treatment is in contrast to the ~4.5°C increase observed in red oak.

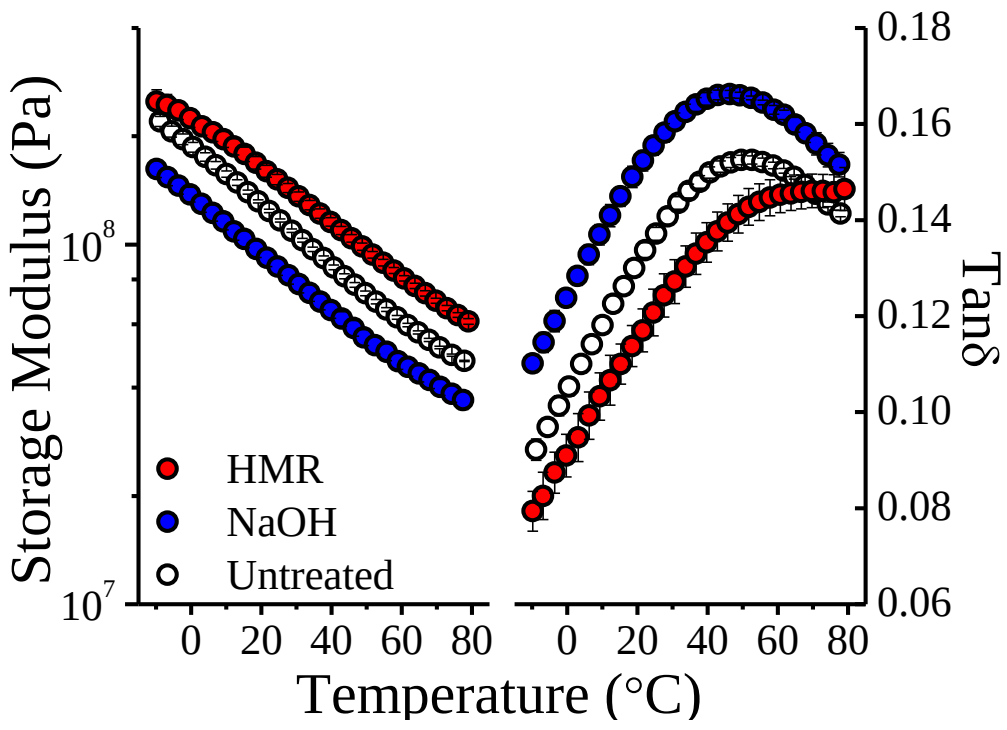

Figure 9-1. Average cooling scans of HMR-treated, NaOH-treated, and Untreated (n = 3) RT SYP specimens submersed in DMF (3°C/min, 5 hz; error bars represent ±1 standard deviation).

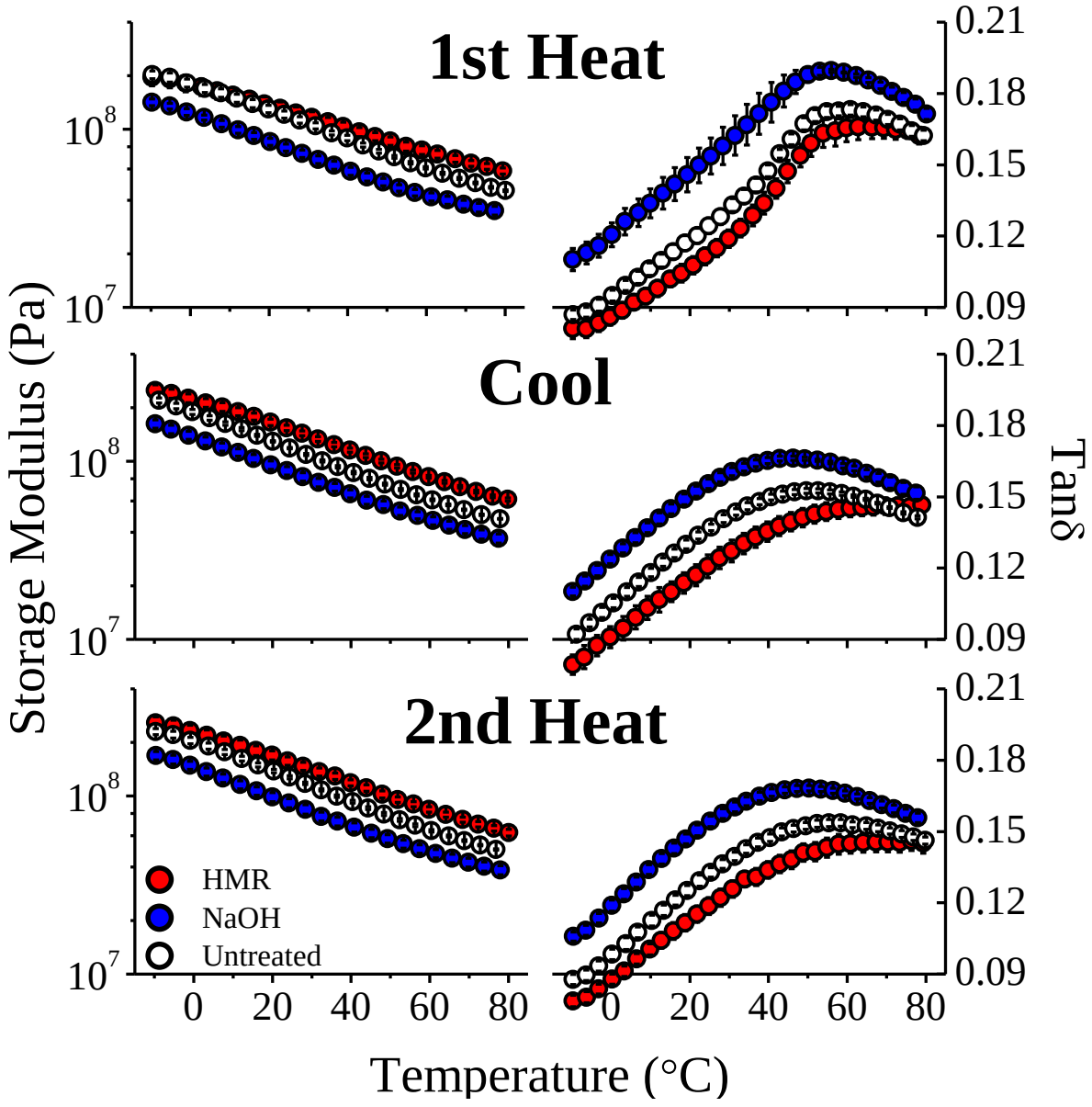

Figure 9-2. Average DMA tan δ and storage modulus curves for each thermal scan (first heat, cool, second heat) of HMR-treated, NaOH-treated, and untreated (n=3) RT SYP samples immersed in DMF (3°C/min, 5 hz; error bars represent ±1 standard deviation).

Appendix B

Polyaniline-treated Wood

Southern yellow pine (*Pinus spp.)* was treated with polyaniline, a known electrically conductive polymer. Two methods were investigated: vacuum impregnation and brush application. In the case of brush application, two methods of polyaniline polymerization were employed: direct application and interfacial polymerization.

Materials

Aniline, ammonium peroxydisulfate, 1M hydrochloric acid (HCl), and toluene were obtained from commercial suppliers and used as received. Southern yellow pine (SYP) lumber was obtained from a local softwood distributor and used as received.

Methods

Sample Preparation

Vacuum Impregnation

SYP compressive-torsion disc specimens (8 mm dia., 6mm thick, TR grain orientation) were vacuum-impregnated (~1 mmHg, 1 hr) with aniline. Specimens were then vacuum-dried (~1 mmHg, 5 min) over analytical wipes to remove excess aniline from wood lumens. Specimens were vacuum-impregnated again (~1mmHg, 30-60 min) with an initiator solution (0.8 mmol ammonium peroxydisulfate per 10 ml 1M HCl) which initiates polymerization. The vacuum was removed and specimens continued to soak (10 min, ambient conditions). Specimens were removed from solution and placed in distilled water (60 min, water replaced after 30 min), after which they were vacuum dried (~1 mmHg, >24 hr). After treatment, samples

appeared dark blue to black in color. After drying, specimens were sputter coated (7nm-thick, gold-palladium) and observed in a LEO (Zeiss) 1550 field emissions scanning electron microscope.

Brush Application

Two methods of polyaniline synthesis were investigated: direct application (DA), in which aniline and a doping acid are mixed and then directly reacted with a polymerization initiator (ammonium peroxydisulfate)-doping acid solution; and interfacial polymerization (IP), in which aniline and an organic solvent are mixed and then added to the initiator-acid solution, with polymerization occurring at the interface of the two mixtures. Both methods were adjusted to use the wood surface as the polymerizing interface.

Direct Application

Two solutions were prepared:

1.) 3.2 mmol aniline per 10 ml 1M HCl, with stirrer bar;

2.) 0.8 mmol ammonium peroxydisulfate (initiator) per 10 ml 1M HCl.

Solution 1 was applied to the tangential-radial plane of a freshly sanded SYP block and allowed to dry (24 hr, ambient conditions). Solution 2 was applied to the wood surface every 30 minutes until a dark green hue was observed (approx. 90 min). The specimen was then fully dried, moistened prior to microtoming, dried again and then sputter coated (7 nm-thick, gold-palladium) for observation in a LEO (Zeiss) 1550 field emissions scanning electron microscope (FESEM).

Interfacial Polymerization

Two solutions were prepared:

1.) 3.2 mmol aniline per 10 ml toluene, with stirrer bar;

2.) 0.8 mmol ammonium peroxydisulfate (initiator) per 10 ml 1M HCl.

Solution 1 was applied to the tangential-radial plane of a freshly sanded SYP block (7 in. x 4 in.) and allowed to dry (24 hr, ambient conditions). Solution 2 was applied to the wood surface every 30 minutes until a dark green hue was observed (approx. 120 min). The specimen was then fully dried, moistened prior to microtoming, dried again and then sputter coated (7 nm-thick, gold-palladium) for observation in a LEO (Zeiss) 1550 field emissions scanning electron microscope (FESEM).

Results

Tangential surface of polyaniline-treated SYP (Vacuum Impregnation)

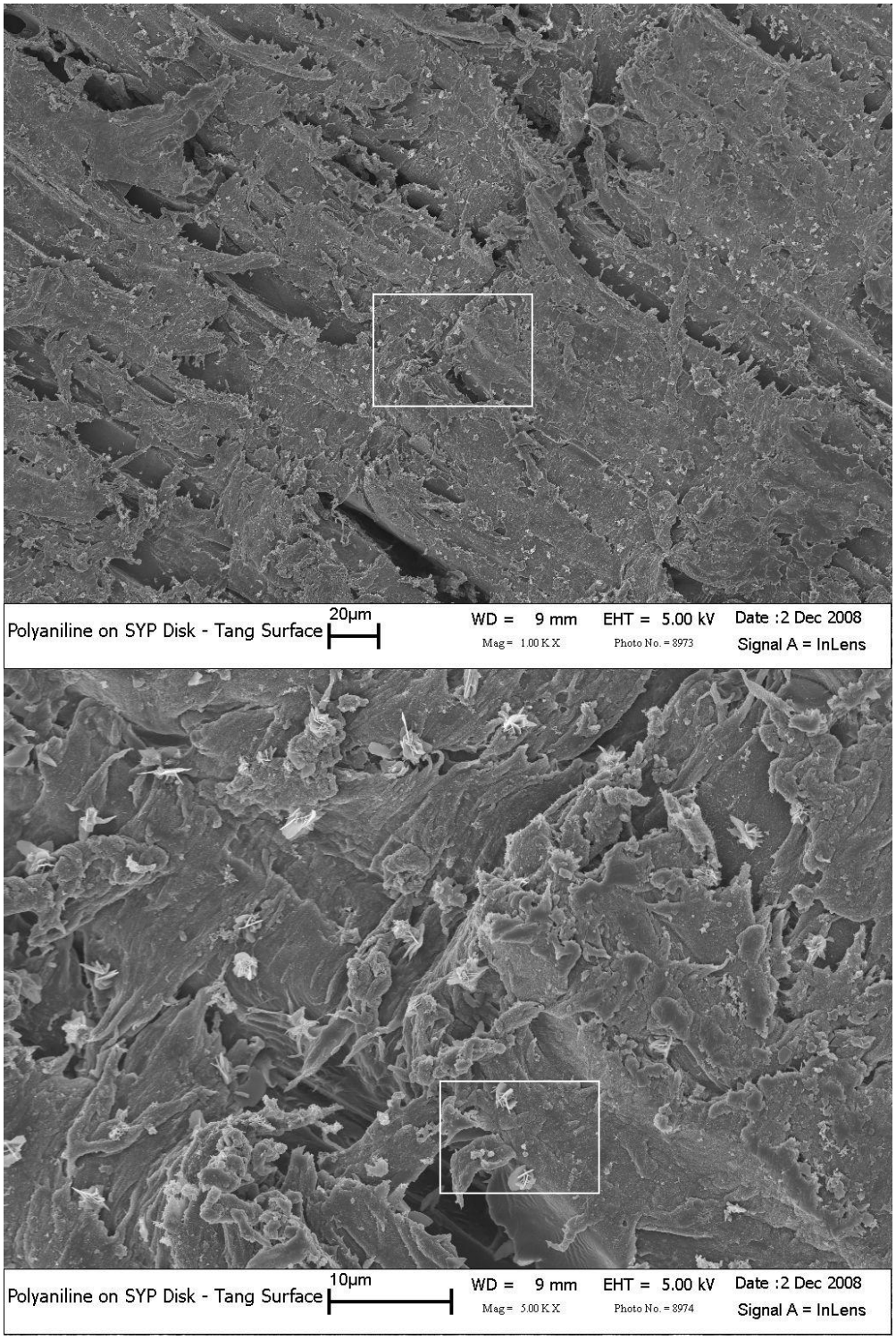

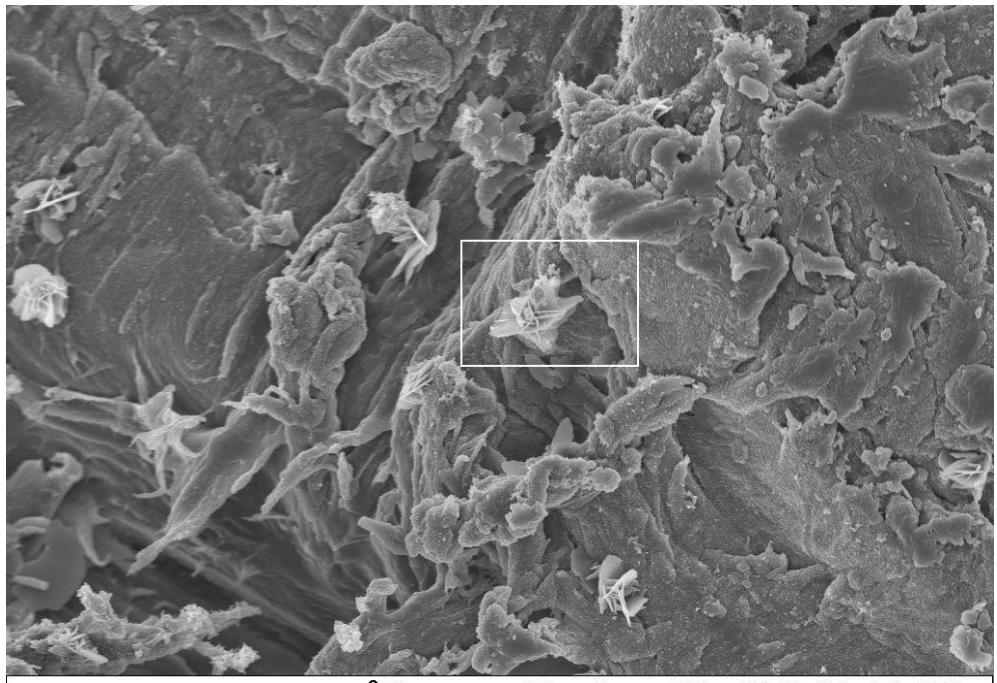
Polyaniline on SYP Disk - Tang Surface
2µm
WD = 9 mm
EHT = 5.00 kV
Date :2 Dec 2008
Mag = 10.00 K X
Photo No. = 8975
Signal A = InLens

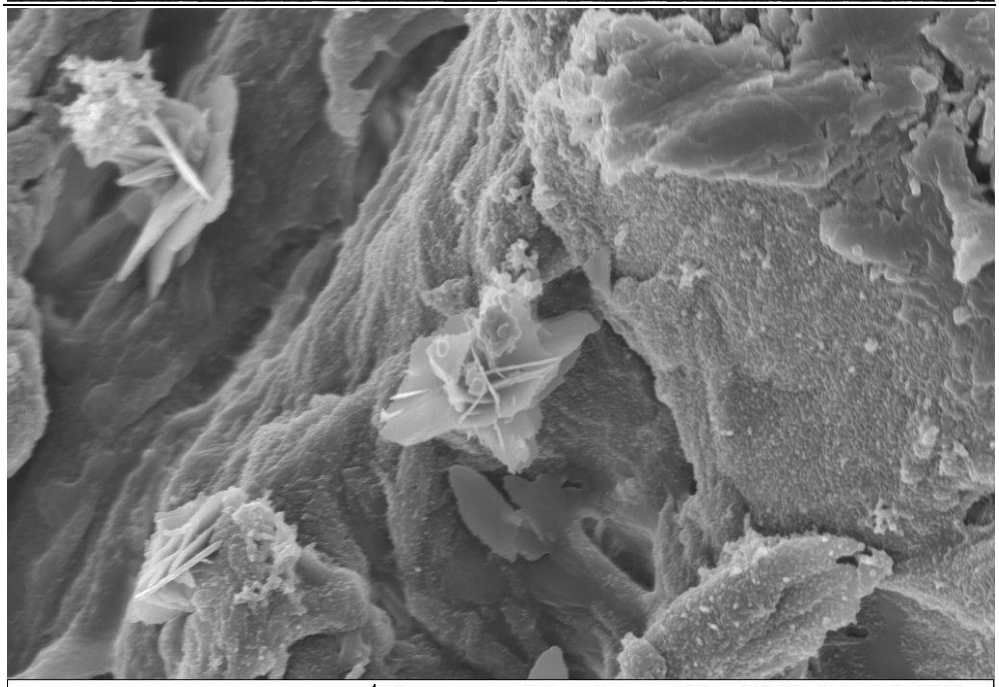
Polyaniline on SYP Disk - Tang Surface
1µm
WD = 9 mm
EHT = 5.00 kV
Date :2 Dec 2008
Mag = 25.00 K X
Photo No. = 8976
Signal A = InLens

Tangential-radial surface of polyaniline-treated SYP (Direct Application)

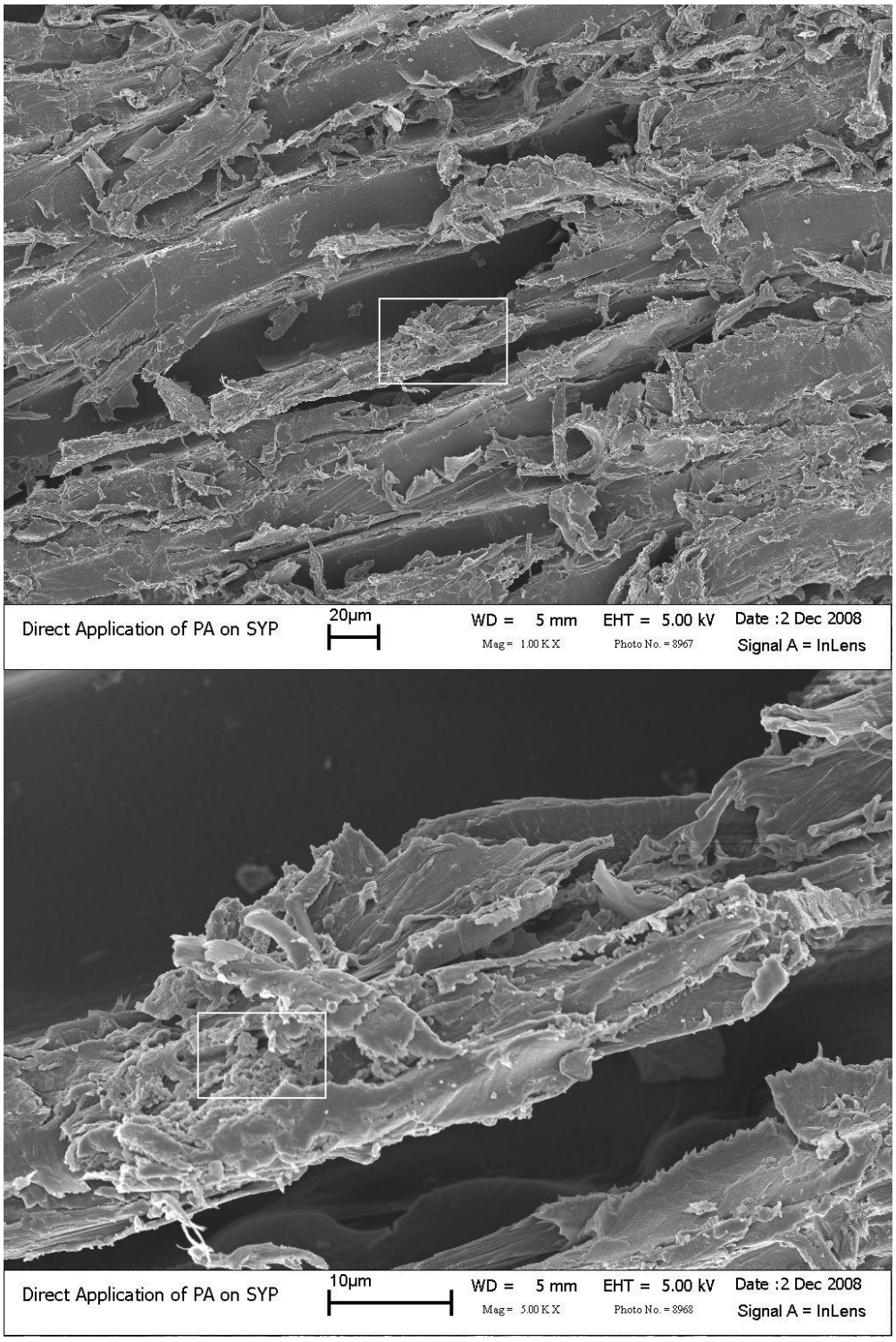

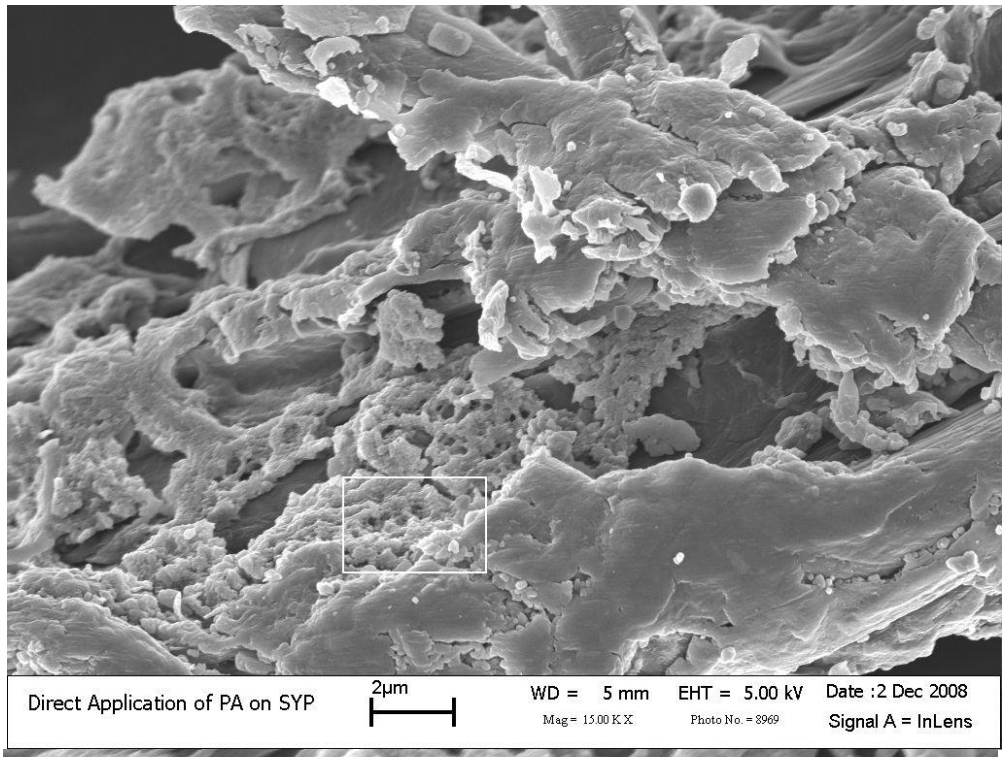
Direct Application of PA on SYP
2µm
WD = 5 mm
EHT = 5.00 kV
Date :2 Dec 2008
Mag = 15.00 K X
Photo No. = 8969
Signal A = InLens

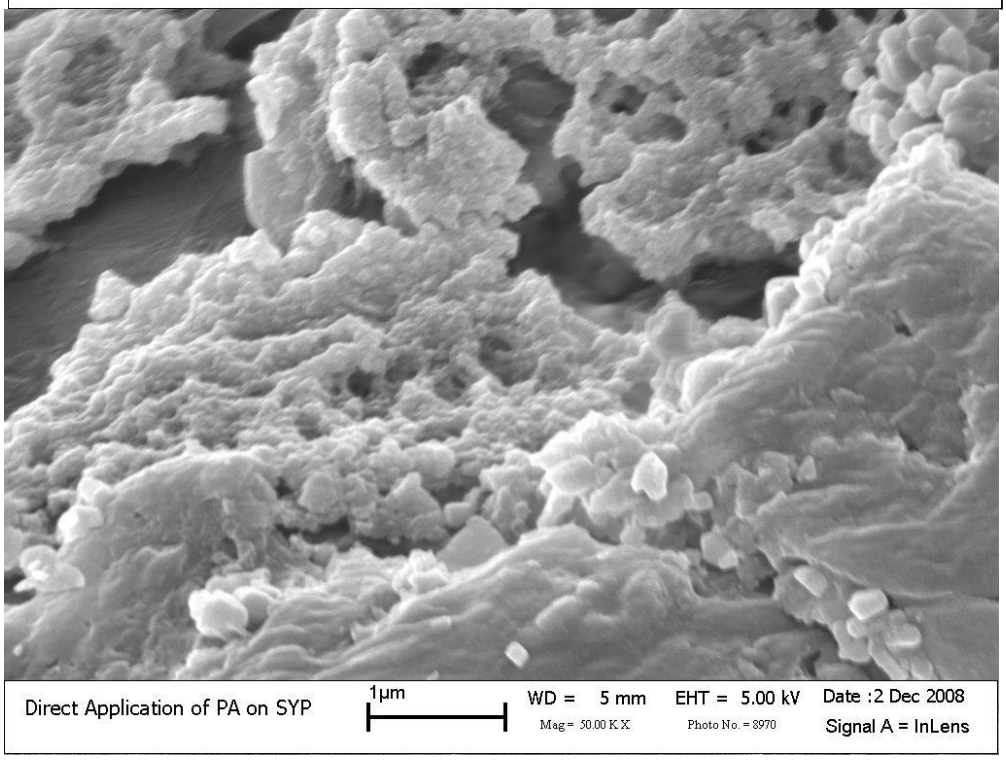
Direct Application of PA on SYP
1µm
WD = 5 mm
EHT = 5.00 kV
Date :2 Dec 2008
Mag = 50.00 K X
Photo No. = 8970
Signal A = InLens

Tangential-radial surface of polyaniline-treated SYP (Interfacial Polymerization)

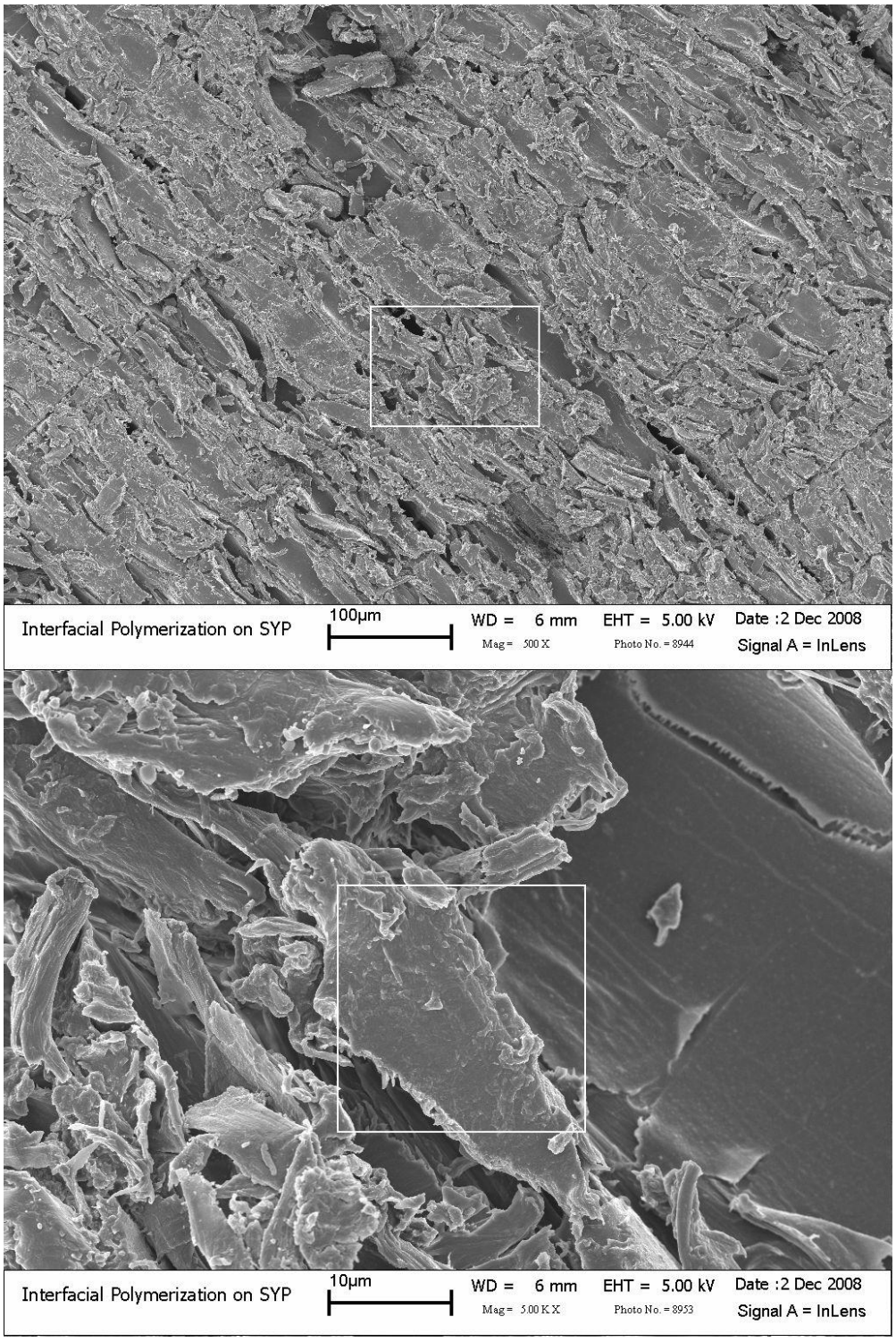

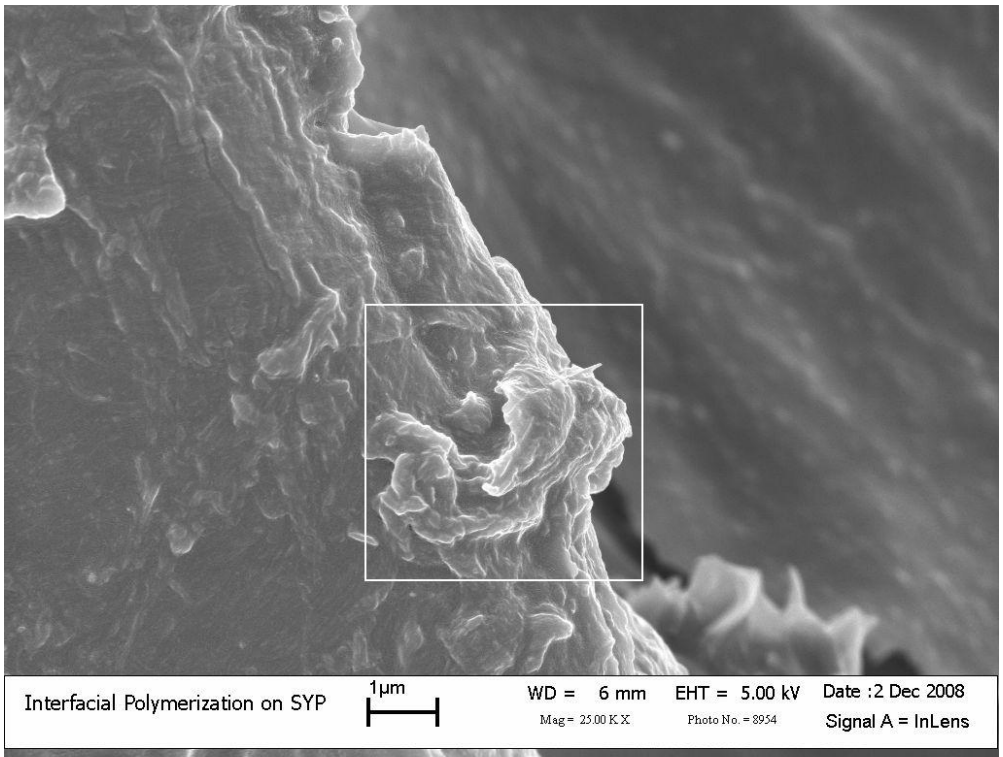
Interfacial Polymerization on SYP
1µm
WD = 6 mm
EHT = 5.00 kV
Date :2 Dec 2008
Mag = 25.00 K X
Photo No. = 8954
Signal A = InLens

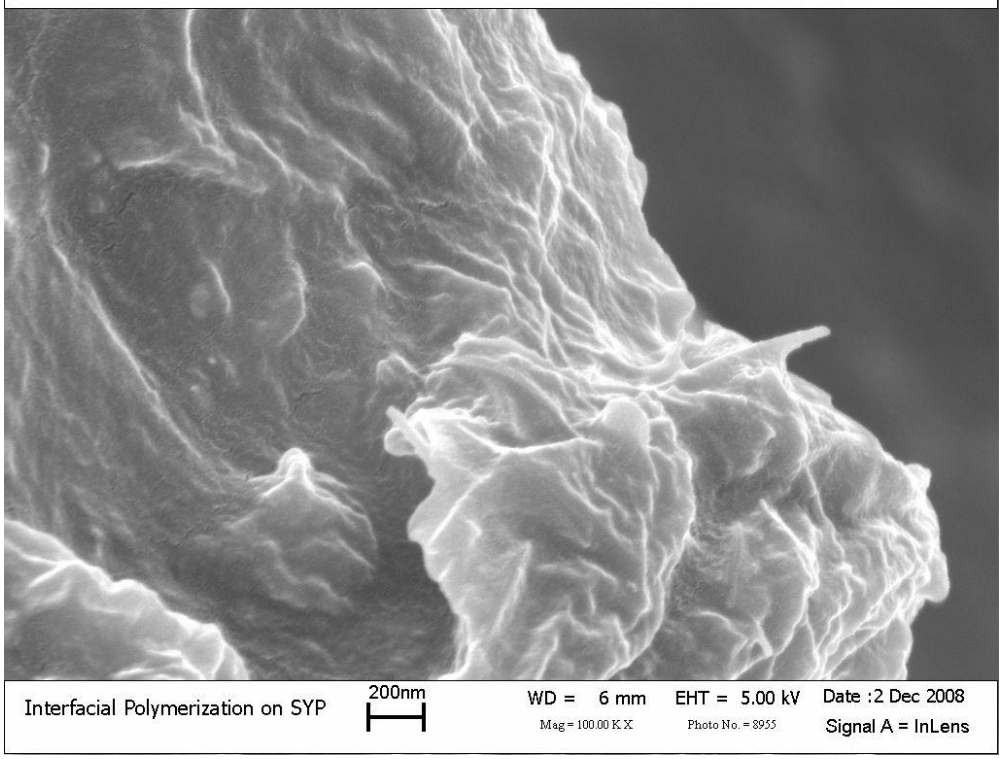
Interfacial Polymerization on SYP
200nm
WD = 6 mm
EHT = 5.00 kV
Date :2 Dec 2008
Mag = 100.00 K X
Photo No. = 8955
Signal A = InLens

Appendix C

Supplementary Data – Chapter 4

Table 9-1. P-values from t-tests performed between critical energies of unweathered primer treatments and control (untreated) ($\alpha = 0.05$); Concurrently-bonded specimens.

Unweathered			
Treatment	a-HMR	HMR	pMDI
Untreated	0.000	0.000	0.034

Table 9-2. P-values from t-tests performed between arrest energies of unweathered primer treatments and control (untreated) ($\alpha = 0.05$); Concurrently-bonded specimens.

	Unweathered		
Treatment	a-HMR	HMR	pMDI
Untreated	0.000	0.000	0.012

Table 9-3. P-values from t-tests performed between critical energies of unweathered and weathered primer treatments and control ($\alpha = 0.05$); Concurrently-bonded specimens.

		Weathered			
	Treatment	a-HMR	HMR	Untreated	pMDI
Unweathered	a-HMR	0.355	---	---	---
	HMR	---	0.090	---	---
	Untreated	---	---	0.377	---
	pMDI	---	---	---	0.001

Table 9-4. P-values from t-tests performed between arrest energies of unweathered and weathered primer treatments and control (α = 0.05); Concurrently-bonded specimens.

		Weathered			
	Treatment	a-HMR	HMR	Untreated	pMDI
Unweathered	a-HMR	0.104	---	---	---
	HMR	---	0.785	---	---
	Untreated	---	---	0.105	---
	pMDI	---	---	---	0.006

Table 9-5. P-values from t-tests performed between critical energies of weathered primer treatments and control (untreated) (α = 0.05); Concurrently-bonded specimens.

Weathered			
Treatment	a-HMR	HMR	pMDI
Untreated	0.000	0.000	0.000

Table 9-6. P-values from t-tests performed between arrest energies of weathered primer treatments and control (untreated) (α = 0.05); Concurrently-bonded specimens.

Weathered			
Treatment	a-HMR	HMR	pMDI
Untreated	0.000	0.000	0.000

Appendix D

Supplementary Data – Chapter 5

The following pages show the average storage modulus and tan δ curves for the first and (when available) second heats for each of the primer treatments and grain orientations. Additionally, p-values from all means comparisons performed in Chapter 5 can be found in Tables 9-7 through 9-10. Stress and strain values from the stress sweeps performed for all treatments and grain orientations can also be found in Tables 9-11 through 9-13.

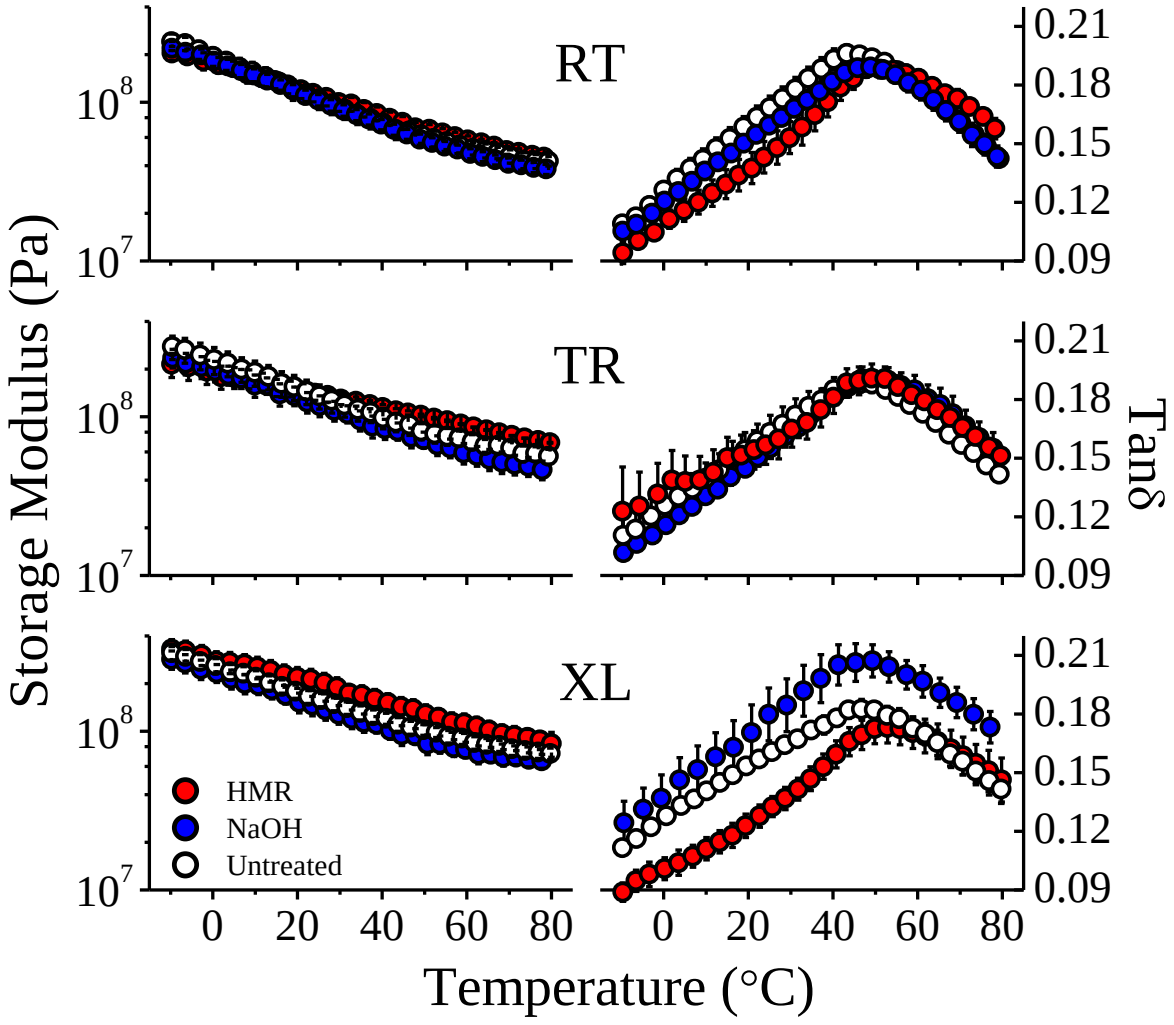

Figure 9-3. First heat. From top to bottom: Average/single DMA scans of HMR-treated (n=4), NaOH-treated (n=4), and untreated (n=6) RT red oak specimens; HMR-treated (n=2), NaOH-treated (n=4), and untreated (n=5) TR red oak samples; and HMR-treated (n=5), NaOH-treated (n=3), and untreated (n=5) XL red oak samples immersed in DMF (3°C/min, 5 hz; error bars represent ±1 standard deviation).

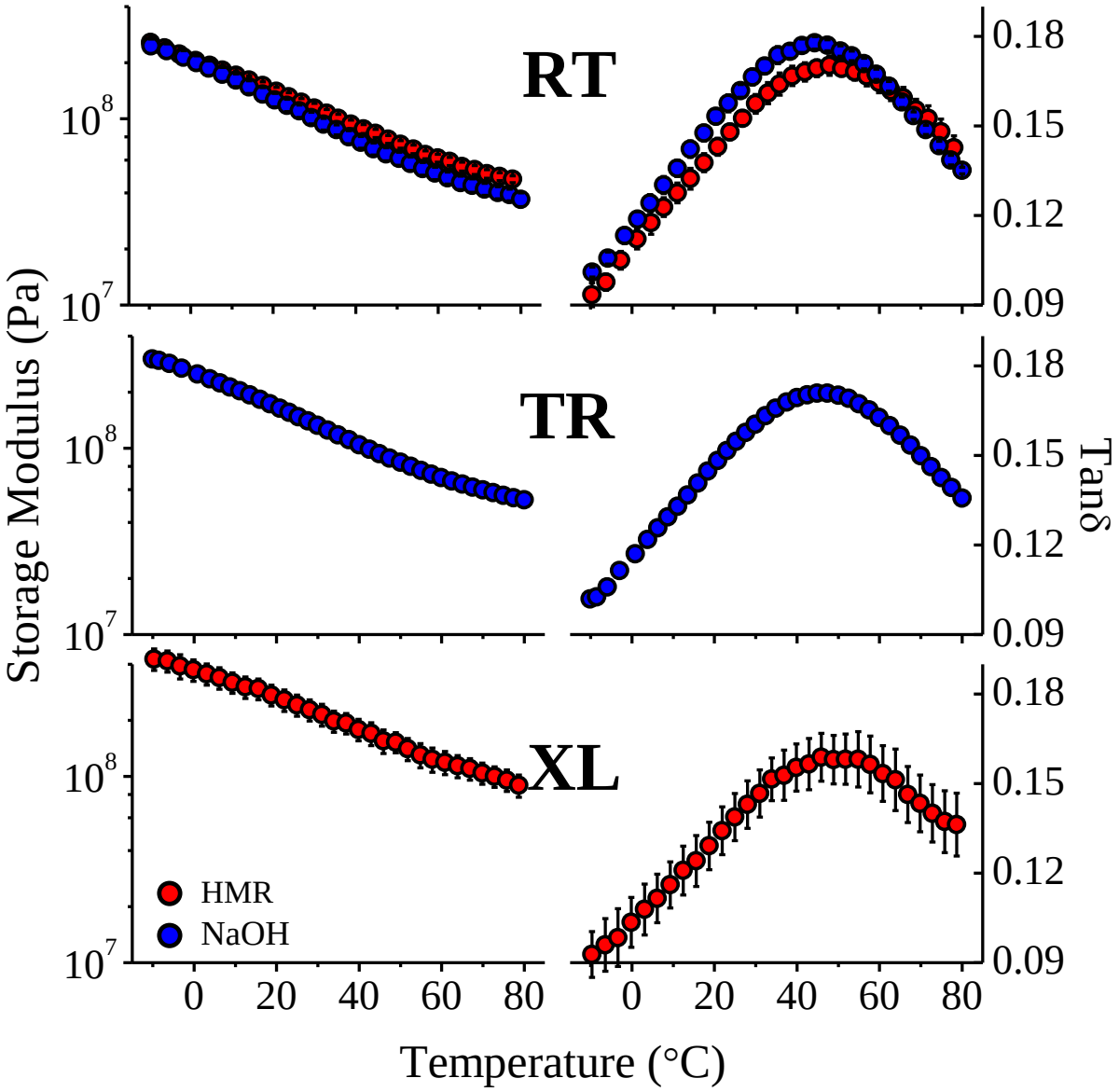

Figure 9-4. Second heat. From top to bottom: Average/single DMA scans of HMR-treated (n=3) and NaOH-treated (n=4) RT red oak specimens; NaOH-treated (n=1) TR red oak sample; and HMR-treated (n=5) XL red oak samples immersed in DMF (3°C/min, 5 hz; error bars represent ±1 standard deviation).

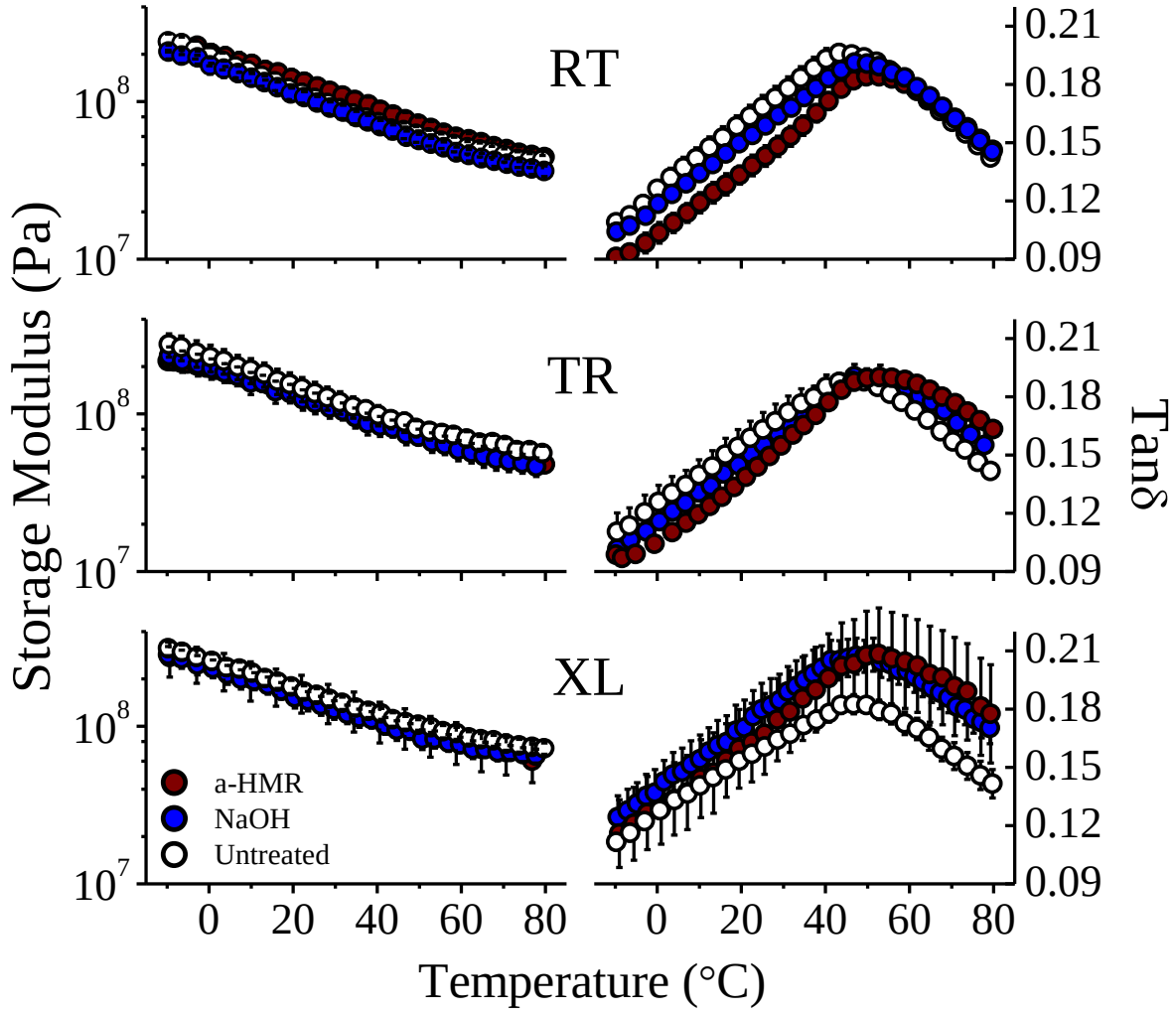

Figure 9-5. First heat. From top to bottom: Average DMA tan δ and storage modulus curves of a-HMR-treated (n=5), NaOH-treated (n=4), and untreated (n=5) RT red oak samples; a-HMR-treated (n=1), NaOH-treated (n=4), and untreated (n=6) TR red oak samples; and a-HMR-treated (n=4), NaOH-treated (n=3), and untreated (n=5) XL red oak samples immersed in DMF (3°C/min, 5 hz; error bars represent ±1 standard deviation)

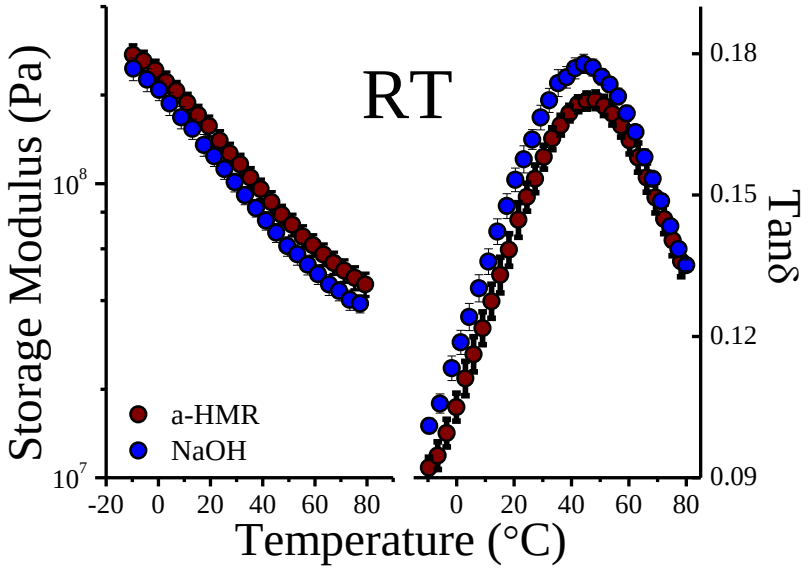

Figure 9-6. Second heat. Average DMA tan δ and storage modulus curves of a-HMR-treated (n=5) and NaOH-treated (n=4) red oak samples immersed in DMF (3°C/min, 5 hz; error bars represent ±1 standard deviation)

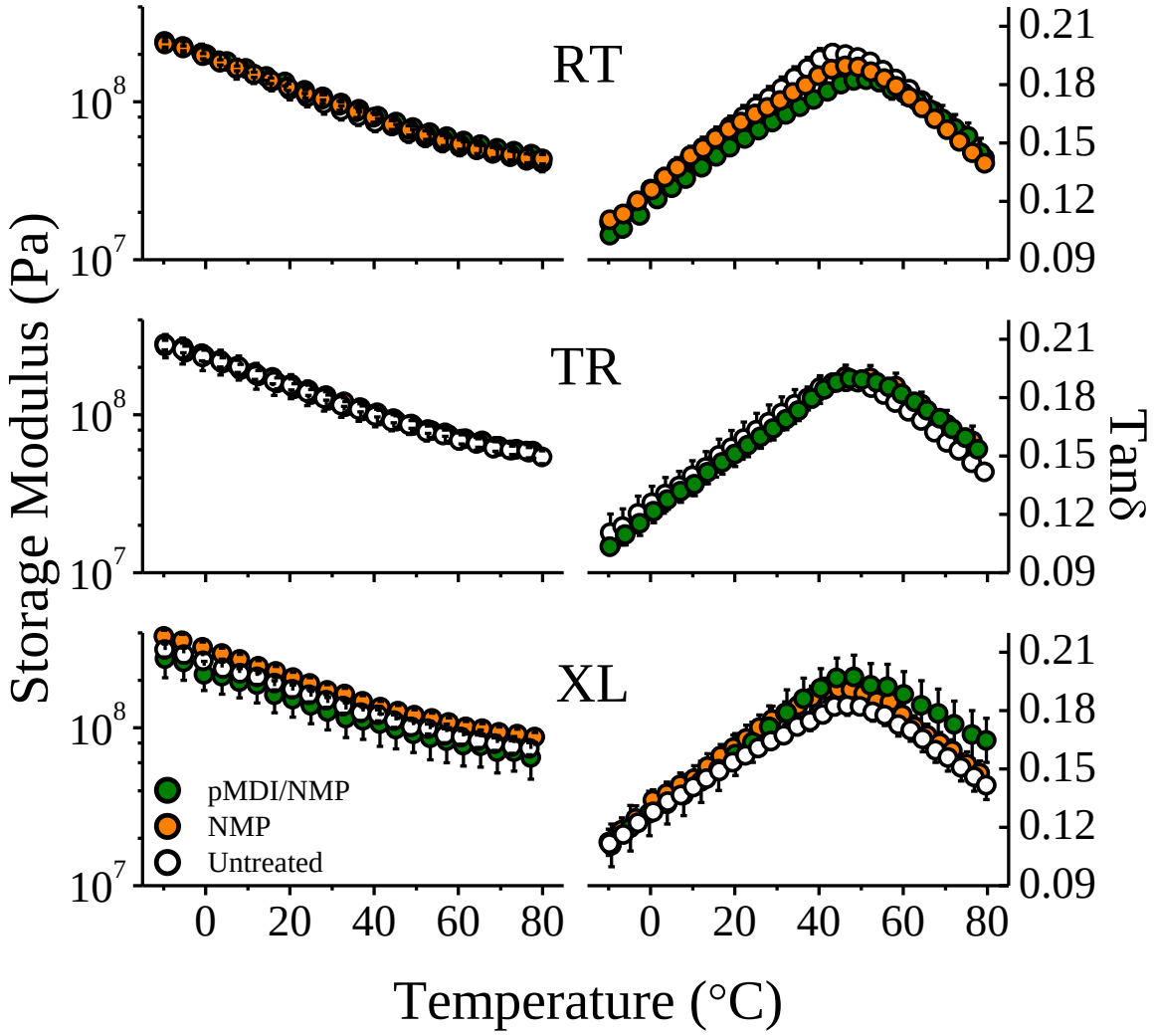

Figure 9-7. First heat. From top the bottom: Average DMA tan δ and storage modulus curves of pMDI-treated (n=2), NMP-treated (n=5), and untreated (n=6) RT red oak samples; pMDI-treated (n=4), NMP-treated (n=5), and untreated (n=5) TR red oak samples; and pMDI-treated (n=4), NMP-treated (n=3), and untreated (n=5) XL red oak samples immersed in DMF (3°C/min, 5 hz; error bars represent ±1 standard deviation).

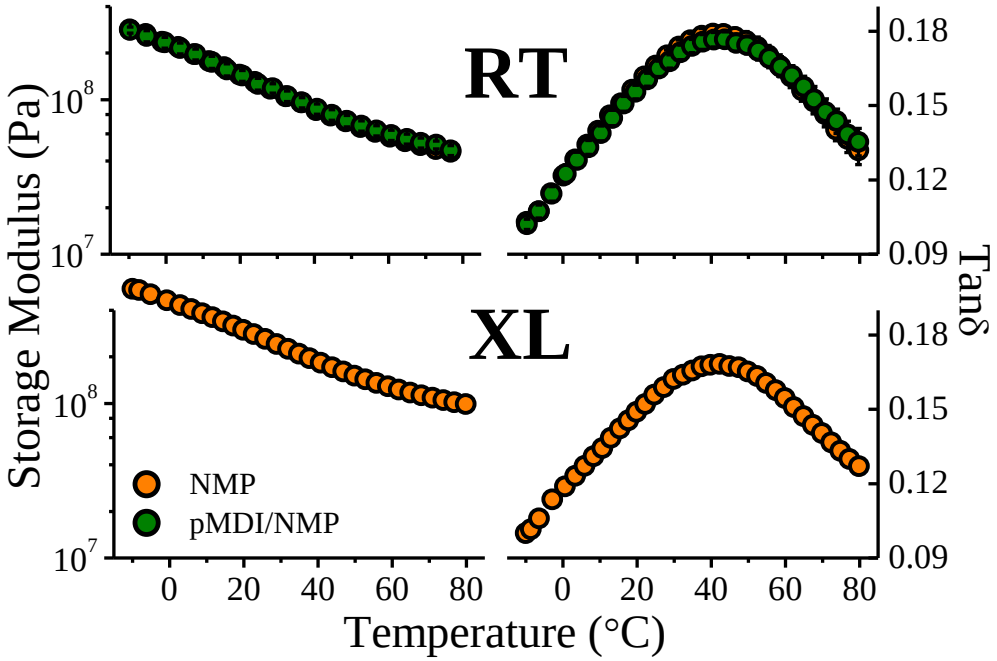

Figure 9-8. Second heat. From top the bottom: Average DMA tan δ and storage modulus curves of pMDI-treated (n=3) and NMP-treated (n=5) RT red oak samples; and NMP-treated (n=1) XL red oak sample immersed in DMF (3°C/min, 5 hz; error bars represent ±1 standard deviation)

Table 9-7. P-values from ANOVA tests performed between T_g values of HMR-treated, NaOH-treated (pH = ~8.34), and untreated specimens with the same grain ($\alpha = 0.10$); hyphens indicate comparison of treatments.

Orientation	HMR-Untreated	HMR-NaOH	NaOH-Untreated
RT	0.000	0.000	0.000
TR	0.000	0.820	0.000
XL	0.001	0.280	0.050

Table 9-8. P-values from ANOVA tests performed between the T_g values of a-HMR-treated, NaOH-treated (pH = ~8.34), and untreated specimens with the same grain ($\alpha = 0.10$); hyphens indicate comparison of treatments.

Orientation	a-HMR-Untreated	a-HMR-NaOH	NaOH-Untreated
RT	0.000	0.180	0.000
TR	0.000	0.074	0.006
XL	0.006	0.401	0.151

Table 9-9. P-values from ANOVA tests performed between the T_g values of pMDI-treated, NMP-treated, and untreated specimens with the same grain ($\alpha = 0.10$); hyphens indicate comparison of treatments.

Orientation	pMDI	pMDI-Untreated	NMP-Untreated
RT	1.00	0.010	0.027
TR	1.00	0.000	0.000
XL	0.001	0.000	0.048

Table 9-10. P-values from ANOVA tests performed between the T_g values of each primer treatment individually as a function of grain ($\alpha = 0.10$); hyphens indicate comparison of grain orientation.

Treatment	RT-TR	RT-XL	TR-XL
Untreated	0.103	0.551	1.00
NaOH	1.00	1.00	1.00
HMR	0.052	0.230	0.900
a-HMR	0.910	1.00	1.00
NMP	0.041	1.00	0.134
pMDI	0.467	0.0328	0.380

Table 9-11. Stress values and percent strain ranges recorded from stress sweeps performed for LVR limit determination – RT, 1st cool.

Treatment	Determined LVR limit (Pa)	LVR limit % Strain	Oscillation stress (Pa)	Actual %Strain
HMR	60,000	0.029 - 0.144	50,000	0.021 - 0.117
a-HMR	80,000	0.031 - 0.163	60,000	0.022 - 0.153
pMDI	60,000	0.029 - 0.136	60,000	0.022 - 0.144
Untreated	70,000	0.021 - 0.153	50,000	0.019 - 0.139
NaOH	80,000	0.037 - 0.212	55,000	0.022 - 0.165
NMP	80,000	0.031 - 0.212	60,000	0.021 - 0.133

Table 9-12. Stress values and percent strain ranges recorded from stress sweeps performed for LVR limit determination – TR, 1st cool.

Treatment	Determined LVR limit (Pa)	LVR limit % Strain	Oscillation stress (Pa)	Actual %Strain
HMR	70,000	0.021 - 0.094	60,000	0.017 - 0.086
a-HMR	70,000	0.031 - 0.143	60,000	0.017 - 0.123
pMDI	60,000	0.029 - 0.093	45,000	0.014 - 0.089
Untreated	70,000	0.026 - 0.130	45,000	0.013 - 0.099
NaOH	60,000	0.026 - 0.151	50,00	0.017 - 0.130
NMP	70,000	0.022 - 0.106	70,000	00.021 - 0.133

Table 9-13. Stress values and percent strain ranges recorded from stress sweeps performed for LVR limit determination – XL, 1st cool.

Treatment	Determined LVR limit (Pa)	LVR limit % Strain	Oscillation stress (Pa)	Actual %Strain
HMR	50,000	0.016 - 0.068	45,000	0.011 - 0.059
a-HMR	60,000	0.016 - 0.076	60,000	0.015 - 0.132
pMDI	32,000	0.015 - 0.044	31,000	0.007 - 0.068
Untreated	50,000	0.013 - 0.059	31,000	0.009 - 0.047
NaOH	60,000	0.016 - 0.090	50,000	0.014 - 0.087
NMP	60,000	0.017 - 0.088	55,000	0.012 - 0.065

Appendix E

References

Chowdhury, S., J. Fabiyi and C. E. Frazier. 2010: Small specimen wood rheology: a novel tool to investigate the HMR coupling mechanism. *International conference on wood adhesives*, Lake Tahoe, CA.